CHALMERS
UNIVERSITY OF TECHNOLOGY

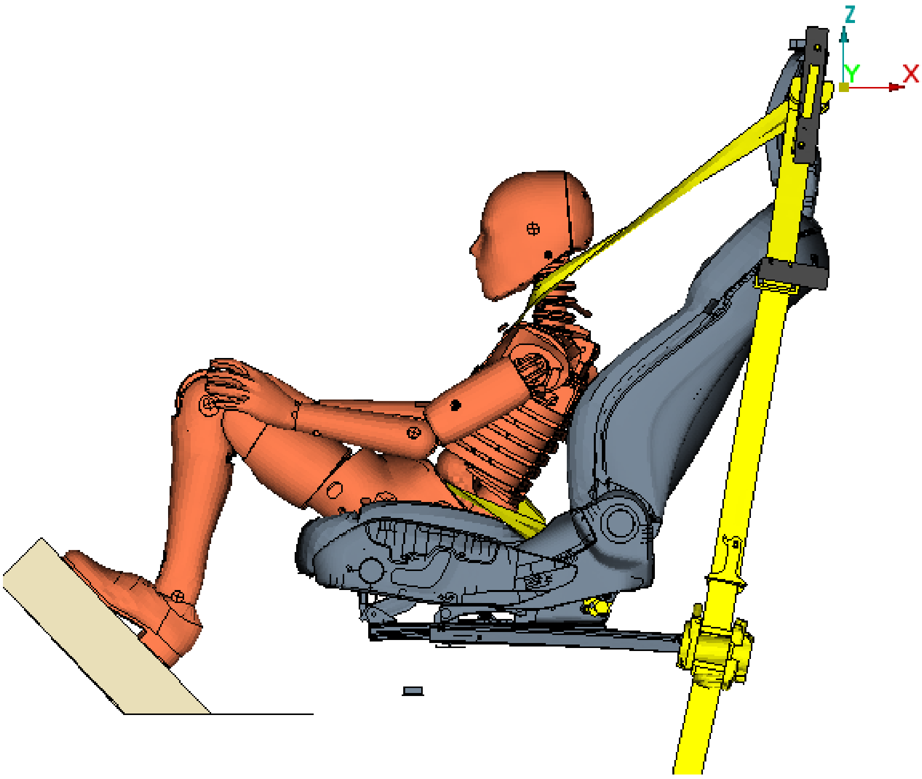

Feasibility of Probabilistic Submarining Prediction in Finite Element Occupant Model Simulations

Master's thesis in M.Sc. Automotive Engineering and M.Sc. Applied Mechanics

VICTORIA RENNER
SUMIT SHARMA

Department of Mechanics and Maritime Sciences
CHALMERS UNIVERSITY OF TECHNOLOGY
Gothenburg, Sweden 2019

Master's thesis 2019:61

Feasibility of Probabilistic Submarining Prediction in Finite Element Occupant Model Simulations

VICTORIA RENNER
SUMIT SHARMA

Department of Mechanics and Maritime Sciences
SAFER - Vehicle and Traffic Safety Centre
Chalmers University of Technology

Gothenburg, Sweden 2019

Feasibility of Probabilistic Submarining Prediction in Finite Element Occupant Model Simulations
VICTORIA RENNER
SUMIT SHARMA

Supervisor: Jonas Östh, Volvo Car Corporation, Volvo Car Safety Centre - Front Crash Interior Team
Examiner: Johan Davidsson, Vehicle Safety, Mechanics and Maritime Sciences, Chalmers University of Technology

Master's Thesis 2019:61
Mechanics and Maritime Sciences
SAFER - Vehicle and Traffic Safety Centre at Chalmers
Chalmers University of Technology
SE-412 96 Gothenburg
Telephone +46 31 772 1000

Cover: HIII 5^{th} submarining in fully frontal rigid barrier sled setup.

Typeset in LaTeX
Printed by Chalmers Reproservice
Gothenburg, Sweden 2019

Feasibility of Probabilistic Submarining Prediction in Finite Element Occupant Model Simulations
VICTORIA RENNER
SUMIT SHARMA
Mechanics and Maritime Sciences
Chalmers University of Technology

Abstract

Current development trends in the automotive industry is heading towards Autonomous Drive (AD) vehicles with novel occupant seating positions, one particular position is reclined seating position. The new seating positions in the car may affect the interaction between the occupant and the seatbelt. In a frontal crash, if the pelvis of an occupant fails to engage properly with the lap-belt, Anterior Superior Iliac Spine (ASIS) slides under the lap-belt and lap-belt loads the abdomen instead of the pelvis bony structures, this is the undesirable event referred to as submarining. To avoid submarining in novel reclined seating position is a key challenge for future AD vehicles. The objective of this thesis was to develop submarining criteria. This master thesis was split into two parts, namely Finite Element (FE) simulations and statistical analysis. The objective of the FE simulations study was to evaluate submarining indicators from the literature and ones developed by thesis student's engineering judgement. The study simulated two Anthropomorphic Test Devices (Hybrid three 5^{th} and Test Device for Human Occupant Restraint 50^{th} percentile) and one Human Body Model (Total HUman Model for Safety 50^{th} percentile) in three different seating configurations (upright, intermediate reclined and reclined) for three different frontal crash pulses (full frontal rigid barrier and two oblique pulses) using a sled setup to generate submarining and non-submarining data. The full frontal rigid barrier pulse is based on a car's response in a staged full scale crash test where the car impacts the rigid wall at 56 km/h and the oblique pulses are based on the struck car being impacted by a 2500 kg moving deformable barrier at 90 km/h having a partial overlap from the driver side and passenger side inclined at 15° and -15° along Z-axis respectively. Several submarining indicators were evaluated for the simulated occupant models and the following were found to indicate submarining: ASIS lever arm, ASIS to belt X distance, ASIS X forces and relative angle between lap-belt and pelvis. The results from the FE simulations study were further analysed using statistical analysis using logistic regression. The objective of the statistical analysis was to find an optimal predictor in relation to submarining and to develop a methodology to derive probability curve for submarining which could be further expanded. The most optimal predictor was identified from the smallest value of the Akaike's Information Criterion and model performance was decided based on the area under the Receiver Operating Characteristics curve. The most optimal predictors were identified as ASIS lever arm and minimum ASIS to belt X distance. The thesis demonstrated that a probabilistic prediction of submarining is feasible, based on analysis of occupant model FE simulation data.
Keywords: Submarining, Probability curve for submarining, Submarining indicators, Logistic regression, FE simulations

Preface

This report presents the work done in a Master's Thesis within the field of occupant safety. The Master's Thesis was conducted at the department of Mechanics and Maritime Sciences at Chalmers University of Technology. The thesis was supervised by Jonas Östh, PhD, First CAE Engineer Safety at Volvo Car Corporation and examination and academic supervision was done by Johan Davidsson, PhD and Associate Professor, researcher at SAFER (Vehicle and Traffic Safety Centre at Chalmers). The thesis work was conducted in the offices of Volvo Cars Safety Centre at Volvo Car Corporation Headquarters.

Acknowledgements

We would like to thank Volvo Car Corporation and SAFER for hosting and supporting us during our thesis work. We would like to express our special gratitude to Jonas Östh at Volvo Car Corporation and Johan Davidsson at Chalmers University of Technology for supervising and supporting us during our thesis work. We would also like to thank Catherine Lef and Henrik Ljungqvist at Volvo Car Corporation for their dedicated support and engagement as well as Nils Lübbe and Erik Brynskog at Chalmers University of Technology for valuable discussions and support.

We also want to thank DynaMore Nordic for giving us the opportunity to attend their introductory course in LS-Dyna for free and thank BETA CAE for setting up a separate licence sever of their software for us thesis students at Volvo Car Corporation.

At last we would like to extend our thanks to our parents, to rest of family and to friends who have consistently supported us and shared the experiences with us during our time at Chalmers.

Victoria Renner & Sumit Sharma, Gothenburg, June 2019

Nomenclature

The terminology used for this thesis is listed below:

ΔV Delta velocity
AIC Akaike's Information Criterion
AIS Abbreviated Injury Scale
ASIS Anterior Superior Iliac Spine
ATD Anthropomorphic Test Device
BTP Belt to pelvis angle
CRS Child Restraint System
CT Computed Tomography
DOE Design of Experiments
EuroNCAP European New Car Assessment Program
FE Finite Element
Fig. Figure
FMVSS208 Federal Motor Vehicle Safety Standards 208
H-point Hip-point
HIII Hybrid Three - Anthropomorphic Test Device
HII Hybrid Two - Anthropomorphic Test Device
Hx H-Point coordinate in x of the occupant
km/h kilometres per hour
max maximum
min minimum
mph miles per hour
MPI Message Parsing Interface
MPP Massive Parallel Computing
NASS-CDS National Automotive Sampling System Crashworthiness Data System
Occupant models HIII05, THOR50 and THUMS50
PMHS Post Mortem Human Subject
Q10 Q series child crash test dummy representing 9 to 12 year old children
ROC Receiver Operating Characteristics
SDG Sustainable Development Goals
THOR50-M Test device for Human Occupant Restraint - an advanced 50^{th} percentile male frontal impact Anthropomorphic Test Device
THOR Test device for Human Occupant Restraint - frontal impact Anthropomorphic Test Device
THUMS Total HUman Model for Safety - Human Body Model
UNECE The United Nations Economic Commission for Europe
UN United Nations

USNCAP United States New Car Assessment Program
WHO World Health Organisation

Contents

1
Introduction

The Sustainable Development Goals (SDG) set up by the United Nations (UN) are a call for action by all countries to promote prosperity while protecting the planet (WHO 2018b). One of these goals set up by the UN is that by 2020, the number of global deaths and injuries from road accidents should be halved relative to the year 2011 (WHO 2018a). The global number of deaths caused by road accidents continues to rise and has reached 1.35 million in 2016 (WHO 2018a). However, the rates of death in relation to the world's population has stabilised in recent years, which suggests that the efforts to improve road safety have mitigated the situation from getting worse, although it also suggests that the efforts made to reach the 2020 SDG remain far from sufficient. Future progress will depend on the success in addressing a wide area of significant challenges in the field of road safety.

Current development trends in the automotive industry is heading towards Autonomous Drive (AD) vehicles, which could improve safety by eliminating human error (Dozza 2018) from causing accidents. Moreover, AD vehicles enable the driver to engage in other tasks than driving (Dozza 2018), as drivers of vehicles no longer need to steer the vehicles themselves. This opens up the possibility for novel occupant seating positions in the car, with particular focus on reclined seating positions. The new seating positions in the car may affect the interaction between the occupant and the restraint systems, where the seatbelt could be one of these restraints. The task of a properly designed seatbelt is to load the structures of the human body which can accept high load without injury (Bohlin 1977). These structures include the rib cage and the pelvis. The lap-belt part of the seatbelt should be worn so that the force is exerted through or below the anterior spines of the iliac crests and the shape of the pelvic bone usually permits the lap-belt to be kept in place if the angle between the lap-belt and the horizontal is not too small; this way the lap-belt is kept at a position between the thigh and torso (Bohlin 1977). If the belt is not worn or positioned in a suitable way, the pelvis (iliac crest) can slide under the lap-belt and lap-belt loads the abdomen instead of the pelvis during the frontal crash, which can cause injuries to the abdominal organs (Bohlin 1977). This undesirable event is what is referred to as submarining. To avoid submarining in novel reclined seating position is a key challenge for future AD vehicles, which are to operate alongside existing vehicles.

Considerable research efforts have already been put into understanding sliding of the pelvis under the lap-belt in vehicle crashes. As summarised in Section 1.2, areas covered are methods to evaluate existing tools used to detect submarining, such as by performing tests with Anthropomorphic Test Devices (ATDs) and Post Mortem

Human Subjects (PHMS) (Uriot, Potier, Baudrit, Trosseille, Richard, et al. 2015), and methods to characterise submarining as a physical event using submarining indicators such as the belt to pelvis angle (Nakane et al. 2015). Other areas involved the methods used to prevent submarining using different countermeasures such as the Pelvic Restraint Cushion (PRC) (Shaw et al. 2018). Research has also been conducted on the consequences of submarining related injuries (Poplin et al. 2015).

1.1 Scope

One of the aims of this master's thesis is to review the available literature and previous work on submarining and submarining detection in vehicle crashes. Another aim is to identify and investigate potential submarining indicators for three occupant models by performing simulations with three occupant models (HIII05, THOR50 and THUMS50). To reach this aim, simulations were carried out with these occupant models in three different pulses (fully frontal rigid barrier and two oblique pulses) and three different seating configurations (upright, intermediate reclined and reclined) using a sled setup to generate submarining and non-submarining data. The final aim is to use the identified indicators to find the optimal indicator in relation to submarining occurrence by performing statistical analysis and check the feasibility of probability curve for submarining to predict the risk of submarining occurrence of occupant models.

1.2 Literature Review

Submarining, the event that the occupant pelvis slides under the lap-belt and the belt loads the soft tissues of the abdomen, has been a concern in the automotive safety research after the three-point seatbelt was introduced (as standard equipment first by Volvo Cars in 1959) and was reported by (Bohlin 1977). There has been continuous studies on the effectiveness of the belt and severity of injuries caused by the belt-occupant interaction in the car, which has also been investigated in recent studies by Luet, Trosseille, Drazétic, et al. (2012), Nakane et al. (2015), Beck, Brown, and Bilston (2014), Richard et al. (2015), Uriot, Potier, Baudrit, Trosseille, Richard, et al. (2015), Poplin et al. (2015), Girard and Cirovic (2012), Shaw et al. (2018) and Trosseille et al. (2018).

Norin, Carlsson, and Korner (1984) wrote a report about the seatbelt usage in Sweden before and after the introduction of the mandatory seatbelt wearing law. They also elaborated on the injury reducing effects that the seatbelt in itself has had. Historically, the usage of the seatbelt increased drastically by making seatbelt usage mandatory in Sweden in 1975. The law stated that all drivers and front seat passengers that are at least 150 cm tall and more than 15 years old must wear seatbelts in cars, trucks and buses where these are installed (although there were some few exceptions from the law). In 1975, the seatbelt usage was about 84% for those travelling in the front seats and in Volvo cars this number was even higher, 93% (Norin, Carlsson, and Korner 1984). Data from the investigation of the injury reducing effects of the seatbelt showed that the seatbelt reduced the injury rate when using a seatbelt compared to not using one. It was also found that the seatbelt was able to reduce the severity of the injuries occurring in a crash. In 1977, Volvo made a study in order to analyse the injury reducing effects of the introduction of the mandatory belt wearing law for Volvo cars involved in accidents (Norin, Carlsson, and Korner 1984). From this study it was found that the injury reducing effect of the law was very positive and that the total injury rate for front seat occupants (belted and unbelted) decreased from 34.6% in 1974 to 28.1% in 1975, which means an injury rate reduction of 19% attributable to the belt use law. It was also found from the study that the rate of severe to fatal injuries decreased by 51% from 1974 to 1975. For the year of 2010, an analysis of the road safety trends was made by the Swedish Transport Administration (Trafikverket) (2011) which stated that the belt usage for front seat occupants in passenger cars was 96%.

Poplin et al. (2015) conducted a study where they investigated the risk factors and mechanisms of hollow-organ, lower abdomen injury in belted automobile occupants in frontal collisions. The hollow-organs include the large intestine, small intestine, and mesentery. In the study, a field data analysis was performed. Furthermore, also an in-depth examination of selected cases demonstrating hollow-organ abdominal injuries was performed. Analysis of data from National Automotive Sampling System-Crashworthiness Data System (NASS-CDS) implied that, on average, occupants that sustained hollow-organ injuries were involved in crashes of higher delta V compared to occupants without hollow-organ injuries (49.2 and 22.8 kilometres per hour (km/h) delta V respectively). They also showed that hollow-organ injuries were not dependent on the seated location of the occupant. About 79% of the hollow organ injuries were isolated in the mesentery and consisted of contusions and hematoma. The authors suggested two reasons for direct loading to the abdominal region in the paper. First, direct loading may be caused by poor initial belt position, resulting from the belt being positioned superior to the Anterior Superior Iliac Spines (ASIS). An ideal belt position would have the lap-belt placed low and tight around the pelvis. Second, direct loading may be caused by submarining, when the belt fails to "catch" on the anterior iliac spines of the pelvis, causing the belt to move into the abdomen. The first reason may be due to static misplacement, while the second reason may be due to dynamic misplacement.

Håland and Nilsson (1991) performed dynamic sled tests with a HIII Anthropomorphic Test Device (ATD) with seat-backrest reclined to 23° in 50 km/h impacts. They varied various parameters such as belt geometry, slack in belt, pre-tensioner in different seat-seatbelt configurations and concluded that occupants are more likely to submarine if the upper belt anchorage is far behind their shoulder, like it is in the rear seat or in the front seat of the two-door car, than if the strap is anchored close to the shoulder. They also said that the risk of submarining increases with the occupant's feet placed close to a seat and with the slack in a belt, and decreases with a buckle pre-tensioner. Håland and Nilsson (1991) also showed that the angle between the lap-belt and pelvis can predict the risk of submarining, measured when the belt force has peaked and dropped to 3 kN.

Richard et al. (2015) did a study to develop a biofidelic FE THOR ATD for prediction of the risk of submarining. First, Luet, Trosseille, Drazétic, et al. (2012) performed some tests on rigid seat and PMHSs, based on that, (Richard et al. 2015) modified an existing FE THOR ATD. Secondly, a comparison study was done by (Richard et al. 2015) with FE results obtained with the FE biofidelic THOR ATD and tests performed by (Uriot, Potier, Baudrit, Trosseille, Petit, et al. 2015) with PMHS in real seats. A wide scope was covered by assessing the FE biofidelic THOR ATD with submarining and non-submarining configurations. Uriot, Potier, Baudrit, Trosseille, Petit, et al. (2015) performed additional PMHS tests to assess the level of predictivity of this new FE model and showed the same submarining ability with the FE THOR ATD as with the PMHS. The authors showed that FE THOR can be used for determination of the risk of submarining. Richard et al. (2015) also discussed three specific mechanisms which they found to be most important for explaining why submarining occurs. Firstly, the initial position of the occupant i.e., when the occupant sits in mid or forward position in seat (Hx -X mm), the pelvis angle is higher compared to occupant sitting at standard position (Hx mm), which increases the risk of submarining of the occupant. Secondly, the relative position between the lap-belt attachment points and the occupant i.e. the risk of submarining is therefore influenced by the orientation of the lap-belt. A more rearward anchorage position of the lap-belt in x will induce a more horizontal lap-belt angle, and thereby increasing the risk of submarining. Thirdly, the type of restraint system is important, as the risk of submarining increases with the amount of belt slack (e.g. if the belt is pre-tensioned or not prior to crash). A pretension device reduces the slack between the occupant and the seatbelt, which then allows to the seatbelt to be more effective in correctly restraining the occupant. The risk of submarining is therefore reduced by the presence of a pre-tensioner.

To assess the submarining ability of existing ATDs, Uriot, Potier, Baudrit, Trosseille, Richard, et al. (2015) performed tests using a real seat with THOR Mod Kit, Hybrid three (HIII) and Hybrid two (HII) ATDs and PMHS. The PMHS were tested in three different configurations to create corridors as reference for ATD testing, with three subjects in each. The first configuration was positioning the test subjects in a standard passenger position with a standard three-point belt having load-limitation of 6 kN at the shoulder belt and a pyrotechnic retractor. The second in a slouched position for which the pelvises of the subjects were translated 60 mm forward in relation to the standard position (in addition the seat was moved forward by 50 mm) intended to generate submarining. The last configuration in slouched position but with separate shoulder- and lap-belt, where the upper shoulder-belt force was limited at 6 kN and the lap-belt force at 4 kN (the lap-belt was equipped with two pyrotechnic retractors). The main corridors created from PMHS testing related to the assessment of submarining were connected to the forces applied to the pelvis and pelvis kinematics: outboard lap-belt forces, seat vertical and horizontal forces, pelvis resultant acceleration and pelvis y-rotation. It was found that submarining occurred in three PMHS tests in the second configuration (slouched) and that no submarining was observed in the other two configurations. Iliac wing fractures were observed for all PMHS in the second configuration and one PMHS sustained an iliac wing fracture in the first configuration and one in the last configuration. It was found that HIII did not submarine in any configuration, while in the slouched position the THOR and HII ATD submarined. In the slouched configuration with lap-belt load-limitation, the submarining of the THOR ATD was unclear. Compared to the PMHS, the HIII ATD did not predict submarining in the slouched position, while the HII and THOR Mod Kit ATDs did. The THOR Mod Kit ATD better predicted the timing of submarining than the HII ATD compared to the timing of submarining of the PMHS. The authors discussed that only analysing the occurrence and timing of submarining is not enough to evaluate the biofidelity of the investigated ATDs, because the conclusions may depend on the test configuration. Thus, it was stated by the authors, a more detailed analysis is required to evaluate the biofidelity of each component leading to submarining. This is because the interaction of the components in itself and its effects on submarining are complex, and therefore, simulations investigating this would be of great help. The paper concluded that the PMHS tests allow for the evaluation of human surrogates in terms of pelvis kinematics and dynamics, and although the tests might not be fully reproducible, they can be used as reference for the development of further, more controlled tests.

Luet, Trosseille, Potier, et al. (2012) performed a study to assess the influence of inter-individual differences on submarining. They conducted nine tests with nine PMHS in three different configurations. Each configuration differed by five features: the deceleration characteristics, initial lap-belt angle, lap-belt slack, seat pan angle and footrest position. Before the tests, both a pre-positioning phase to define the PMHS's natural sitting position as well as static behaviour characterisation of the lumbar spine of the PHMS was performed. The pre-positioning phase involved recording of the position using angular sensors mounted on the sacrum on T1 and T12 levels. For the static behaviour characterisation, a Y moment sensor was used and adjusted so that it approximately went through the middle of the sacral plate. The sacrum and T12 vertebrae angles and the Y moment were recorded at the same time as forward and rearward movement was imposed onto the thorax to characterise the static behaviour of the lumbar spine. After the sled tests were performed, simulations using the Labman model were run. The Labman model was developed by Lizee et al. (1998) and, is a 3D finite element model of the human body that can be used in automotive safety engineering. The simulations with the Labman model were run to assess how inter-individual differences influence submarining; this was done by first performing a numerical sensitivity study and then using the results from this to personalise the Labman model to match the nine PMHS's CT scans and responses. The personalised Labman models were then used to reproduce the sled tests in simulation and validate such that the identified personalisation parameters allowed submarining to be captured correctly. The authors found that in the first and third test configuration, all PMHS submarined, whereas in the second configuration, only one PMHS out of three submarined. Therefore, the occurrence of submarining was observed to depend on the test severity and restraint geometry on the one hand and only the specimen features on the other hand. Moreover, the authors state in the paper that flexion of the lumbar spine mostly occurs in submarining. It was also found that the initial orientation of pelvis and the geometry of the ASIS seem to play an important role in the lap-belt interaction.

Luet, Trosseille, Drazétic, et al. (2012) did a study to validate the biofieldity of Anthropomorphic Test Devices (ATDs) (HII and HIII against PMHS for a front sled using 2 ATDs and 9 PMHS) for different parameters such as deceleration pulse, initial lap-belt angle, lap-belt slack, seat pan angle, footrest position and discussed the prediction of submarining. HIII ATD had the most human like behaviour. However, the interaction causing submarining in HIII were not similar to interactions causing submarining in the PMHS. More precisely, the Hybrid III pelvis rotation matched the three corridors despite the difference in the thorax kinematics. HIII has a similar pelvis rotation as PMHS due to rearward tilting of thorax. The lap-belt ended on the abdomen, risking producing injuries irrespective of fractures caused submarining or submarining caused fractures. They concluded that HII has more propensity to submarine compared to HIII and none of the HII and HIII demonstrate better biofidelity.

Nakane et al. (2015) discussed two factors which have large impact on abdominal injuries for the rear seat occupants: submarining and the incorrect static routing of the seatbelt on the abdomen which causes lap-belt intruding into abdominal region in car crash. They first established the frequency of the abdominal injuries caused by submarining by analysis of accident data of 555 injury cases of belted rear seat occupants from 2007 to 2011 from the National Automotive Sampling System Crashworthiness Data System (NASS-CDS) database. It was found that injuries due to belt restraint system accounts for nearly 28% in the rear seat, of which 34% were injuries in abdominal region. Out of this 34% injuries in abdominal region, 65% were distributed in the lower abdomen such as the intestine or the mesentery. Later, they experimentally determined the influence on abdominal internal organs using the THUMS HBM in 56 km/h full-width rigid barrier impact simulations. Important finding in their study were the mechanics of the submarining, and the importance of lap-belt forces (Figure 1.1) and angles in the pelvis region which influence the submarining. The authors proposed the hypothesis that continuously maintaining a small belt to pelvis angle (BTP) (see Figure 1.1) is important to control the submarining. They also proposed incorrect belt fit as the cause for the increase in abdominal injuries and supported the claim with two main findings. Firstly, when the lap-belt was fitted on the abdomen, the maximum abdomen deflection increased approximately 3.4 times compared with proper fitted lap-belt on the iliac spine. Secondly, the abdomen deflection velocity increased by 2.3 times. They proposed the importance of proper belt routing on the iliac spine to restrain the occupants. Their study was limited to an occupant sitting in proper position and proper posture.

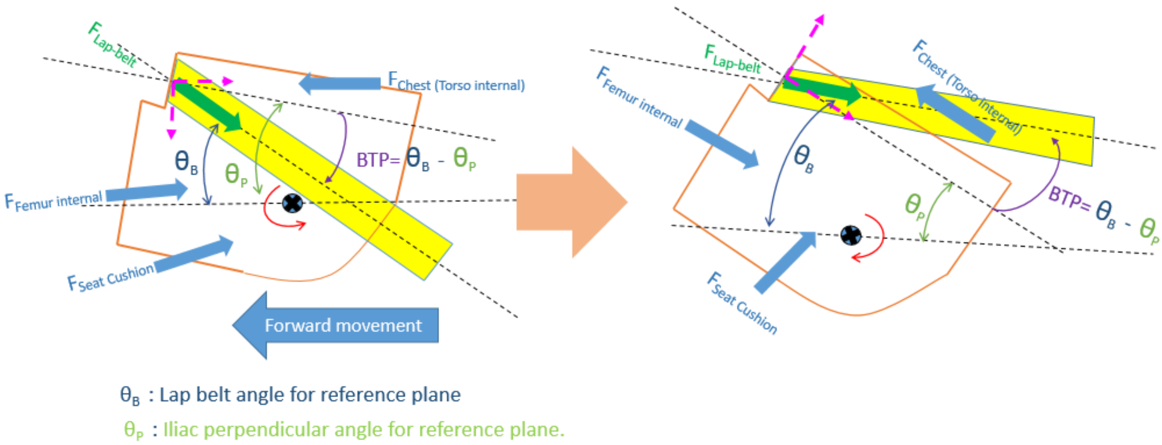

Figure 1.1: Forces acting on pelvis and BTP (belt to pelvis angle), adapted from Nakane et al. (2015), page 3)

Another set of sled tests with PMHS, and three types of ATDs to study submarining was conducted by Uriot, Baudrit, et al. (2006). The study compared the interaction between the belt and pelvis for three different types of ATDs: THOR NT, Hybrid III 50th and Hybrid III 95th percentile, and for PMHS. The study also aimed at identifying parameters which may influence how the lap-belt hooks the pelvis. The tests were performed using a hydraulic test device, which reproduced the belt kinematics of a frontal impact. The belt tension was kept constant and dynamic rotation was imposed on the lap-belt anchorages during the tests. Submarining was automatically identified by a software of a servo controller used in the tests as soon as the magnitude of drop in the belt tension reached a threshold (threshold not specified). A submarining angle was defined as the angle between the lap-belt relative to the pelvis at the time when the occurrence of submarining was identified to generate a comparative metric. This angle was measured in two different coordinate systems, where the first was the HI line (H-point to imaginary midpoint between left and right ASIS) pelvis coordinate system and the second was in a seated pelvis position coordinate system (to take the difference of pelvis position in the car seat into account). The test results showed that for submarining cases, the submarining angle was larger for the tested ATDs than for the PMHSs. Increased belt tension also resulted in a larger submarining angle for both ATDs and PMHS. Uriot, Baudrit, et al. (2006) also performed a parametric analysis by performing a multiple linear regression analysis on the test results. For this analysis they used the type of surrogate, initial angle of the lap-belt relative to the pelvis in the X-Z plane, load exerted by the lap-belt onto the pelvis and rotation velocity of the lap-belt relative to the pelvis as explanatory variables and submarining angle as a dependent variable. The results of the multiple linear regression showed that in this test sample, only the type of surrogate and the belt tension were significant parameters. The belt tension refers to the load exerted by the lap-belt onto the pelvis. The belt tension was defined as the average values measured in both strands of the belt.

Girard and Cirovic (2012) conducted fifty UNECE REG.44 (i.e. a 52 km/h ΔV

impact) sled tests using nine different Child Restraint Systems (CRS) with the Q10 ATD. They recorded the trajectory of the head, thighs, arms, the CRS's base, backrest and headrest. They found that the submarining cases had distinct patterns of the head-torso-leg complex trajectory. They proposed that it may be possible to use lower limb motion for detection of submarining.

In the assessment protocol for adult occupant protection for the full width impact assessment set up by the European New Car Assessment Programme (Euro NCAP 2017), modifiers are applied to the score if submarining is occurring during a test. If a 1 kN drop in force is measured within 1 ms in any of the two iliac load cells of an ATD in testing and when submarining can be confirmed on a high speed film, the modifier is applied. If submarining occurs, the score for Knee, Femur and Pelvis is reduced by 4 points.

Shaw et al. (2018) performed a study involving sled tests which approximated high and low speed frontal impacts. In the sled tests four female PMHS were used. The study evaluated the performance of a submarining countermeasure called a Pelvic Restraint Cushion (PRC). The PRC is an improvement of the existing "anti-submarining bar", which typically is a sheet metal ramp commonly employed under front seat cushions (Shaw et al. 2018). The PRC deploys under the thighs when a crash is detected in order to block the forward motion of the pelvis (Shaw et al. 2018). The tests were performed with and without the PRC. The results from the tests showed that the PRC is effective in reducing forward motion of the pelvis and that it reduces the risk of abdominal injury due to lap-belt loading in a high speed frontal crash. To quantify the position of the pelvis in relation to the lap-belt throughout the event, the researchers developed a parameter called submarining distance. It was defined as the right ASIS X-axis position relative to the X-axis position of the lap-belt at the mid-line of the subject. Positive values of the submarining distance indicated that the ASIS is forward of the lap-belt at the mid-line.

Beck, Brown, and Bilston (2014) demonstrated the importance of adjustable upper anchorages to allow good seatbelt fit, upright seating posture, belt buckle positioned near the seat, pre-tensioner and load limiter equipped seatbelt and anti-submarining seat pan for rear seat occupants. These features can be used to improve the design of a system of restraints to reduce injuries to rear seat occupants. They visually assessed the submarining and in addition to that, they also used femur displacement and pelvic rotation as a supplementary measure for the assessment of submarining. They also considered lap-belt force measurement as another potential measure of submarining. The authors varied the seating posture parameter and found that HIII 5^th ATD seated in slouched posture caused submarining in all cases. They also pointed that in all slouched postures pelvis has a more backward rotation with a longer webbing, the lap-belt angle is more horizontal and, as a result, the pelvis slides up more easily under the lap-belt. Beck, Brown, and Bilston (2014) found that for both the standard three-point seatbelt and the pre-tensioning belt in tests, webbing length on the buckle resulted in submarining with the abdominal penetration initiated from the buckle side. Therefore, Beck, Brown, and Bilston (2014) suggested that, to avoid long webbing or buckle stalks, manufacturers should aim for the buckle to be located as close as possible to the seat. They also found reduced chest injury measures and improved HIII 5^th ATD kinematics with anti-submarining seat pan when compared to a flat seat pan commonly found in the rear seat. This is because of the concave shape of the seat pan which provides resistance to forward motion of the pelvis of the occupant. Beck, Brown, and Bilston (2014) also pointed out that if the forward motion of pelvis is well controlled, the rearward pelvic rotation is not necessarily accompanied by submarining. However, the limitation in their study was, no use of front seat and subsequently, there was no knee or lower leg restriction during the forward excursion of the HIII 5^th ATD. (Beck, Brown, and Bilston 2014).

2

Methods

This study utilises Finite Element (FE) simulations of three occupant FE models, a FE model of a Hybrid III 5^{th} female ATD (HIII05), a FE model of a THOR 50^{th} male ATD (THOR50) and SAFER THUMS 50^{th} male Human Body Model (THUMS50), positioned in three seating positions (upright, intermediate reclined and reclined) for three pulses (fully frontal rigid barrier and two oblique pulses). Simulations were run with LS-DYNA version R9.3.0 to generate submarining and non-submarining data. Data post-processing was done in META. The data was investigated and analysed in MATLAB to find the most promising indicators in relation to submarining. Statistical analysis of the data was done in MATLAB to find the most optimal predictor using logistic regression and to investigate risk of submarining occurrence.

2.1 FE Simulations

The sled model setup for the three occupant models was done using pre-processors. The simulations were performed according to the design of experiments (see Fig. 2.2) in an FE solver and post-processing was done to analyse the results. The details of these steps can be found in the subsections below.

2.1.1 Design of Experiments

The design of experiments was comprised of the combination of components shown in Fig. 2.2. The following points below represent the experimental set-up and variations performed in the study.

- Sled model.
- Postures: Upright, Intermediate reclined, Reclined.
- Sled pulses: Fully Frontal Rigid Barrier (FFRB) and two oblique pulses.
- Occupant models.

2.1.1.1 Sled Model

A reduced correlated FE sled model was used for the study. The model is correlated for the test scenario when the belted occupant is hitting the car with a rigid barrier at 56 km/h. The sled model has all necessary parts depicting the environment for driver to seat and seat-belt interaction such as floor, mounted seat, mounted belt assembly and routed belt and a positioned occupant model at the respective H-points as in testing. In this sled setup, some parts were not considered such as an instrument panel, knee airbag, steering wheel and driver airbag. The sled setup can be seen in Figure 2.1.

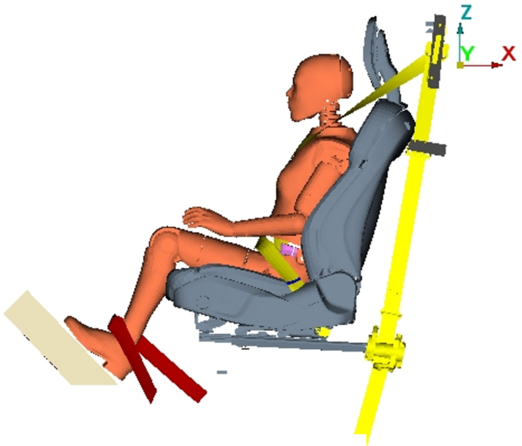

(a)

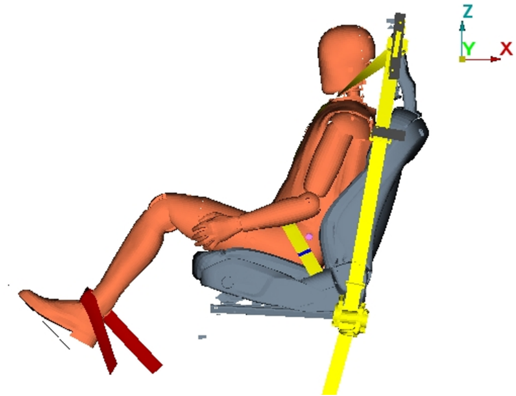

(b)

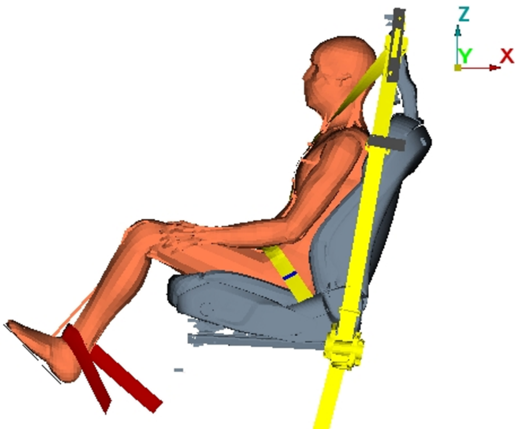

(c)

Figure 2.1: Sled setup for occupant models, left side view. (a) HIII05, (b) THOR50, (c) THUMS50

2.1.1.2 Sled Pulses

The experiment was designed to be evaluated for three sled pulses: Fully Frontal Rigid Barrier (FFRB) pulse, oblique left pulse and oblique right pulse. The FFRB pulse is based on a car's response in a staged full scale crash test where the car impacts the rigid wall at 56 km/h. The oblique left pulse is based on the struck car getting impacted by a 2500 kg moving deformable barrier at 90 km/h having a partial overlap from the driver side inclined at 15° (Saunders and Parent 2013) along

Z-axis. The oblique right pulse was generated so that it mirrored the kinematics of the oblique left pulse and it is based on the struck car getting impacted by a 2500 kg moving deformable barrier at 90 km/h having a partial overlap from the passenger side inclined at -15° along Z-axis. The oblique left pulse is in positive yaw rotation (directing the driver to move diagonally towards the a-pillar) and the oblique right pulse is in negative yaw rotation (directing the driver to move diagonally towards the passenger/centre-console).

2.1.1.3 Occupant Models

The experiment was designed to be evaluated for three occupant models: HIII05, THOR50 and THUMS50.

1. **HIII05**: The Hybrid III (HIII) 5^{th} ATD represents the smallest portion of the adult population. The HUMANETICS HIII5F V2.0 harmonized FE model was used in this study. The FE model has a number of 233255 nodes and 429254 elements. The FE model has load cells at various modelled body parts which can provide all six output channels: three forces and three moments. The ones which were used in this master's thesis are: lumbar spine load cell, left iliac load cell and right iliac load cell. The local axis for the load cells is defined by the use of coordinate systems. The orientation of the local coordinate system used in the ASIS/iliac load cells can be seen in Figure 2.11. The FE model has accelerometers at various modelled body parts and the ones used in this study are the upper thoracic spine, middle thoracic spine, lower thoracic spine and pelvis centre accelerometer. The measuring capabilities of HIII05 ATD in FE simulations, can be measured in hardware testing and are mentioned in Appendix A.1.

2. **THOR50**: Test device for Human Occupant Restraint (THOR) 50^{th} ATD is an advanced frontal impact ATD and represents the 50^{th} percentile adult male of the population. The HUMANETICS THOR-50TH V1.6 FE model was used in this study. The FE model has a number of 441857 nodes and 715165 elements. The FE model has load cells at various modelled body parts which can provide all six output channels: three forces and three moments. The ones which were used in this master's thesis are: Thoracic Spine Load Cell, ASIS load cell left and ASIS load cell right. The orientation of the local coordinate system in the ASIS load cells of this occupant model is the same as in HIII05 and can be seen in Figure 2.11. The FE model has accelerometers at various modelled body parts and the ones used in this study are the T1 accelerometer, T4 accelerometer, T12 accelerometer and pelvis accelerometer. The measuring capabilities of THOR50 ATD in FE simulations, can be measured in hardware testing and are mentioned in Appendix A.2.

3. **THUMS50**: This study used the SAFER Total Human Model for Safety (THUMS) Human Body Model (HBM) v9.0.1, which is a 50^{th} percentile adult male HBM based on the THUMS v3 but substantially updated by the partners of the SAFER Vehicle and Traffic Safety Centre at Chalmers in Gothenburg. The FE model has a number of 180570 nodes and 237476 elements. The FE

model has load cells at various modelled body parts which can provide all six output channels: three forces and three moments. The ones which were used in this master's thesis are: right ASIS load cell, left ASIS load cell and L5 vertebra load cell. The orientation of the local coordinate system in the ASIS load cells of this occupant model is the same as in HIII05 and THOR50 and can be seen in Figure 2.11. The FE model has accelerometers at various modelled body parts and the ones used in this study are the T1 accelerometer, T4 accelerometer, T12 accelerometer and Sacrum anterior accelerometer.

2.1.1.4 Seating Postures Used

The experiment was designed to be evaluated for three different seating postures: upright, intermediate reclined and reclined of HIII05, THOR50 and THUMS50. The seating postures of the occupant models were achieved with seat-backrest rotation.

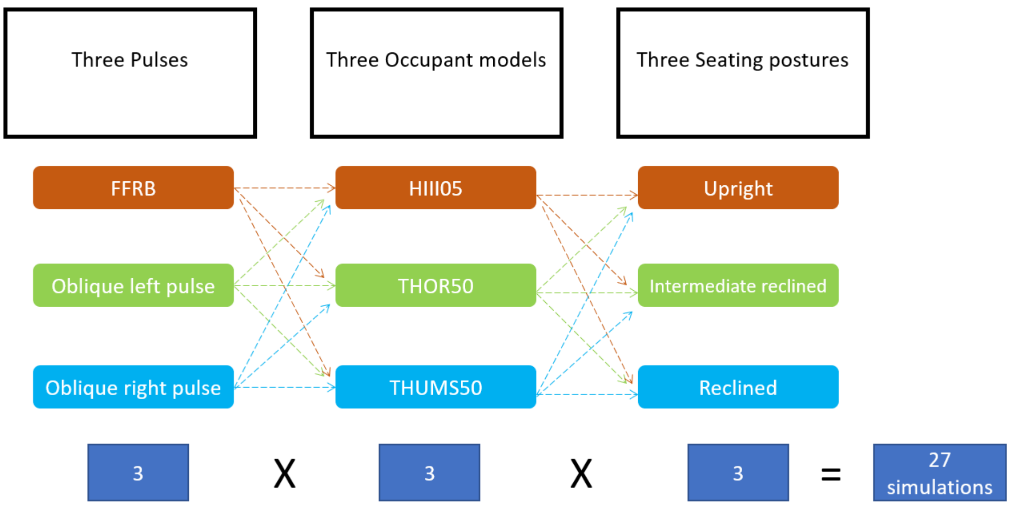

Figure 2.2: Flowchart of design of experiments performed.

2.1.2 Tools and Instrumentation

The FE models of HIII 5^{th} harmonized ATD version 2.0 and THOR 50^{th} ATD version 1.6 by HUMANETICS (Farmington Hills, MI, USA) and SAFER THUMS 50^{th} Human Body Model (HBM) version 9.0.1 by SAFER (Gothenburg, Västra Götaland County, Sweden) were used in this master's thesis to understand the submarining event in the virtual environment.
The pre-processing was done in ANSA (BETA CAE Systems, Root D4, Switzerland), ATD positioning and belt-routing in PRIMER (Oasys Ltd., London, United Kingdom), post-processing was done using META post-processor (BETA CAE Systems, Root D4, Switzerland) and MATLAB® (The Mathworks Inc., Natick, MA, USA). All Simulations were performed on LS-DYNA® MPP R9.3.0 (930_128342) revision 98312 (LSTC Inc., Livermore, CA, USA) solver on Volvo Cars distributed computer cluster using Message Parsing Interface (MPI) technology.

2.1.3 Model Set-Up

Three positions were simulated in this study: upright, intermediate reclined and reclined. For each seating position, the occupant models were positioned using the marionette method, in which one dimensional elements are used to pull the parts of the model into position during a pre-simulation as shown in Fig. 2.3. The parts of the occupant models were positioned into the correct position into the corresponding seat as per the testing position data. For all the generated seating configurations, a seat-squashing procedure was carried out in ANSA to depenetrate the seat according to the outer occupant model profile positioned in the seat. A new seatbelt was generated and positioned for each occupant posture. The seat was depenetrated with the belt profile placed in contact to the seat to ensure there were not any intersections and penetrations in the model. For each occupant posture, one of the three pulses was used to generate all possible cases as presented in Fig. 2.2.

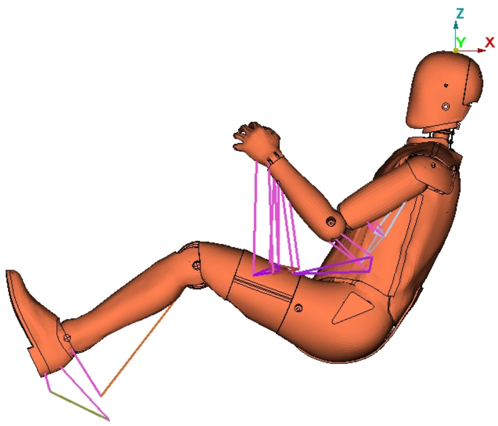

(a)

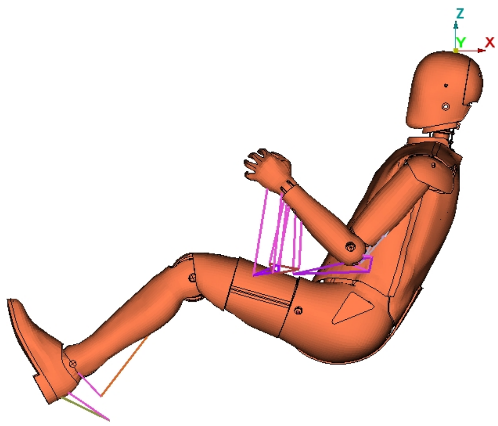

(b)

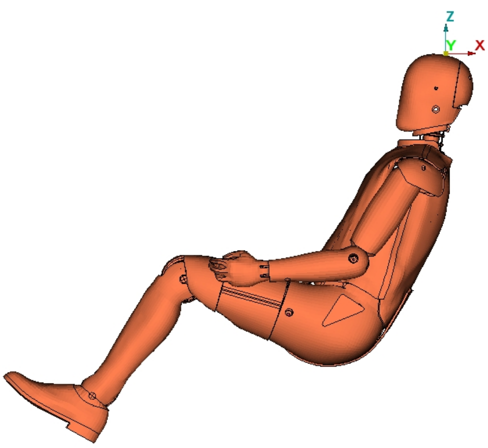

(c)

Figure 2.3: Marionette method: Occupant model pre-simulation using cables (a) initial stage, (b) intermediate stage, (c) final stage. Images showing the THOR50 ATD.

2.1.4 Submarining Assessment

The left (anchor side) ASIS/iliac block sliding under the lap-belt was considered as left submarining while the right (buckle side) ASIS/iliac block sliding under the lap-belt was considered as right submarining. The submarining and submarining time information as observed visually in simulation for HIII05, THOR50 and THUMS50 are tabulated in Table 3.2, 3.3, 3.4 corresponding to upright, intermediate reclined and reclined configurations of the seat backrest for the FFRB and two oblique pulses. In the results Section (3) for the FE simulations, the green colour in Table 3.2, 3.3 and 3.4 depicts the simulations which did not submarine while the red colour depicts the simulations which submarined and for the simulations which submarined, the timing of submarining is given in the same tables.

2.2 Evaluated Submarining Indicators

Based on the literature review in Section 1.2, a number of possible submarining indicators were selected, which are summarised in Table 2.1. In addition to the indicators previously used in the literature, a few indicators were added based on the authors' engineering judgement. Both categories of indicators are specified in Table 2.1 and are explained in the following subsections.

Table 2.1: Identified submarining indicators arranged into different categories.

Category	Submarining Indicators		
Angles	1. Relative angle between lap-belt and pelvis - 3D left	2. Relative angle between lap-belt and pelvis - 2D left	3. Relative angle between lap-belt and pelvis - 2D right
Trajectories	4. Belt mid-point XZ trajectory	5. H-point XZ trajectory	
Forces & Moments	6. Iliac X forces	7. Iliac Y moments	8. Lap-belt cross-sectional forces
	9. Lumbar spine forces	10. Lumbar spine moments	11. Abdomen region forces - force transducer
Submarining Distances	12. Belt mid-point to spine X distance	13. Left ASIS to belt X distance	14. Right ASIS to belt X distance
Accelerations	15. Pelvis acceleration	16. Spine T1 acceleration	17. Spine T4 acceleration
	18. Spine T12 acceleration		
Miscellaneous	19. Belt pay-in & pay-out	20. Initial belt position in relation to ASIS	21. Iliac/ASIS lever arm

2.2.1 Indicator 1-3 - Relative Angle between Lap-Belt and Pelvis

From the literature review in Section 1.2, it was found that Uriot, Baudrit, et al. (2006) defined an angle of the lap-belt relative to the pelvis. In their study, the researchers defined this angle as the angle between two straight lines, where the first line for the lap-belt went through the the anchorage of the belt projected onto the mid-sagittal plane and the centre of the lap-belt in the mid-sagittal plane. The second line went through the H-point and an imaginary midpoint between left and right ASIS (denoted as I). Their angle was a 2D angle.

The differences between how this project defined the angle between the lap-belt and pelvis and how Uriot, Baudrit, et al. (2006) defined their angle, is that this project investigated the angle on both sides of the pelvis (left and right ASIS), a 3D skew angle was added to the analysis of this study and the lap-belt cross-sectional forces were used instead to define the belt vector. The cross-sectional forces provide the direction of the forces in the lap-belt and is meant to approximate the orientation of the lap-belt in relation to the global coordinate system. The forces are assumed to be aligned along the longitudinal axis of the lap-belt.

This project defined two 2D angles and one 3D skew angle to describe the relative orientation between the lap-belt and pelvis. The procedure used to define such angles is presented below:

1. First, for the lap-belt, a belt force vector was defined using the belt cross-section forces on left (anchor side) and right side (buckle side) respectively. The cross-section in the lap-belt is indicated by the blue lines and the force vectors are displayed using black lines in Figure 2.4 and 2.5.
2. Second, for the pelvis, vectors between the H-point and iliac crest (further denoted as I) were defined as either a vector connecting the H-point to left or right ASIS (for the 2D angle, see Figure 2.4 and 2.5) or a vector connecting the H-point to an imaginary point in the middle between left and right ASIS (for the 3D angle, see Figure 2.4). For the left side, the initial point was the I point and terminal point was the H-point. For the right side, the initial point was the H-point, while the terminal point was the I point. The reason for the shift of the terminal and initial point between left and right side, was that the time-history curves of the angles should be comparable between both sides.
3. Third, to determine the 2D angles, the two vectors were projected onto the XZ-plane and then the angle between them was calculated. For the 3D angle, a skew angle was determined by calculating the dot product between and determining the lengths of the two vectors. The 3D angle was then determined using equation (2.1) below.

$$\theta \;=\; cos^{-1}\left(\frac{\overrightarrow{v_{HI}} \bullet \overrightarrow{v_{Force}}}{|\overrightarrow{v_{HI}}||\overrightarrow{v_{Force}}|}\right) \tag{2.1}$$

Where $\overrightarrow{v_{HI}}$ is the vector between point H and I (which as mentioned before also can be defined as: $\overrightarrow{v_{IH}}$), $\overrightarrow{v_{Force}}$ is the force vector in the cross-section of the lap-belt and θ is the angle between the two vectors.

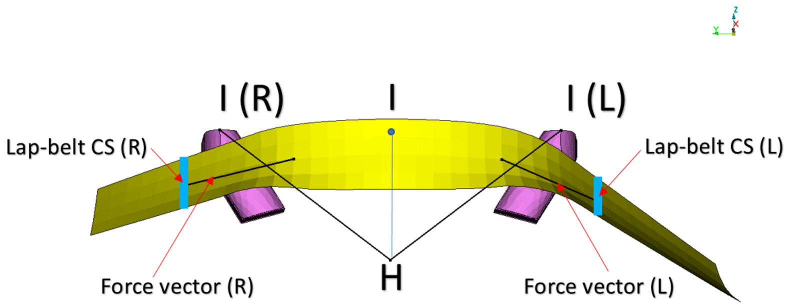

Figure 2.4: Front view describing the vectors between H and I and vectors created from the forces in the lap-belt cross-sections. Showing the position of H-point, I-points, lap-belt cross-sections (CS) and vectors. Image displaying the iliac blocks of HIII05 and the lap-belt.

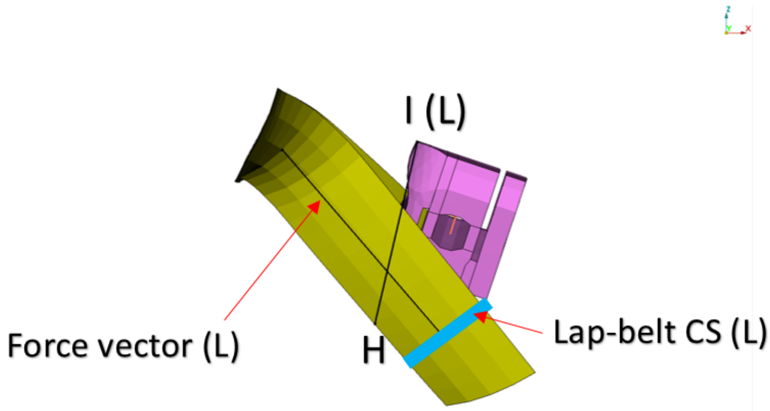

Figure 2.5: Side view describing the vector between H and I (on anchor side) and vector created from the forces in the lap-belt cross-section on anchor side. Image displaying the left iliac block of HIII05 and the lap-belt.

2.2.2 Indicator 4 - Belt Mid-Point Trajectory

The belt mid-point kinematics were investigated in a study performed by Uriot, Baudrit, et al. (2006). There the authors analysed the X and Z displacement of the belt mid-point. In this study, the belt mid-point trajectory was investigated by extracting the X and Z coordinates of a node in the middle of the lap-belt throughout the simulation time and a graph showing the X coordinates on one axis and the Y coordinates on the other axis was plotted. The node was identified in the middle of the lap-belt for all performed simulations with a Y coordinate as close to the H-point Y coordinate as possible. The lap-belt mid-point node is not static in relation to the occupant model pelvis during the simulations. However, for all simulations analysed, it was verified that the node did not move more than 20 *mm* in either positive or negative Y direction. Below images present the node locations in which the lap-belt mid-point trajectory was extracted for the used occupant models:

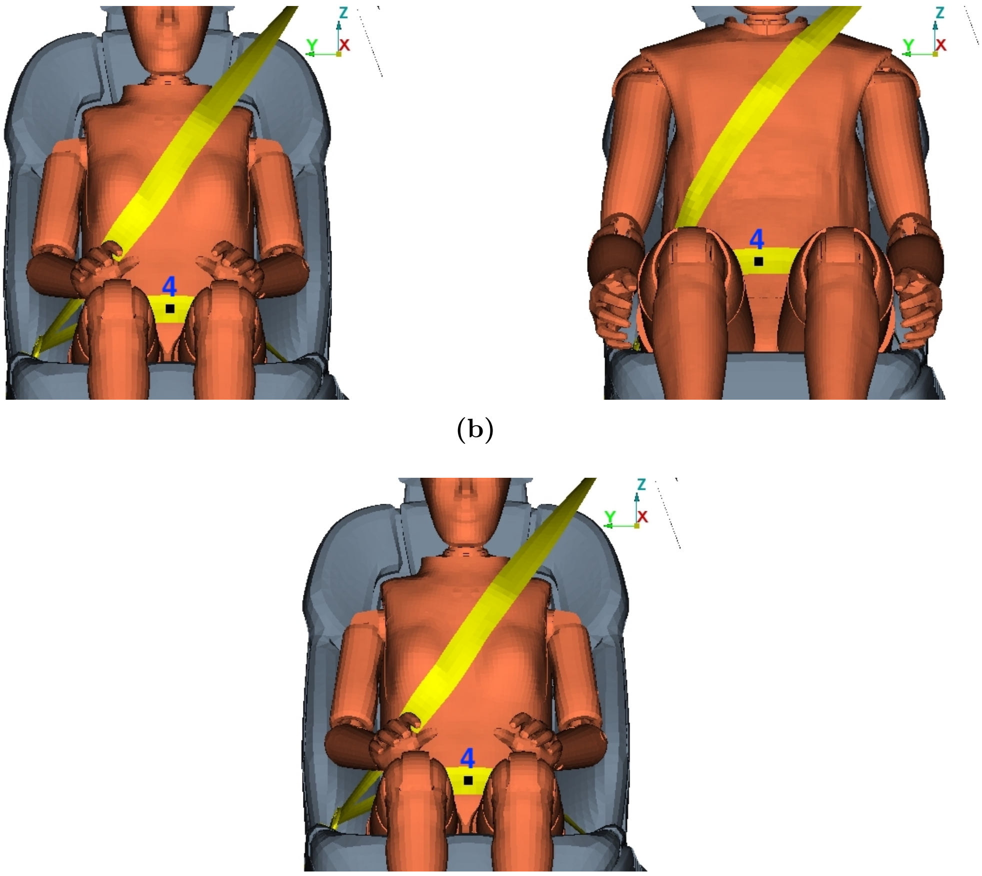

(a) (b) (c)

Figure 2.6: Front view: Position of lap-belt mid-point node for belt mid-point trajectory. (a) HIII05, (b) THOR50, (c) THUMS50.

2.2.3 Indicator 5 - H-Point Trajectory

Luet, Trosseille, Drazétic, et al. (2012) investigated the H-point X and Z displacement over time and Girard and Cirovic (2012) analysed the thigh trajectory in their studies. Thus, the thesis students chose to combine the work from both studies and investigate the H-point trajectory. To analyse the H-point trajectory, the X and Z coordinates of a node located at the H-point of the used occupant models were extracted throughout the simulation time and a graph showing the X coordinates on one axis and Z coordinates on the other axis was plotted. The H-point location in the different occupant models can be seen in Figure 2.7.

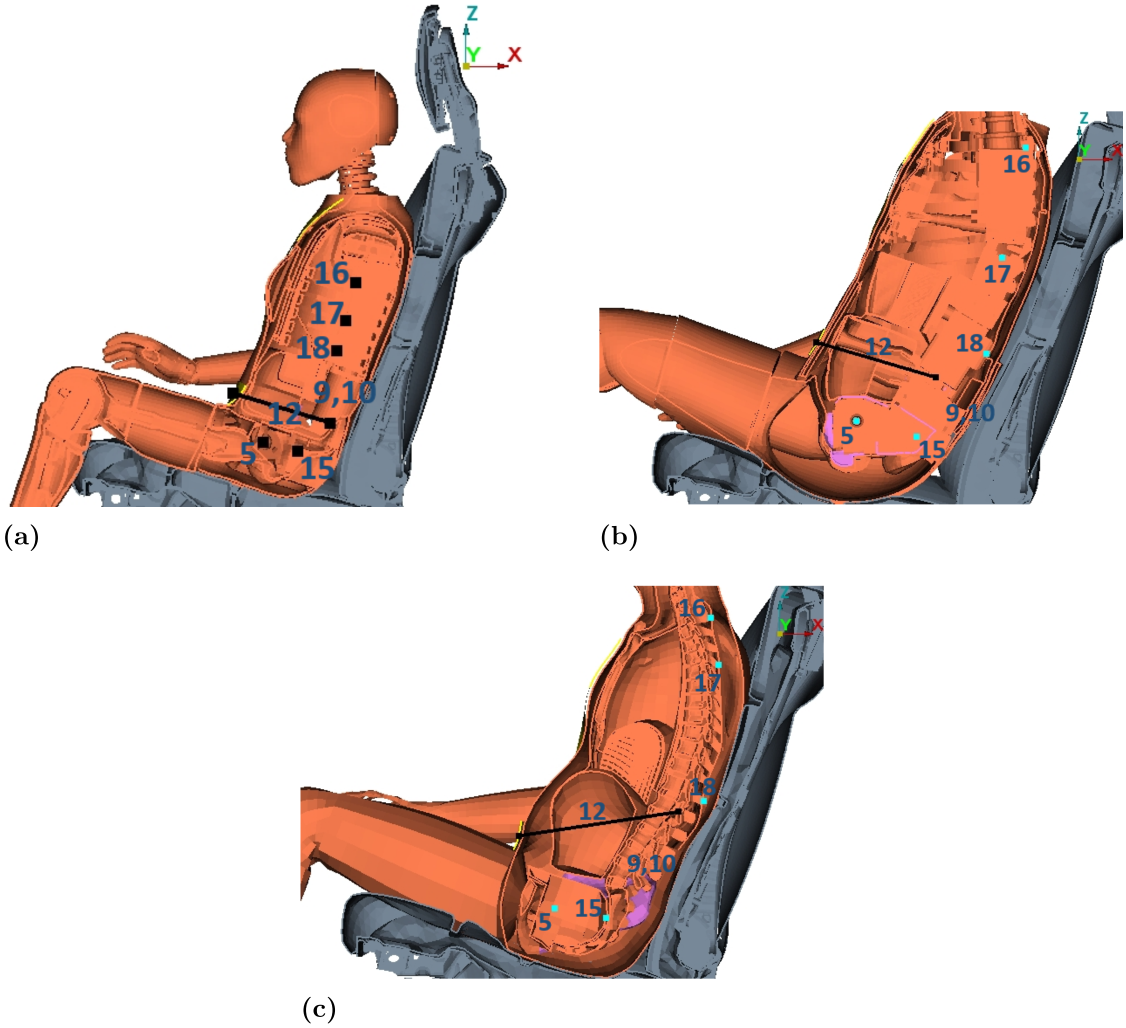

Figure 2.7: Side cross-section view: Position of indicators 5. H-point trajectory, 9-10. Lumbar spine forces and moments, 12. Belt mid-point to spine X-distance, 16. Spine T1 acceleration, 17. Spine T4 acceleration and 18. Spine T12 acceleration. (a) HIII05, (b) THOR50, (c) THUMS50.

2.2.4 Indicator 6 - ASIS X Forces

As described in Section 1.2, the iliac forces are monitored in the frontal full width impact assessment for adult occupant protection by Euro NCAP (2017) (the ASIS is the the outermost point on the iliac wings). To investigate the forces acting on the ASIS on left and right side for the used occupant models in this study, X force data was extracted from load cells in the ASIS blocks. The load cells in the pelvis have a local coordinate system and the direction of the local coordinate system in these load cells can be seen in Figure 2.11. In relation to submarining, the X force was of interest, since a drop in force over a short period of time may indicate if submarining has occurred or not. The position of these load cells in the used occupant models can be seen in the figures below:

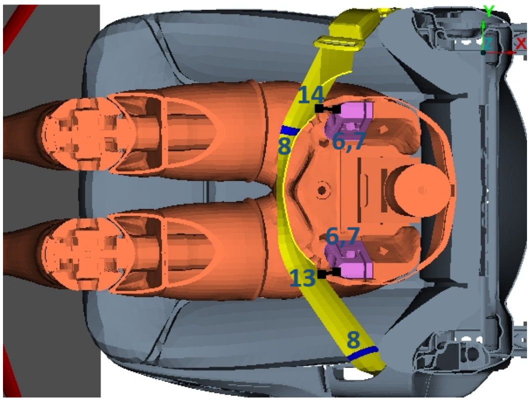

(a)

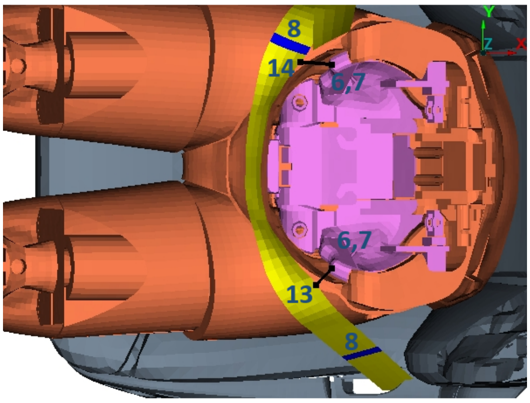

(b)

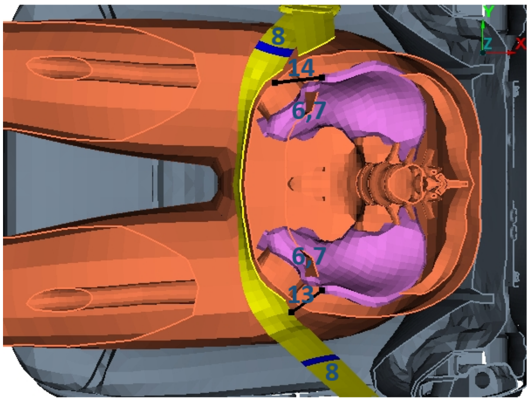

(c)

Figure 2.8: Top cross-section view: Position of indicators 6-7. Iliac X forces and Y moments, 8. Lap-belt cross-sectional forces and 13-14. Left and right ASIS to belt X distance. (a) HIII05, (b) THOR50, (c) THUMS50.

2.2.5 Indicator 7 - ASIS Y Moments

This submarining indicator was added based on the authors' engineering judgement. To investigate the moments acting on the ASIS on left and right side, Y moment data was extracted from load cells in the ASIS blocks. As described in the section about ASIS X forces, the load cells in the pelvis have a local coordinate system and the direction of the local coordinate system in the ASIS load cells can be seen in Figure 2.11. In relation to submarining, the Y moment was of interest. This is of interest since the sign of the Y moment value may indicate whether the lap-belt is positioned below or above the load cell throughout the simulation and a sudden drop in combination with the sign of the Y moment value may indicate if submarining has occurred or not. The position of the load cells where the Y moment data was extracted in the used occupant models, can be seen in Figure 2.8.

2.2.6 Indicator 8 - Lap-Belt Cross-Sectional Forces

As described in Section 1.2, Uriot, Baudrit, et al. (2006) monitored the belt tension and drop in belt tension throughout their tests. This project investigated the resultant cross-sectional forces of the lap-belt by extracting force data from the cross-sections on the lap-belt on both right (buckle side) and left side (anchor side). The locations at which these forces were extracted can be seen in Figure 2.8 for the used occupant models.

2.2.7 Indicator 9-10 - Lumbar Spine Forces and Moments

In their study, Luet, Trosseille, Drazétic, et al. (2012) measured the lumbar spine loads (X- and Z-axis) and moment (Y-axis) for the ATDs they used in their tests. To investigate the resultant lumbar spine forces and moments in this project, force and moment data was extracted from the load cells corresponding to lumbar spine location in the used occupant models. In the test device for human occupant restraint - an advanced 50^{th} percentile male dummy (THOR50-M), no lumbar spine load cell is defined, so the load cell located at the lowest point on the thoracic spine was used. Figure 2.7 presents the locations at which the forces and moments were extracted in the used occupant models.

2.2.8 Indicator 11 - Abdomen Region Forces - Force Transducer

This submarining indicator was added based on the authors' engineering judgement. To investigate the force acting on the abdomen and pelvis, a force transducer was defined. This was done by defining a set of elements on the abdomen and pelvis region of the used occupant models which may be loaded by the lap-belt only. The figures below show parts of these elements for the different occupant models:

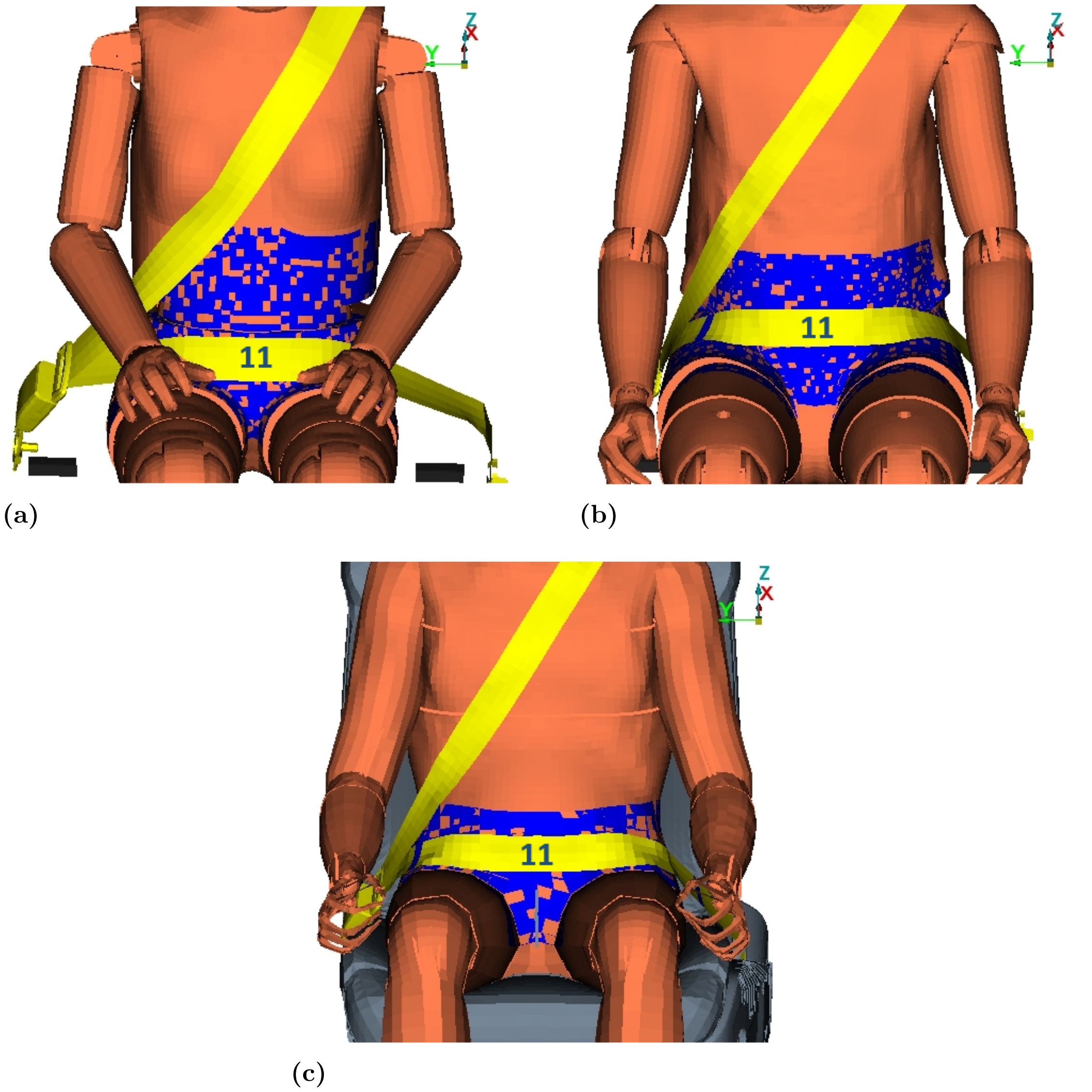

Figure 2.9: Front view: Figure showing parts of the elements chosen on the abdomen and pelvis region for the force transducers. (a) HIII05, (b) THOR50, (c) THUMS50.

2.2.9 Indicator 12 - Belt Mid-Point to Spine X Distance

Also this submarining indicator was added based on the authors' engineering judgement. To investigate the lap-belt position in relation to the spine, the belt mid-point to spine X distance was calculated. This indicator may indicate if the lap-belt is intruding into the abdomen or not and thus, if submarining has occurred or not. The same belt node as used to calculate the belt mid-point trajectory was used here. A node in the lumbar spine for HIII05 and THUMS50 and a node in the thoracic spine for THOR50 was chosen to calculate this indicator. The black lines at number 12 in Figure 2.7 show the total distance between these points for the used occupant models.

2.2.10 Indicator 13-14 - ASIS to Belt X Distance

As described in Section 1.2, Shaw et al. (2018) developed a parameter to quantify the position of the pelvis relative to the lap-belt. To investigate this position, the researchers determined the X-axis position of the right ASIS relative to the X-axis position of the lap-belt at the midline of the test subject. This project investigated the position of left and right ASIS blocks in relation to the lap-belt. For this, the minimum distance between either left or right ASIS block and the lap-belt was extracted and the X component of the minimum distance was further analysed. The minimum distance function in META was used for this calculation. To define an area on the lap-belt for which META picked the minimum distance, an element group was defined on the lap-belt. For the ASIS blocks, the same nodes on the ASIS as used in calculating the relative angles between lap-belt and pelvis were used, which were the outermost points on left and right ASIS blocks. The two lines indicated with number 13 and 14 in Figure 2.8 visualise the minimum total distance between ASIS and belt for the different used occupant models.

2.2.11 Indicator 15 - Pelvis Acceleration

Luet, Trosseille, Drazétic, et al. (2012) measured the resultant pelvis acceleration in their tests. To investigate the resultant acceleration of the pelvis in the used occupant models in this project, acceleration data was extracted from accelerometers inside or close to the pelvis. For HIII05 and THOR50, accelerometers inside the pelvis were used and for THUMS50, an accelerometer at anterior sacrum position was used. Figure 2.7 presents the locations at which the used accelerometers are located for the different occupant models.

2.2.12 Indicator 16-18 - Spinal T1, T4 and T12 Accelerations

Luet, Trosseille, Drazétic, et al. (2012) measured the T1 resultant acceleration in their tests. To measure the accelerations in the spine of the used occupant models in this project, accelerations were extracted from accelerometer data in the occupant models' spines. Accelerations were extracted from three locations in the thoracic spine at T1, T4 and T12 level. Figure 2.7 presents the locations at which the acceleration data was extracted in the used occupant models.

2.2.13 Indicator 19 - Belt Pay-In and Pay-Out

This submarining indicator was added based on the authors' engineering judgement. To investigate how much the seatbelt is pulled in and out during the crash simulations, the Z-displacement of the end node of the seatbelt was extracted for all simulations with all the used occupant models. Below images present the locations at which the displacement data was extracted in the seatbelts for the used occupant models:

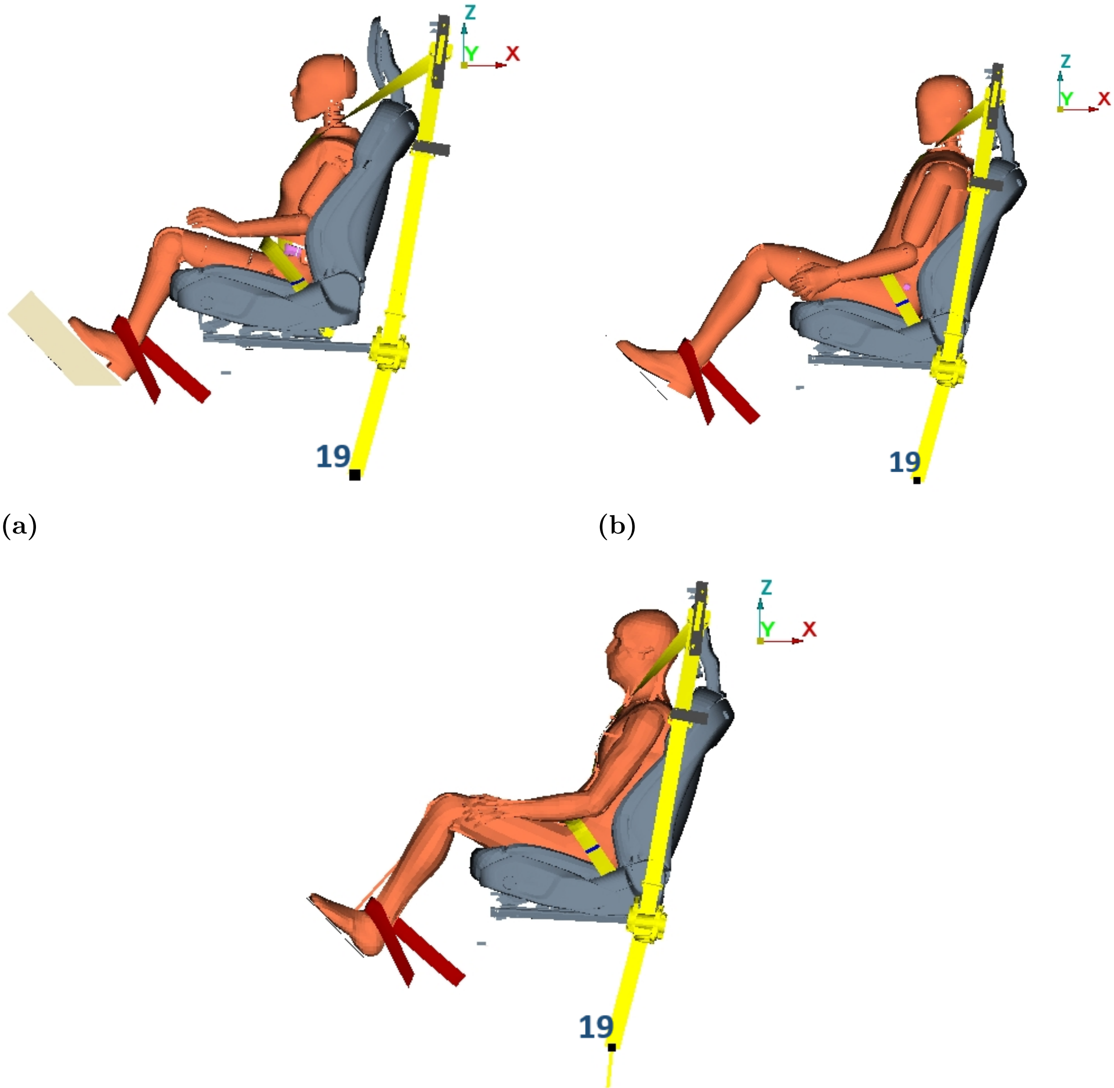

(a) (b) (c)

Figure 2.10: Side view: Position of the node on the belt used for investigation of belt pay-in and pay-out. (a) HIII05, (b) THOR50, (c) THUMS50.

2.2.14 Indicator 20 - Initial Belt Position in Relation to ASIS

This submarining indicator was added based on the authors' engineering judgement. To investigate the initial belt position in relation to ASIS, the distance between the belt and either the left or right ASIS block was calculated in both global X and Z direction. The same element group on the belt as used to calculate the ASIS to Belt X Distance was used in META to calculate this indicator.

2.2.15 Indicator 21 - ASIS Lever Arm

This submarining indicator was added based on the authors' engineering judgement. Normalising the ASIS Y moment with the ASIS X force measured in the ASIS load cells on both left and right side, gives the lever arm along the Z-axis in the local coordinate system defined in the ASIS load cells. The equation below describes the calculation of the lever arm:

$$LA_Z = \frac{M_Y}{F_X} \tag{2.2}$$

Where M_Y is the ASIS Y moment and F_X is the ASIS X force. The figure below shows a schematic description of the left iliac wing and ASIS together with the axis directions of the local coordinate system of the ASIS load cells existing in all the used occupant models.

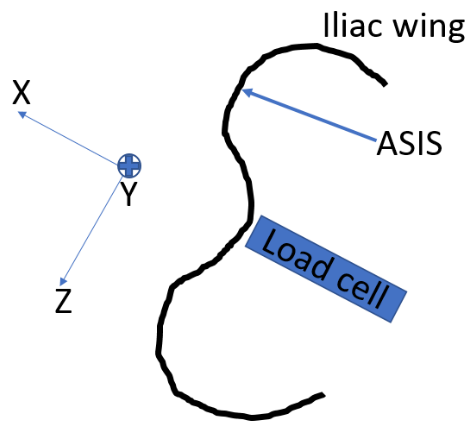

Figure 2.11: Schematic description of the left iliac wing with the ASIS load cell location and local coordinate directions.

2.2.16 Data Filtering

The data extracted using META were filtered using the filters specified in Table 2.2.

Table 2.2: Indicator filtering information. *NF = Not Filtered.

Indicators	**HIII05**	**THOR50**	**THUMS50**
Angles	CFC180	CFC180	CFC180
Trajectories	NF	NF	NF
ASIS Forces & Moments	CFC1000	CFC1000	CFC1000
Cross-Sectional Lap-Belt Forces	NF	NF	NF
Lumbar spine forces & moments	CFC600	CFC600	CFC600
Abdomen region forces - force transducer	NF	NF	NF
Submarining distances	NF	NF	NF
Pelvis accelerations	CFC1000	CFC1000	CFC1000
Spine T1, T4 & T12 accelerations	CFC180	CFC180	CFC180
Belt pay-in & pay-out	NF	NF	NF

2.3 Statistical Analysis

Logistic regression was used in this study to predict submarining occurrence (categorical variable - Yes/No) based on logistic regression models of independent predictors and combinations of independent predictors (submarining indicators). The choice of predictors/variables to be used in the statistical analysis was made from selection of submarining indicators in relation to their ability to show information relevant to submarining occurrence (see Chapter 3) and was aggregated in a biomechanical matrix (see Table A.3 and A.4). This analysis has been done to incorporate biomechanical knowledge in combination with data analysis. The following subsections describe the predictors used for this statistical study and a brief theory together with the methodology used to find the model which best describes the risk of submarining occurrence using logistic regression and the model performance evaluation.

2.3.1 Input Data - Predictor Data Aggregation

The input data to the logistic regression analysis is taken from the outcomes of the simulations from the design of experiment matrix, as described in Fig. 2.2. From the data presented in Section 3.1, 3.2 and 3.3, a number of submarining indicators were chosen to be evaluated in the statistical analysis of this study, based on the information they provided in relation to submarining occurrence (see discussion Section 4.1). To be able to use the data in the statistical analysis, relevant data had to be extracted from the submarining indicator data. A biomechanical matrix was constructed containing the individual parameters chosen for this analysis. The data was extracted for anchor and buckle side using MATLAB and was stored in the biomechanical matrix to be used for the logistic regression analysis in MATLAB. The data is considered as left censored and exact, since the time of submarining is known from the visual checks as mentioned in Table 3.2, 3.3 and 3.4. For all selected submarining indicators, the corresponding graphs were inspected to ensure that the MATLAB code picked the correct value to be inserted into the biomechanical matrix. Anchor and buckle side data were stored separately in the matrix since both sides can submarine independently of each other and since they have different kinematics. The words variable and predictor are used synonymously throughout the analysis. The following paragraphs describe the predictor data that was extracted.

ASIS Lever Arm

When the ASIS slips under the lap-belt, no or little amount of force and moment will be exerted on the iliac wing. Thus, the lever arm acting on the ASIS can only be defined as long as the force is higher than a certain threshold. The authors of this report defined a threshold force of 100 N. For all the performed simulations, the lever arm data was extracted and plotted using the threshold requirement specified above. For submarining cases, the lever arm was extracted just before or at submarining time. For non-submarining cases, an average value was calculated between the time of the first case submarining minus 10 ms and the time of the last case submarining plus 10 ms which were part of that particular pulse and occupant model group of simulations. The data inserted into Equation 2.2 was filtered with CFC180 to reduce the noise. For all simulations, a visual check of the graphs was made to ensure that the correct value was picked for the data aggregation. The aggregated data can be found in the biomechanical matrix in Table A.3 and A.4 in the Appendix.

ASIS to Belt X-Distance

The minimum ASIS to belt X-distance was extracted from the simulations for both buckle and anchor side respectively, and aggregated in the biomechanical matrix (see Table A.3 and A.4 in the Appendix) for all the performed simulations. For all simulations, a visual check of the graphs was made to ensure that the correct value was picked for the data aggregation.

ASIS X Forces

As described in Section 1.2, the force drop in the iliac is included in the full width impact assessment of Euro NCAP to assess submarining occurrence. Similarly, for the X forces on the ASIS extracted from the simulations in this project, the maximum force drop observed over a 1 ms time period was extracted from the data. The data was extracted for both the anchor and buckle side respectively and stored in the biomechanical matrix (see Table A.3 and A.4 in the Appendix).

Relative Angle between Lap-Belt and Pelvis (2D)

For the relative 2D angle between lap-belt and pelvis, the minimum angle observed throughout the crash event was extracted from the data of each performed simulation. The data was extracted for both the anchor and buckle side respectively and stored in the biomechanical matrix (see Table A.3 and A.4 in the Appendix).

2.3.2 Logistic Regression

In the logistic regression model, the log of odds of the submarining (dependent variable) is modelled as a linear combination of the independent predictors (here submarining indicators). In this project, submarining is the dependent variable in the data-set, with categories of failure and success (Yes/No) and the independent predictors are the submarining indicators. Logistic regression models the logit-transformed probability as a linear relationship with the predictor variables (see Equation 2.3). Let y be the binary outcome variable which indicates failure or success taking a value of either 0 or 1 and p be the probability of y to be equal to 1, $p = prob(y = 1)$. Let $x_1, ..., x_k$ be a number of predictors, then the logistic regression of y on the predictor variables $x_1, ..., x_k$ estimates parameter values of the model for $\beta_0, \beta_1, ..., \beta_k$. Logistic regression models are fit using the maximum likelihood method.

$$logit(p) \;=\; log\left(\frac{p}{1-p}\right) \;=\; \beta_0 + \beta_1 \cdot x_1 + ... + \beta_k \cdot x_k \tag{2.3}$$

Transforming the above equation into terms of probability, the following equation is obtained:

$$p \;=\; \frac{e^{\beta_0 + \beta_1 \cdot x_1 + ... + \beta_k \cdot x_k}}{1 + e^{\beta_0 + \beta_1 \cdot x_1 + ... + \beta_k \cdot x_k}} \tag{2.4}$$

Since the left hand side and middle part of Equation 2.3 represents the log odds of the investigated outcome, the interpretations of the coefficients for the model, $\beta_0, \beta_1, ..., \beta_k$, can be made in terms of log odds. If we perform logistic regression with a single continuous predictor variable, x_1, the estimated intercept value, β_0, represents the log odds for the outcome if the value of the continuous predictor would be held at zero. The coefficient for the predictor variable, β_1, represents the expected change in log odds of the outcome when the value of x_1 is increased by one unit. If we perform logistic regression with multiple continuous predictor variables, $x_1, ..., x_k$, and no interaction terms, each estimated coefficient represents the change in log odds of the outcome for a one unit increase in the corresponding predictor variable while holding the other predictor variables constant at a certain value.

If the probability of success for some event is p, then the probability of failure is $1 - p$. The odds of success are then defined as the ratio of the probability of success over the probability of failure. For the estimated parameters in logistic regression, each exponentiated coefficient represents the ratio of two odds (the change in odds in the multiplicative scale for a one unit increase in the value of the corresponding predictor variable holding the other predictor variables at a certain value).
For this study, a number of independent predictor variables were evaluated to find models which best predict the outcome of submarining occurrence. Model estimation was done using single continuous predictor variables as well as using multiple continuous predictor variables without interaction terms. The following list presents the logistic regression models of independent predictors or combination of independent predictors evaluated in this study. More predictors are not selected to avoid the problem of over-fitting of data.

1. Lever arm.
2. Min. ASIS to belt X distance.
3. Max. Force drop.
4. Min. relative angle between lap-belt and pelvis.
5. Lever arm + Min. ASIS to belt X distance.
6. Lever arm + Max. Force drop.
7. Lever arm + Min. relative angle between lap-belt and pelvis.
8. Min. ASIS to belt X distance + Max. Force drop.
9. Min. ASIS to belt X distance + Min. relative angle between lap-belt and pelvis.
10. Max. Force drop + Min. relative angle between lap-belt and pelvis.
11. Lever arm + Min. ASIS to belt X distance + Max. Force drop.
12. Lever arm + Min. ASIS to belt X distance + Min. relative angle between lap-belt and pelvis.
13. Lever arm + Max. Force drop + Min. relative angle between lap-belt and pelvis.
14. Min. ASIS to belt X distance + Max. Force drop + Min. relative angle between lap-belt and pelvis.
15. Lever arm + Min. ASIS to belt X distance + Max. Force drop + Min. relative angle between lap-belt and pelvis.

2.3.3 Model Performance Evaluation

The following sections describe the steps performed in this study to assess the performance of the constructed logistic regression models.

2.3.3.1 Akaike's Information Criterion Value

Akaike's Information Criterion (AIC) provides a relative measure of model quality compared to other logistic regression models obtained by simulating the situation where the model is tested on a different data set. After computing several different models, they can be compared using this criterion. According to Akaike's theory, the most accurate model has the smallest AIC.
The methodology used in this study, involved calculating the AIC values for all the logistic regression models of predictor and predictor combinations and identifying the models with the least AIC values. The logistic regression model with the least AIC value was identified as the most optimal model. The AIC values for all the models are tabulated in Table 3.5. AIC only tells about the relative performance of the model but does not give any information about the quality of the model which has the least AIC value.

2.3.3.2 Area Under Receiver Operator Curve (AU-ROC)

The ROC curve shows the trade-off between the true positive rate (TPR/sensitivity) and false positive rate (FPR/specificity), which shows the decrease in sensitivity results in an increase in specificity. Sensitivity measures the actual positives that are correctly identified. Specificity measures the proportion of actual negatives that are correctly identified.

$$\text{Sensitivity} = \frac{\text{number of true positives}}{\text{number of true positives} + \text{number of false negatives}} \tag{2.5}$$

$$\text{Specificity} = \frac{\text{number of true negatives}}{\text{number of true negatives} + \text{number of false positives}} \tag{2.6}$$

In general, positive = identified and negative = rejected. So it can be said:

1. True positive = correctly identified
2. False positive = incorrectly identified
3. True negative = correctly rejected
4. False negative = incorrectly rejected

The optimum logistic regression model was identified by the AIC value and qualitative performance of the model was chosen based on the area under the Receiver Operator Curve (ROC) value. This was done to make sure the chosen variable was most likely to produce the best statistical model, i.e. the variable best able to distinguish between the injury outcomes. The methodology involved finding the area under ROC curve for identified logistic regression models of predictors and combination of predictors. It represents the measure of predictive ability of the model in terms of specificity and sensitivity. The model producing an AU-ROC greater than 0.7 is in general considered to be a good model.

The higher the AU-ROC, the higher measure of separability the predictor in the logistic regression model has, i.e. the predictor is better at predicting 0s as 0s and 1s as 1s. The AU-ROC of a perfect predictive model equals 1. If AU-ROC is 0, it implies that the predictor is perfectly incorrect, i.e. it predicts all 0s as 1s and all 1s as 0s. A predictor which makes random guesses has an AU-ROC score of 0.5. For example, if AU-ROC is 0.7, it means that there is 70% chance that the model will be able to distinguish between 0s and 1s.

2.3.3.3 Determination of Confidence Intervals

This study determined the 95% Confidence Intervals (CI) for the obtained probability curve for submarining, which is normal approximation for the distribution of the estimated risk.

2.3.3.4 MATLAB Functions

Model fit was performed in MATLAB using the glmfit and fitglm functions. The MATLAB glmval function was used to calculate the predicted values for the models and estimate the 95% confidence bounds for the predicted values.

3

Results

The results presented for the occupant models are grouped by the pulses used, first the FFRB pulse and then two oblique pulses. For the latter, all criteria were not considered to be relevant due to the angled movement of the occupant model and hence some indicators are omitted from the results presentation.
The uniform colour scheme for all occupant models and pulses are used according to Table 3.1 in the results.

Table 3.1: Graph colours for occupant models for all pulses.

HIII05	
Colour	Seat config.
	Upright
	Intermediate
	Reclined

THOR50	
Colour	Seat config.
	Upright
	Intermediate
	Reclined

THUMS50	
Colour	Seat config.
	Upright
	Intermediate
	Reclined

3.1 FE Simulations: Fully Frontal Rigid Barrier Pulse (FFRB)

The left (anchor side) ASIS/iliac block sliding under the lap-belt is considered as left submarining while the right (buckle side) ASIS/iliac block sliding under the lap-belt is considered as right submarining. The submarining and submarining time information as observed visually in simulation for HIII05, THOR50 and THUMS50 occupant models are tabulated in Table 3.2 corresponding to upright, intermediate reclined and reclined configurations of seat backrest. The green colour in Table 3.2 shows the simulations which did not submarine while the red colour shows the simulations which submarined.

Table 3.2: FFRB: submarining time information for HIII05, THOR50, THUMS50.

	FFRB (Fully Frontal)	
HIII05	Left Submarining	Right Submarining
Upright		
Intermediate	50 ms	46 ms
Reclined	43 ms	40 ms

THOR50	Left Submarining	Right Submarining
Upright		
Intermediate		50 ms
Reclined	58 ms	56 ms

THUMS50	Left Submarining	Right Submarining
Upright		
Intermediate	85 ms	60 ms
Reclined	62 ms	48 ms

Legend	
	Non Submarining
	Submarining

3.1.1 Indicator 1-3 - Relative Angle between Lap-Belt and Pelvis: 3D Left Side, 2D Left Side and 2D Right Side

The change in relative angle between lap-belt and pelvis: 3D left side, 2D left side and 2D right side, is shown in Fig. 3.1, 3.2, 3.3 for the span of the crash event for the HIII05, THOR50 and THUMS50 sitting in upright, intermediate reclined and reclined positions for the FFRB pulse.
For the left side, It can be seen for HIII05 (Fig. 3.1 a, 3.2 a) and THUMS50 (Fig. 3.1 c, 3.2 c) that there is an initial transient drop in the the curves and this is due to the pre-tensioner firing. For THOR50 (Fig. 3.1 b, 3.2 b), the initial drop is not seen as there is not any part/flesh in front of ASIS block and lap-belt directly loads the ASIS throughout while for HIII05 and THUMS50, there are some soft parts/flesh in front of ASIS block and loading on ASIS comes from soft part/flesh, which gets loaded from lap-belt first. In HIII05 (Fig. 3.1 a, 3.2 a) and THOR50 (Fig. 3.1 b, 3.2 b), the minimum angle decreases as the backrest is further reclined and the local minima in the graphs gives information about submarining and submarining time of the left side which is inline with Table 3.2.
For the right side, HIII05 and THOR50 (Fig. 3.3 a, 3.3 b), the minimum angle on right side decreases as seat backrest is reclined while for THUMS50 (Fig. 3.3 c), graphs are inconclusive. For HIII05 (Fig. 3.3 a), the local minima in the graph gives information about the right submarining time in the simulations which is inline with Table 3.2. The results in right side are different from the results in left side and which may be because of different of direction of belt force vector in right side compared to left side.

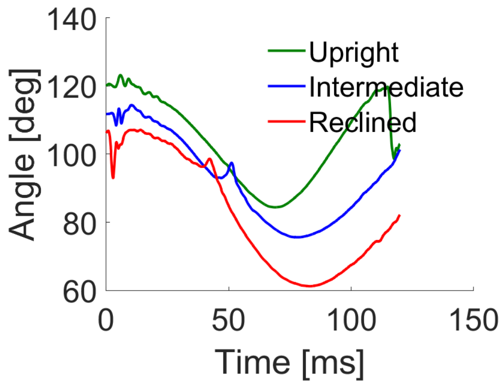

(a)

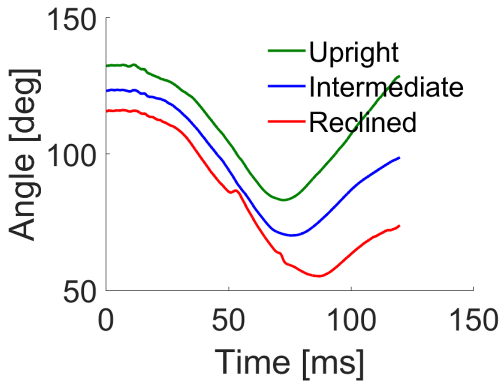

(b)

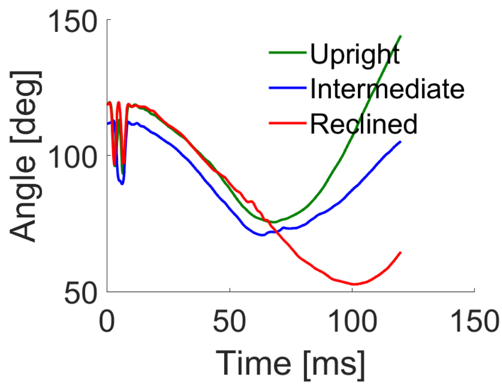

(c)

Figure 3.1: Relative 3D left angle between lap-belt and pelvis in the FFRB pulse. (a) HIII05, (b) THOR50, (c) THUMS50

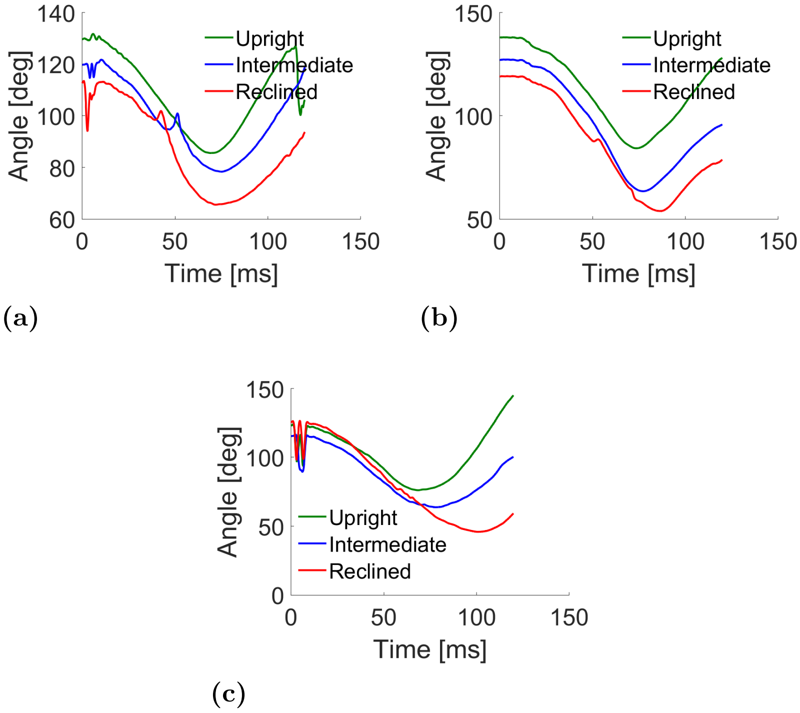

Figure 3.2: Relative 2D left angle between lap-belt and pelvis in the FFRB pulse. (a) HIII05, (b) THOR50, (c) THUMS50

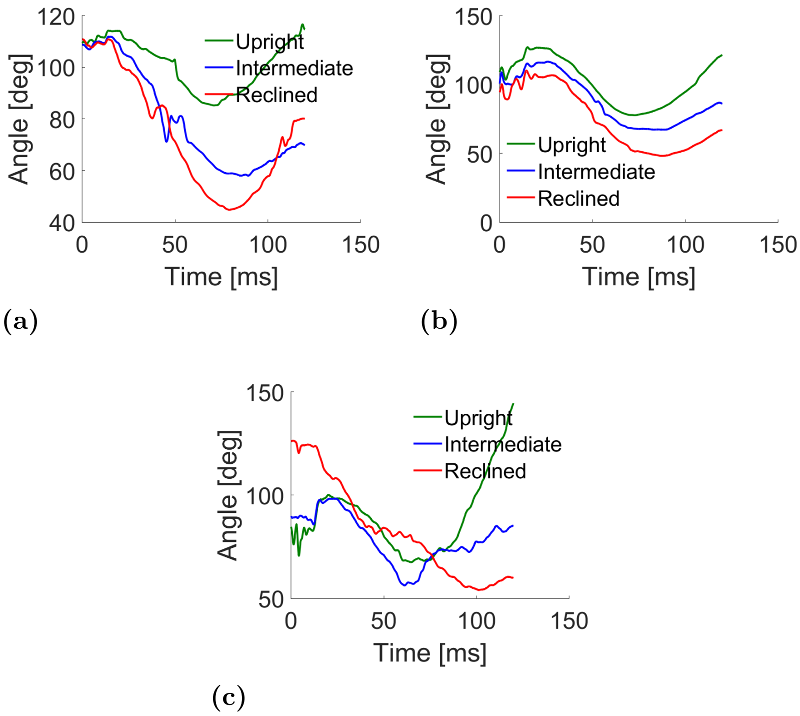

Figure 3.3: Relative 2D right angle between lap-belt and pelvis in the FFRB pulse. (a) HIII05, (b) THOR50, (c) THUMS50

3.1.2 Indicator 4 - Lap-Belt Mid-Point XZ Trajectory

The XZ trajectory of the mid-point of the lap-belt is shown in Fig. 3.4 for the span of the crash event for the HIII05, THOR50 and THUMS50 sitting in upright, intermediate reclined and reclined positions for the FFRB pulse. It can be seen for the HIII05 and THOR50 (Fig. 3.4 a, 3.4 b), cases undergoing submarining show exaggerated forward excursion (X coordinate). The submarining cases show reduced excursion in Z compared to non-submarining cases. In THUMS50 (Fig: 3.4 c), no trend is observed and the graph remains inconclusive.

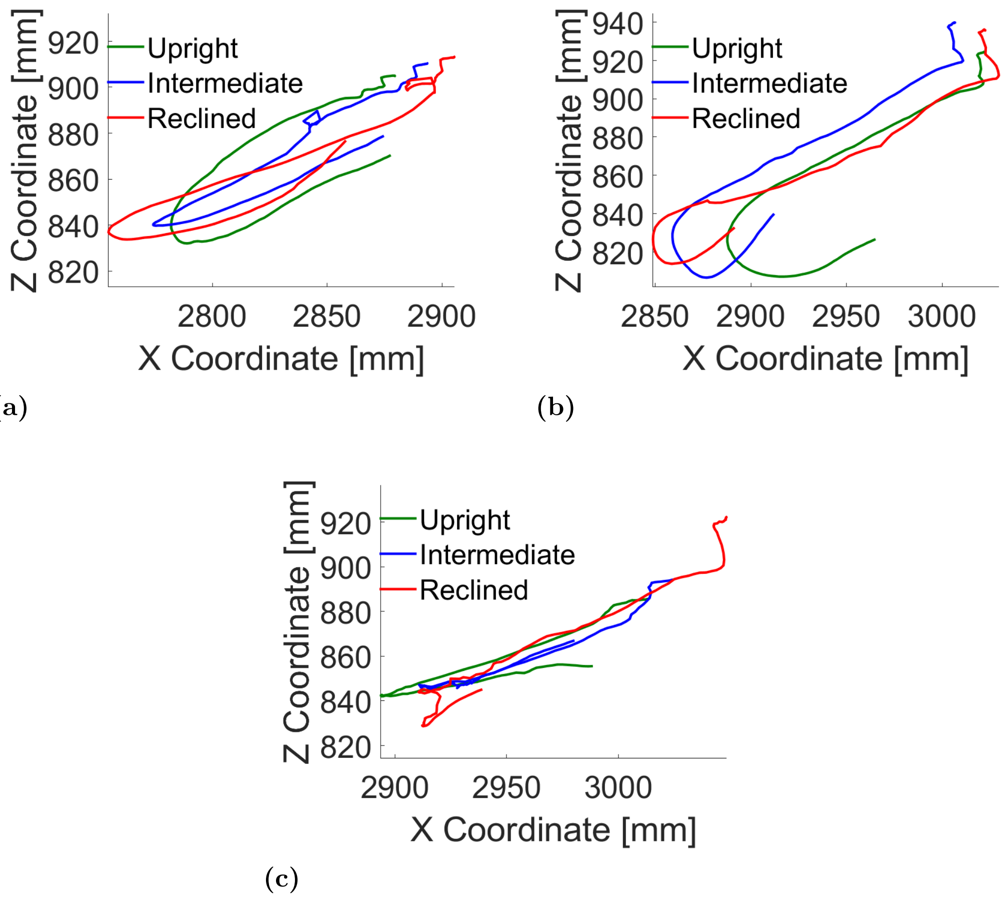

Figure 3.4: Lap-belt mid-point trajectory in the FFRB pulse. (a) HIII05, (b) THOR50, (c) THUMS50

3.1.3 Indicator 5 - H-Point XZ Trajectory

The XZ trajectory of the H-point is shown in Fig. 3.5 for the span of the crash event for the HIII05, THOR50 and THUMS50 sitting in upright, intermediate reclined and reclined positions for the FFRB pulse. It can be seen for all occupant models, that the cases undergoing submarining have exaggerated forward excursion (smaller X coordinate). It can be seen in THUMS50 (Fig. 3.5 c), that the pelvis moves up in submarining cases and in HIII05 and THOR50 (Fig: 3.5 a, 3.5 b), the pelvis moves down in Z in all cases.

For HIII05 and THOR50, X coordinate in H-point XZ trajectory can be explained with the lumbar spine to belt X distance i.e. When the lumbar spine to belt X distance is more in upright position (Fig. 3.15 a and 3.15 b), the ATD's pelvis is restrained well and H-point does not do much excursion in X (Fig. 3.5 a and 3.5 b). Additionally in reclined case for H-point XZ trajectory as seen in Fig. 3.15 a and 3.15 b, the lumbar spine to belt X distance decreases as the pelvis slides under the belt and belt moves into the abdomen, thus, the pelvis is not restrained well and the H-point does excursion in X (Fig. 3.5 a and 3.5 b). For THUMS50, in reclined case Fig. 3.15 c, the belt moves in more in abdomen, so H-point has maximum excursion and pelvis is very poorly restrained by lap-belt.

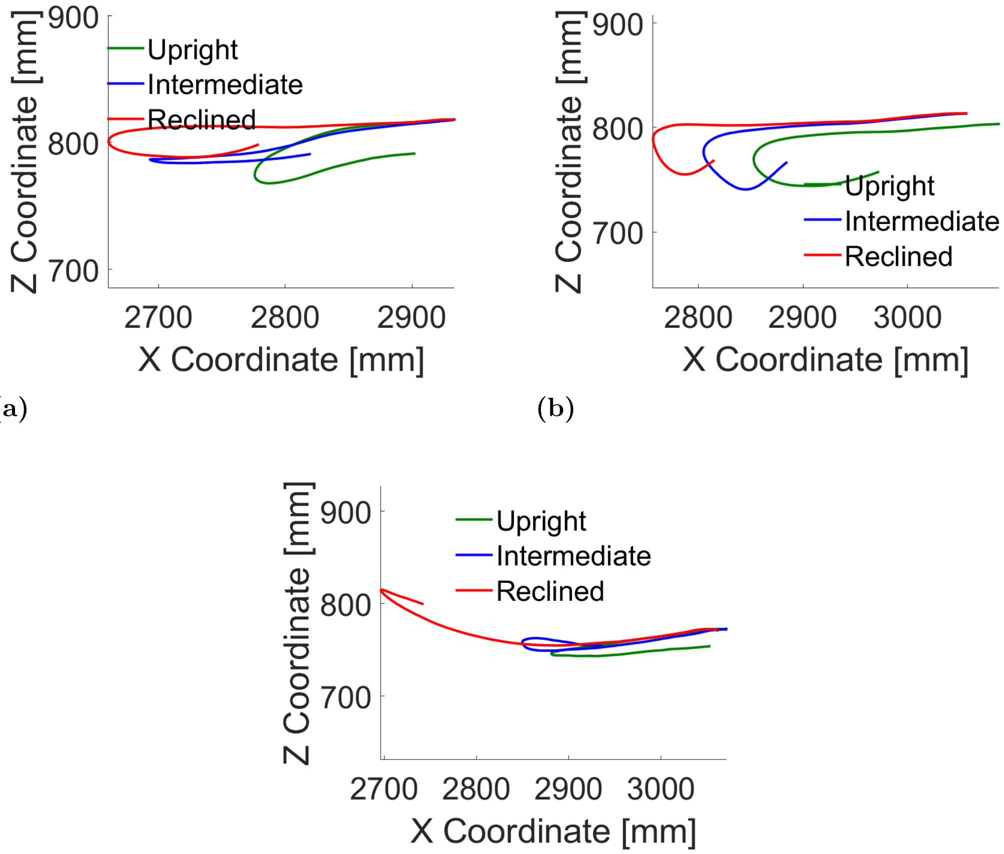

(a) **(b)** **(c)**

Figure 3.5: H-Point XZ trajectory in the FFRB pulse. (a) HIII05, (b) THOR50, (c) THUMS50

3.1.4 Indicator 6 - Iliac/ASIS X Forces Left & Right

The Iliac/ASIS X forces are shown in Fig. 3.6 for the span of the crash event for the HIII05, THOR50 and THUMS50 sitting in upright, intermediate reclined and reclined positions for the FFRB pulse. It can be seen for HIII05 and THOR50 (Fig. 3.6 a, 3.6 b), that the cases undergoing submarining have considerably lower iliac peak forces than non-submarining cases. Additionally, submarining cases for

THUMS50 (Fig. 3.6 c) also show that the peak forces are lower compared to non-submarining cases. It can also be seen for all occupant models, for cases undergoing submarining, that the force buildup and drop happens in smaller time interval, which may be considered as a submarining flag.

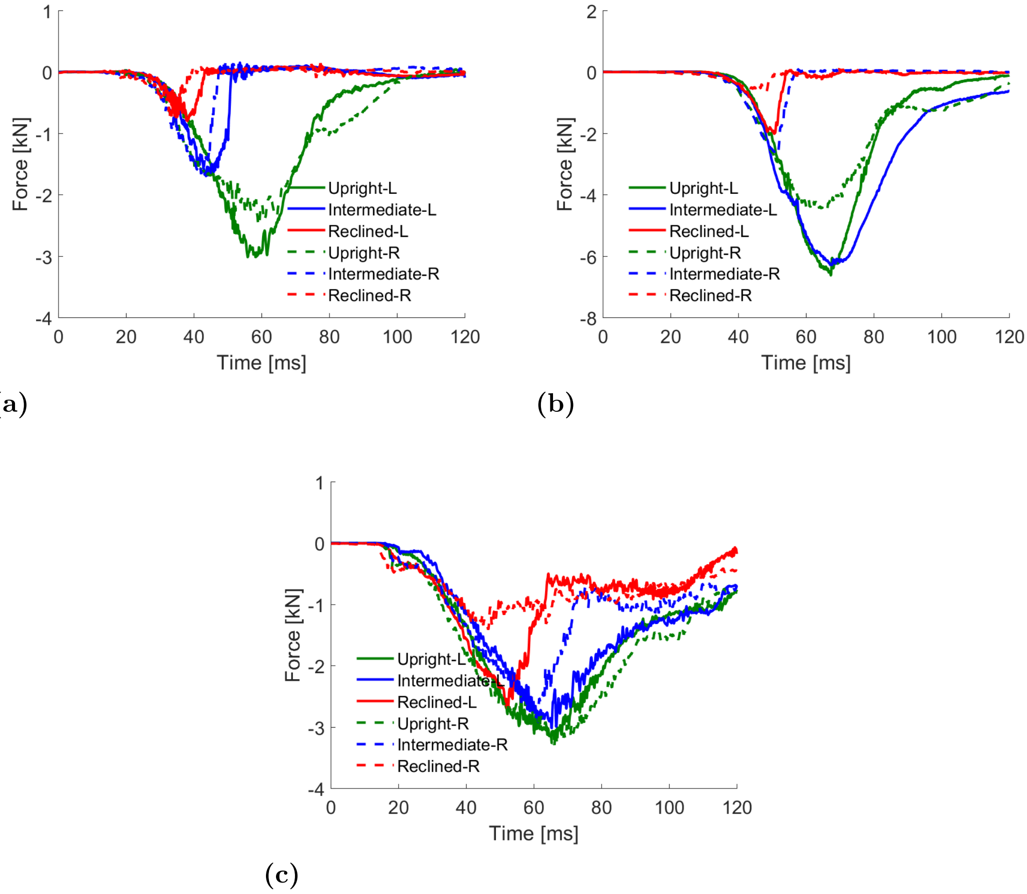

Figure 3.6: Iliac/ASIS X forces left & right in the FFRB pulse. (a) HIII05, (b) THOR50 (c) THUMS50

3.1.5 Indicator 8 - Lap-Belt Cross-Sectional Resultant Forces

The cross-sectional forces of the lap-belt are shown in Fig. 3.7 for the span of the crash event for the HIII05, THOR50 and THUMS50 sitting in upright, intermediate reclined and reclined positions for the FFRB pulse. For HIII05 (Fig.3.7 a) and THOR50 (Fig.3.7 b), it can be seen in the submarining cases, that the force buildup and drop happens in smaller time interval. It can also be seen that local minima/fluctuation in the curves give information about the submarining time, which is in line with the timings presented in Table 3.2. This can be a possible flag for submarining detection. For THUMS50 (Fig.3.7 c), it can be seen, as seat backrest angle increases, lap-belt forces decrease but there is not any information to identify submarining.

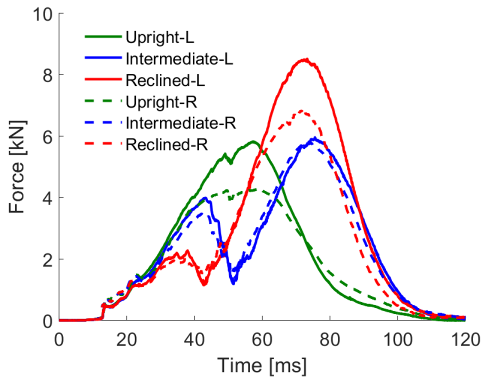

(a)

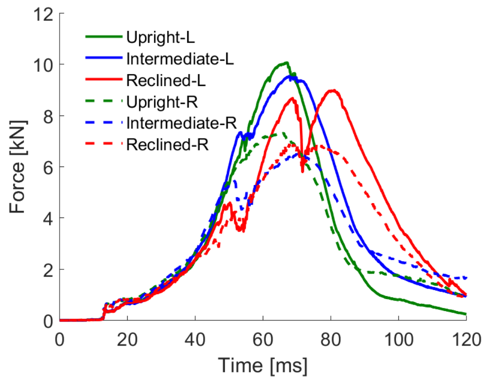

(b)

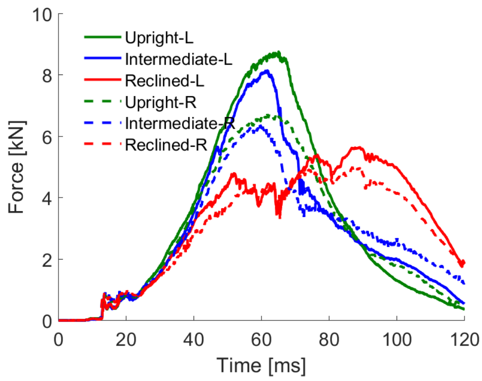

(c)

Figure 3.7: Lap-belt cross-section resultant forces in the FFRB pulse. (a) HIII05, (b) THOR50 (c) THUMS50

3.1.6 Indicator 7 - Iliac Y Moments

The iliac Y moments are shown in Fig. 3.8, 3.9, 3.10 for the span of the crash event for the HIII05, THOR50 and THUMS50 sitting in upright, intermediate reclined and reclined positions for the FFRB pulse. It can be seen for all occupant models that submarined, that the moment is positive before submarining, which represents the belt loading the iliac wing on the negative side of the local coordinate system (see Fig. 2.11) in the ASIS/iliac load cells. It can be seen for the HIII05 (Fig. 3.8), the submarining cases show sudden drop in moment and remain negative afterwards throughout the span of simulation time. The cause of negative moment in the occupant model was investigated but exact reason could not be known. For THOR50 (3.9), a similar drop in moment for submarining cases can be observed and because of the exposed ASIS blocks of the THOR50 occupant model, the moment remains close to zero once the belt has slid off the ASIS. For the non-submarining cases in THUMS50 (Fig. 3.10), negative moments can be observed in parts of the crash event, which are due to that the belt is engaging with the iliac wing on the positive side of the local coordinate system of the ASIS/iliac load cell (see Figure 2.11). Furthermore, for the same occupant model, it can be seen that the moment remains positive after submarining, which may be due to the flesh being pulled by the lap-belt which in turn transfers some load to the ASIS/iliac load cells and gives a positive moment.

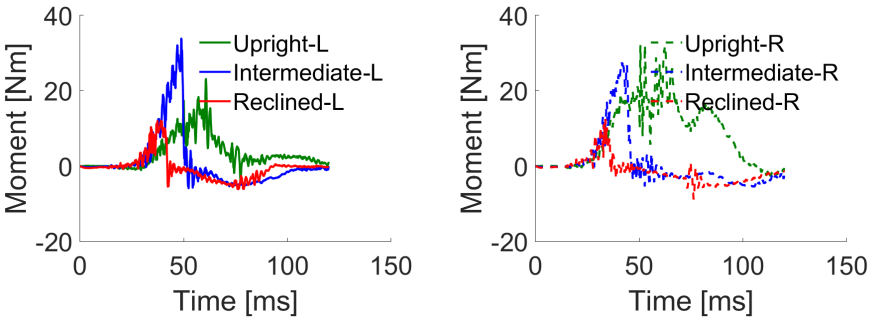

(a) **(b)**

Figure 3.8: Iliac Y moment in the FFRB pulse for HIII05. (a) left side, (b) right side

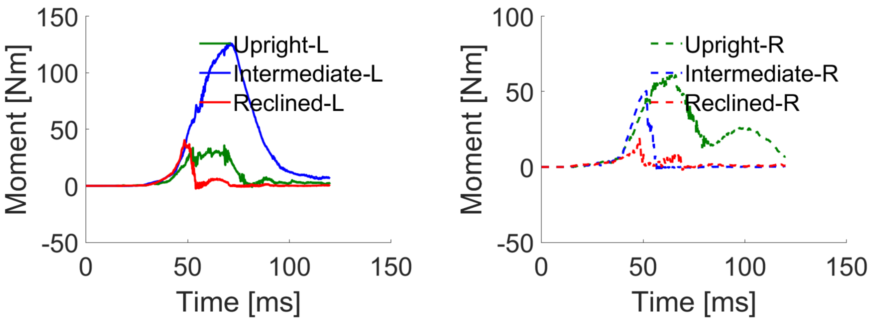

(a) **(b)**

Figure 3.9: Iliac Y moment in the FFRB pulse for THOR50. (a) left side, (b) right side

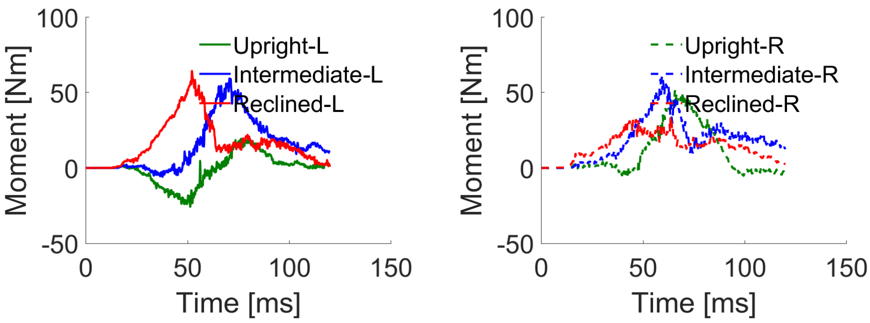

(a) **(b)**

Figure 3.10: Iliac Y moment in the FFRB pulse for THUMS50. (a) left side, (b) right side

3.1.7 Indicator 9-10 - Lumbar Spine Forces & Moments

The lumbar spine forces and moments are shown in Fig. 3.11, 3.12, 3.13 for the span of the crash event for the HIII05, THOR50 and THUMS50 sitting in upright, intermediate reclined and reclined positions for the FFRB pulse. It can be seen for HIII05 (Fig. 3.11 (a)), cases undergoing submarining show considerable higher lumbar spine forces. It can also be seen in (Fig. 3.11 (b)), local minima/fluctuations in curves shows occurrence of submarining and gives information about the submarining time. Therefore, for HIII05, the high lumbar spine forces and minima/fluctuations in moment curve show occurrence of submarining and may be considered as a submarining flag. It can be seen for THOR50 (Fig: 3.12 (a)), that the forces remain inconclusive while, the moments are considerably higher for the submarining cases (Fig. 3.12 (b)) compared to non-submarining cases. So higher moment can be a possible submarining flag. For THUMS50 (Fig: 3.13), both force and moment graphs are inconclusive.

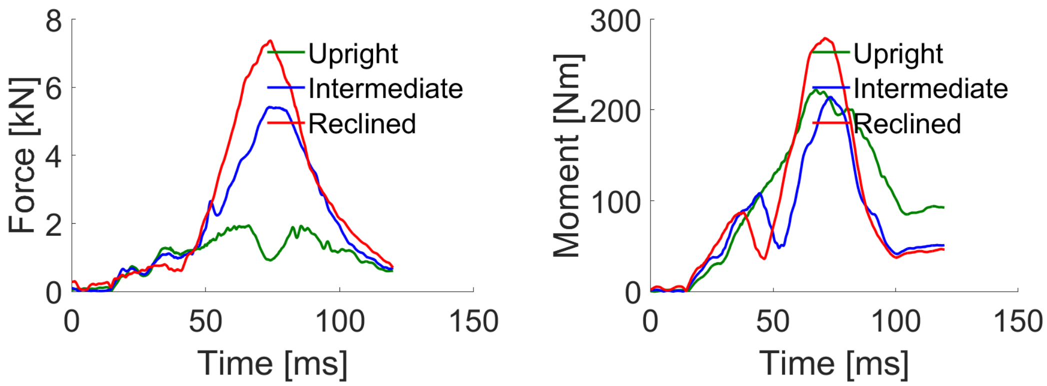

(a) **(b)**

Figure 3.11: For HIII05 in the FFRB pulse. (a) Lumbar spine forces and (b) Lumbar spine moments

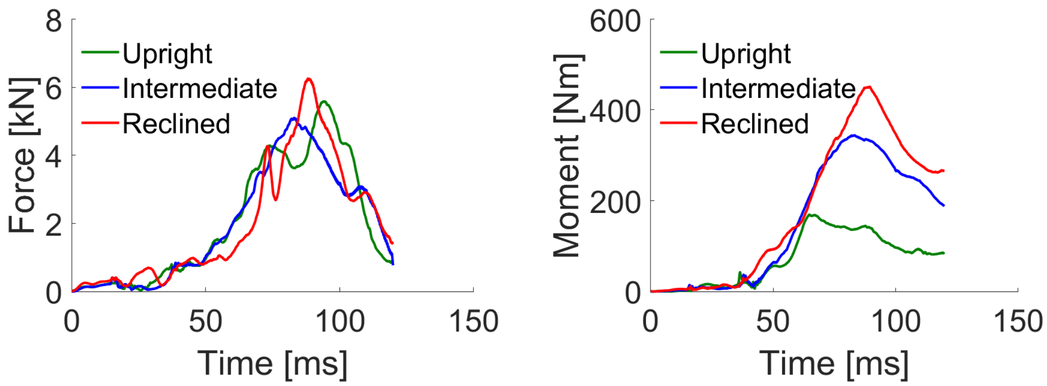

(a) **(b)**

Figure 3.12: For THOR50 in the FFRB pulse. (a) Lumbar spine forces and (b) Lumbar spine moments

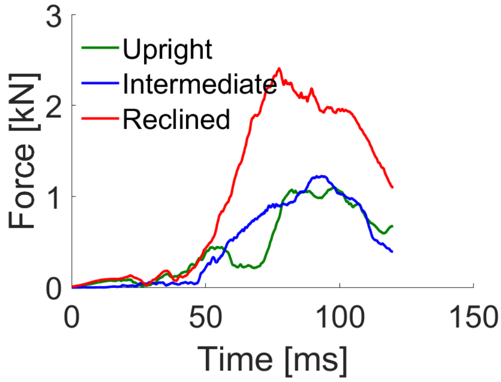

(a)

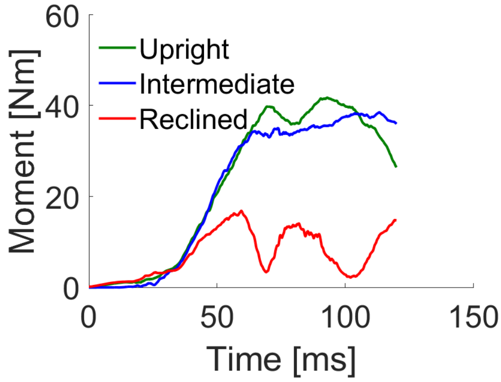

(b)

Figure 3.13: For THUMS50 in the FFRB pulse. (a) Lumbar spine forces and (b) Lumbar spine moments

3.1.8 Indicator 11 - Abdomen Region Forces

The abdomen region forces are shown in Fig. 3.14 for the span of the crash event for the HIII05, THOR50 and THUMS50 sitting in upright, intermediate reclined and reclined positions for the FFRB pulse. It can be observed for HIII05 (Fig. 3.14 a), that the peak forces are delayed for the cases undergoing submarining. It can also be seen that the first minima shows submarining and gives the information about the submarining time which may be considered as a submarining flag. For THOR50 (Fig. 3.14 b), the forces are higher for the submarining cases. The submarining time information can not be seen here. For THUMS50 (Fig. 3.14 c), the peak forces are lower for the submarining cases, which is not very distinctive.

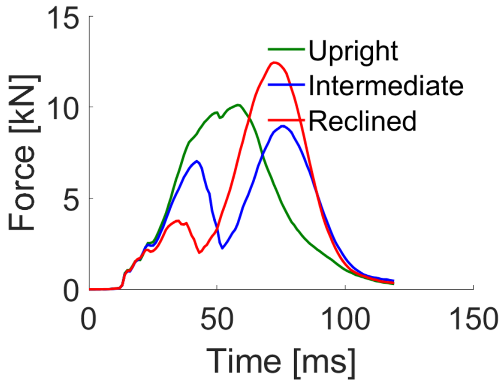

(a)

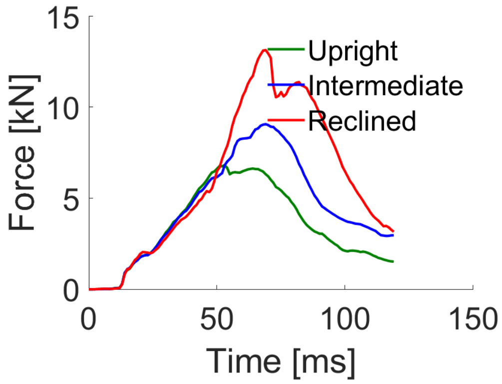

(b)

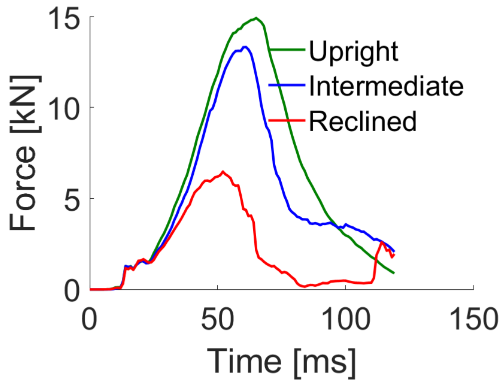

(c)

Figure 3.14: Abdomen region forces in the FFRB pulse. (a) HIII05, (b) THOR50, (c) THUMS50.

3.1.9 Indicator 12 - Belt Mid-Point to Spine X Distance

The belt mid-point to spine X distance is shown in Fig. 3.15 for the span of the crash event for the HIII05, THOR50 and THUMS50 sitting in upright, intermediate reclined and reclined positions for the FFRB pulse. For HIII05 and THOR50 (Fig. 3.15 a & 3.15 b), the cases undergoing submarning show that the distances are smaller than the non-submarining cases. This can be because of the more belt-intrusion into the abdomen in submarining cases. Smaller belt mid-point to spine X distance may be considered as a submarining flag. For THUMS50 (Fig: 3.15 c), the graph remains inconclusive.

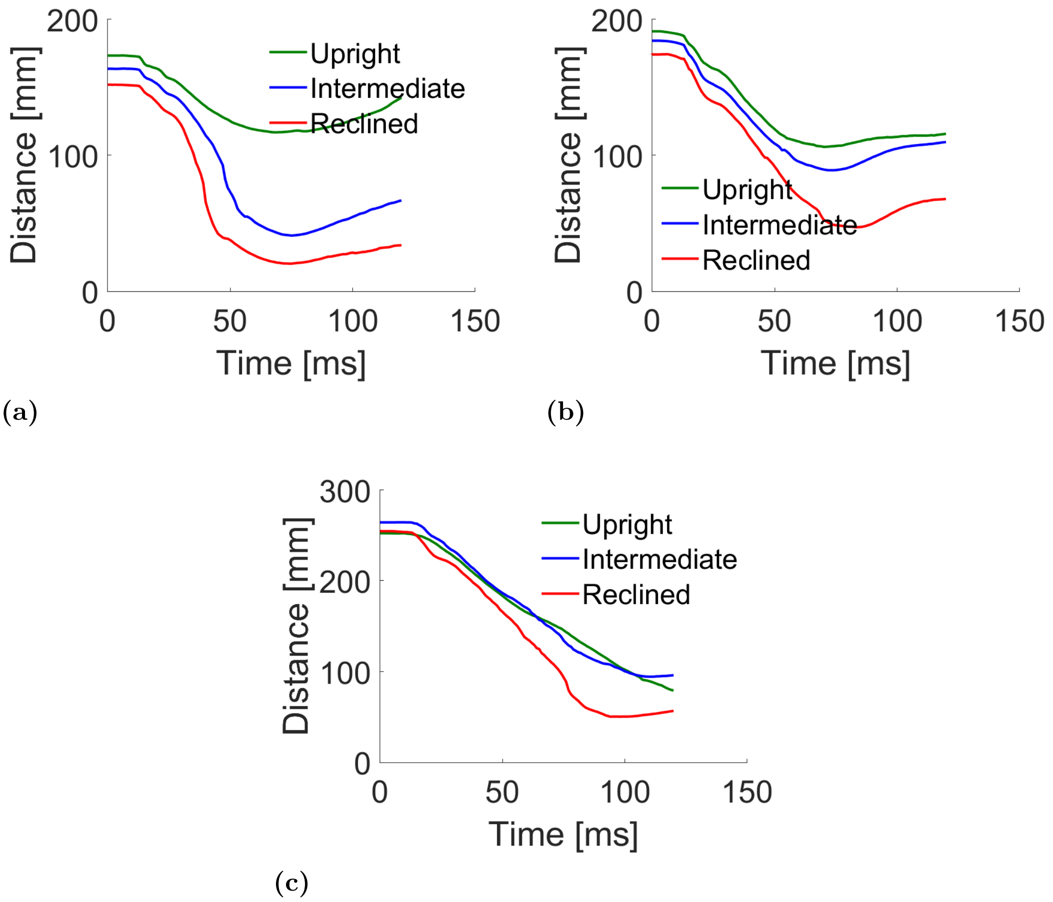

Figure 3.15: Belt mid to Spine X distance in the FFRB pulse. (a) HIII05, (b) THOR50, (c) THUMS50

3.1.10 Indicator 13-14 - ASIS/Iliac (Left/Right) to Belt X Distance

The ASIS/iliac (Left/Right) to belt X distance is shown in Fig. 3.16 for the span of the crash event for the HIII05, THOR50 and THUMS50 sitting in upright, intermediate reclined and reclined positions for the FFRB pulse. It can be seen that the change in the sign of the distance shows submarining and submarining time for left and right submarining respectively. This represents that pelvis(ASIS/iliac) has slid under the belt at that particular instant of time. The cases where distance does not become negative and is close to the zero shows the lap-belt is still loading the ASIS/iliac block and ASIS/iliac block has not slid under the lap-belt. The change in sign of distance may be considered as a submarining flag.
The position of the belt with respect to ASIS block is shown for one of the cases

in Fig.3.17, which also shows that the belt to ASIS X distance becomes negative as soon ASIS block has sled under the lap-belt .

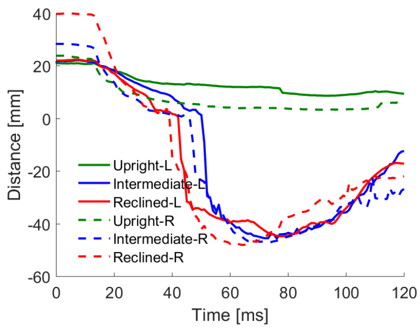

(a)

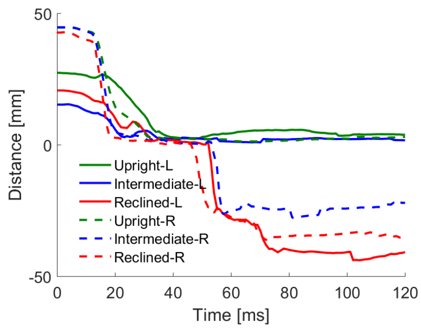

(b)

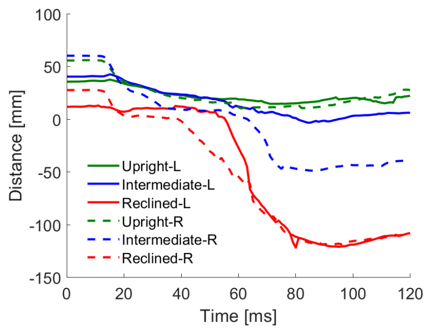

(c)

Figure 3.16: ASIS/Iliac (Left/Right) to Belt X Distance in the FFRB pulse. (a) HIII05, (b) THOR50, (c) THUMS50

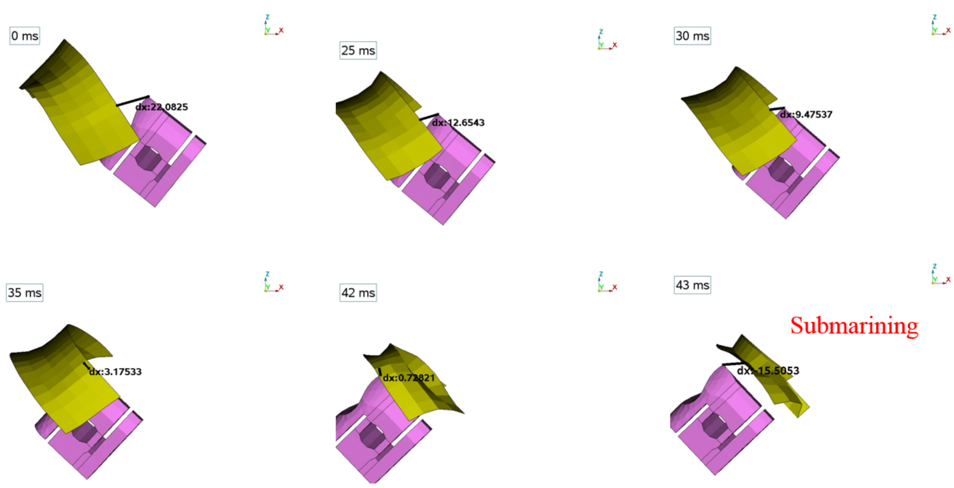

Figure 3.17: The ASIS (left) to belt X distance at different time in simulation, for HIII, Reclined, Left side. Fig. 3.16 a

3.1.11 Indicator 15-18 - Spine T1, T4, T12 & Pelvis Accelerations

The T1, T4, T12 and pelvis resultant accelerations are shown in Fig. 3.18, 3.19, 3.20 and 3.21 for the span of the crash event for the HIII05, THOR50 and THUMS50 sitting in upright, intermediate reclined and reclined positions for the FFRB pulse. It can be seen, the graphs are inconclusive for all occupant models (Fig. 3.18, 3.19, 3.20 and 3.21). It can also be seen that for THUMS50, the values of the T1,T4,T12 and pelvis accelerations acceleration are very high and non-physical (Fig. 3.18 c,3.19 c,3.20 c, 3.21 c), and seems there is something wrong with the measurement.

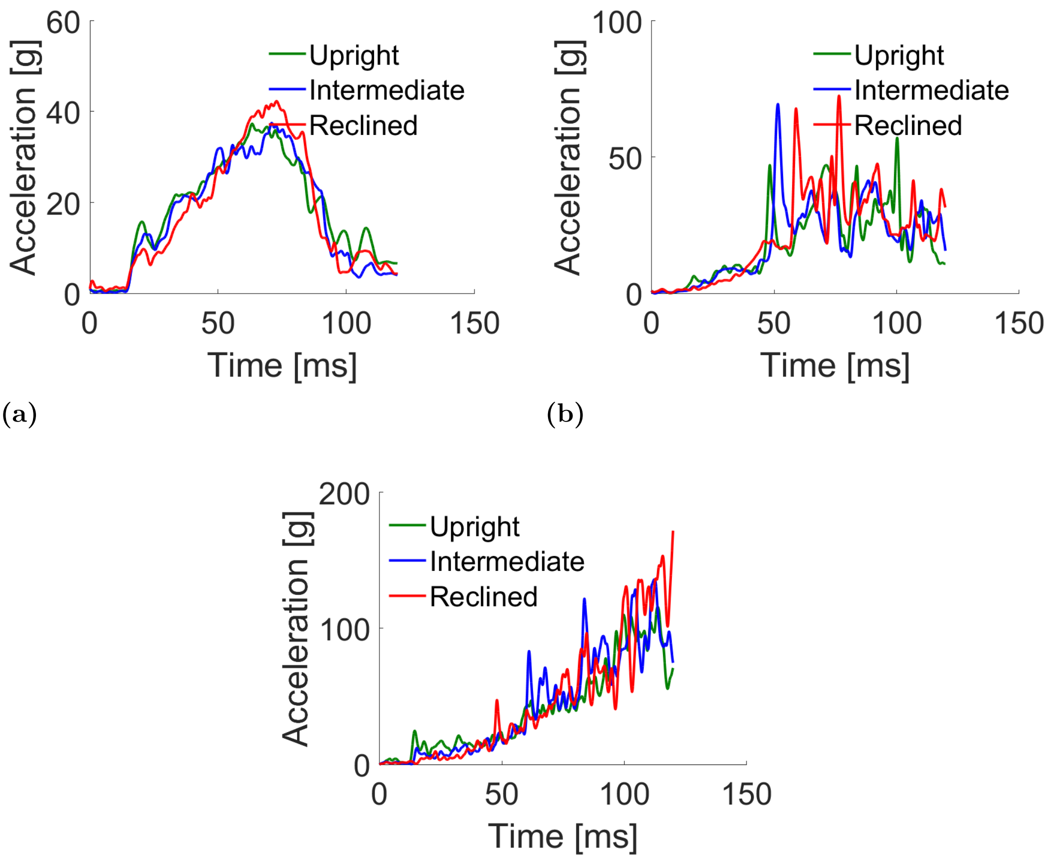

(a) (b) (c)

Figure 3.18: Spine T1 accelerations in the FFRB pulse. (a) HIII05, (b) THOR50, (c) THUMS50

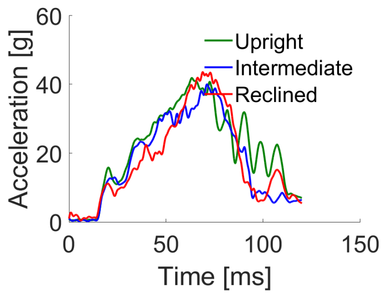

(a)

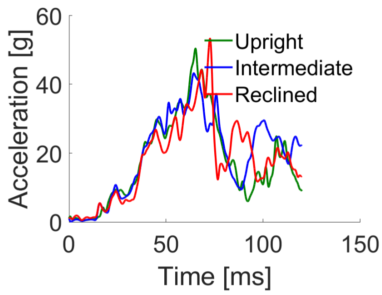

(b)

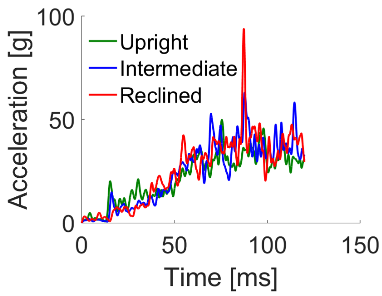

(c)

Figure 3.19: Spine T4 accelerations in the FFRB pulse. (a) HIII05, (b) THOR50, (c) THUMS50

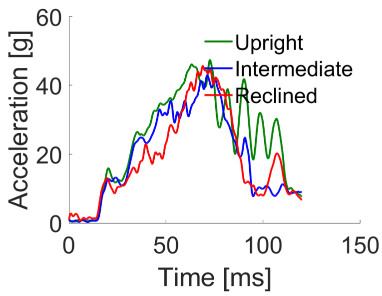

(a)

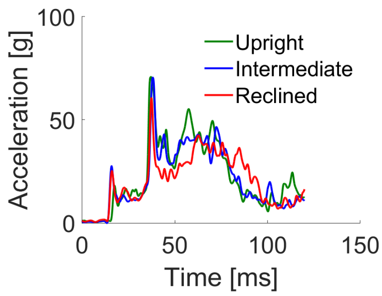

(b)

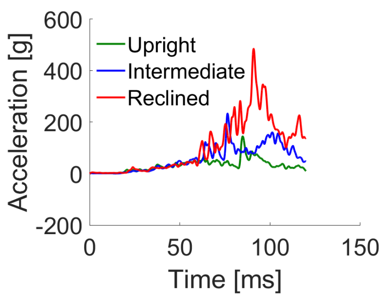

(c)

Figure 3.20: Spine T12 accelerations in the FFRB pulse. (a) HIII05, (b) THOR50, (c) THUMS50

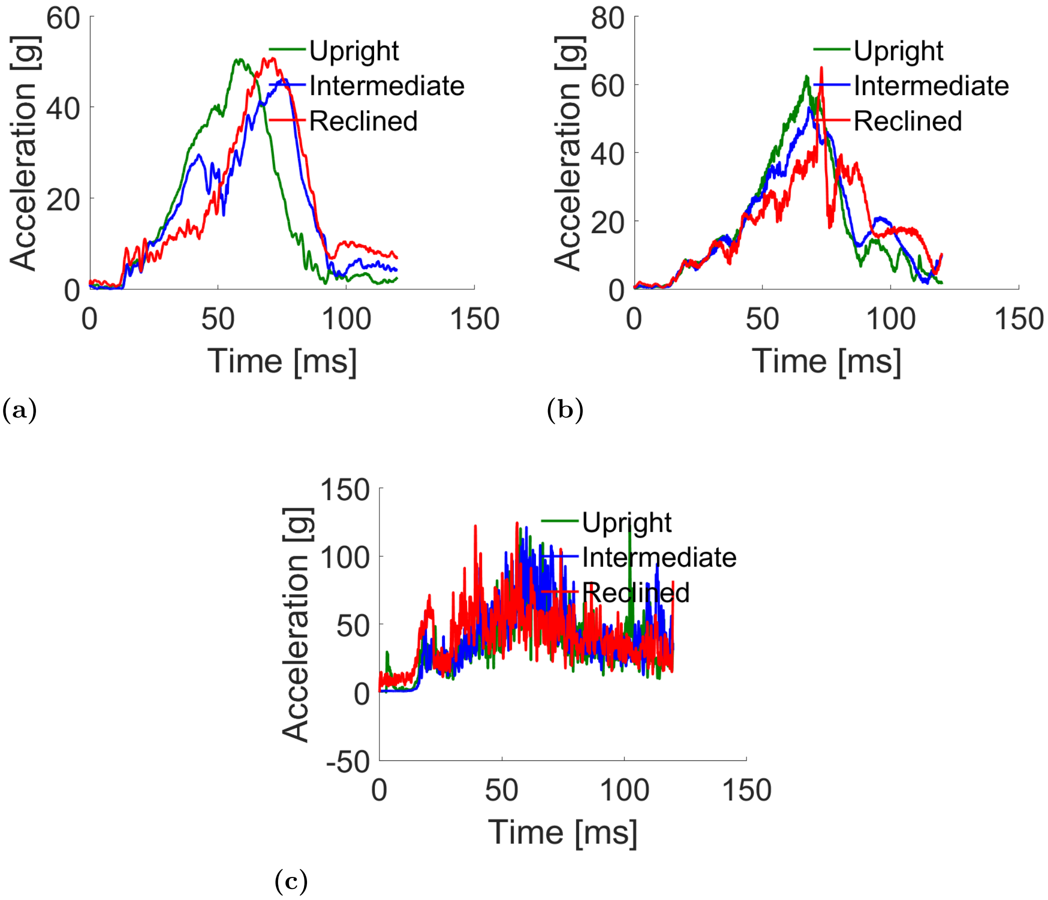

Figure 3.21: Pelvis resultant acceleration in the FFRB pulse. (a) HIII05, (b) THOR50, (c) THUMS50

3.1.12 Indicator 19 - Belt Pay-In and Pay-Out Distance

The belt pay-in and pay-out distance is shown in Fig. 3.22 for the span of the crash event for the HIII05, THOR50 and THUMS50 sitting in upright, intermediate reclined and reclined positions for the FFRB pulse. For all occupant models (Fig. 3.22), the belt pay-in pay-out is less for the submarining cases compared to non-submarining cases. This can possibly be, because in submarining cases, the H-point moves more forward and occupant model slips under the belt, so there is a less belt pay-out.

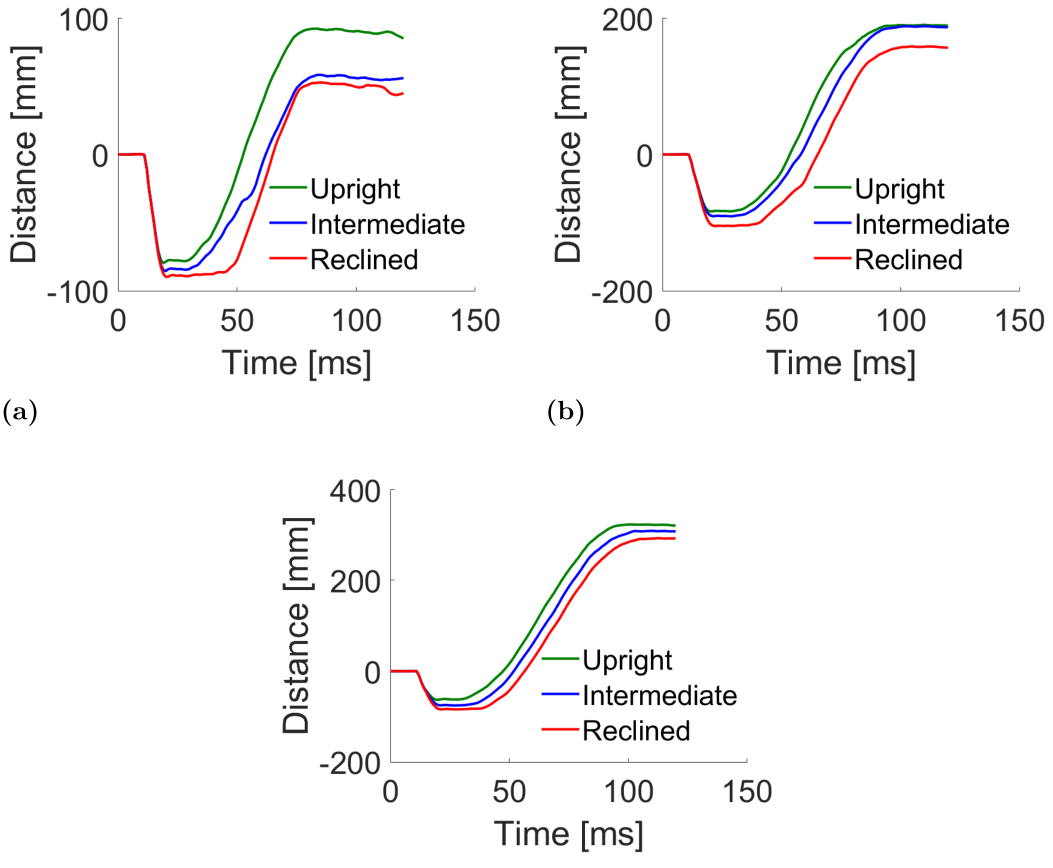

(a) (b) (c)

Figure 3.22: Belt pay-in pay-out distance in the FFRB pulse. (a) HIII05, (b) THOR50, (c) THUMS50

3.1.13 Indicator 20 - Initial Lap-Belt Position in Relation to ASIS Block

The initial lap-belt position in relation to the ASIS blocks for HIII05, THOR50 and THUMS50 is shown in Fig. 3.23, 3.24, 3.25 for both left (anchor side) and right (buckle side) side. It can be seen for HIII05 in Fig. 3.23, as the seat back-angle increases, the routed lap-belt shifts upwards in +Z direction. It can also be said that the upper the belt is routed in Z with respect to ASIS block, the more the

ASIS is likely to slip under the lap-belt and the more likely the occupant model is to submarine on the respective side. In all occupant models (Fig. 3.23, 3.24 and 3.25), the left side lap-belt is routed slightly below in Z with respect to the ASIS comparative to the right side lap-belt position with respect to the ASIS block. Additionally, it can also be seen that the lap-belt is comparatively closer to the ASIS in X direction for the left side compared to the right side for all occupant models.

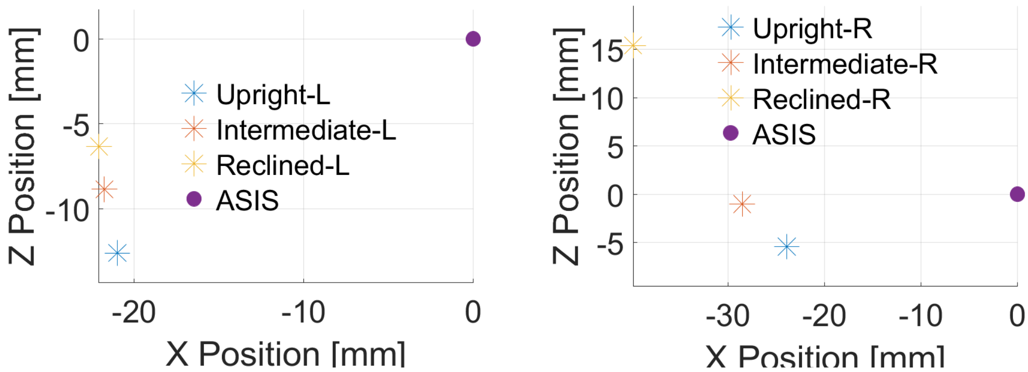

(a) (b)

Figure 3.23: For HIII05: Initial lap-belt position in relation to the ASIS blocks (a) Left (anchor side) and (b) right (buckle side)

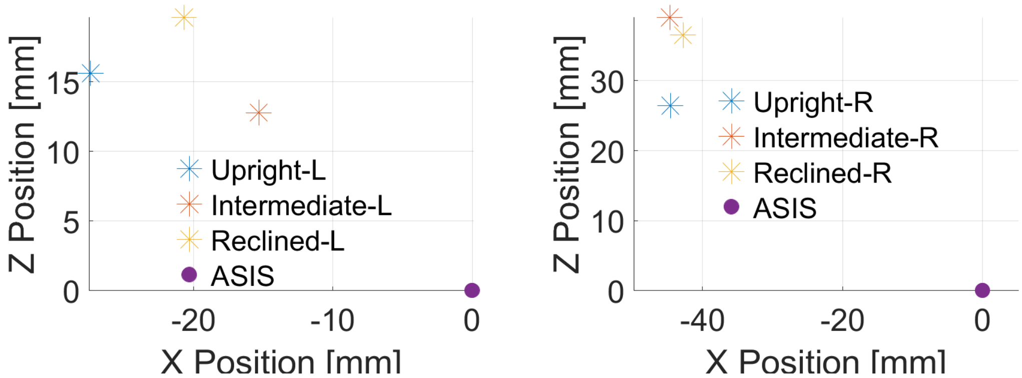

(a) (b)

Figure 3.24: For THOR50: Initial lap-belt position in relation to the ASIS blocks (a) Left (anchor side) and (b) right (buckle side)

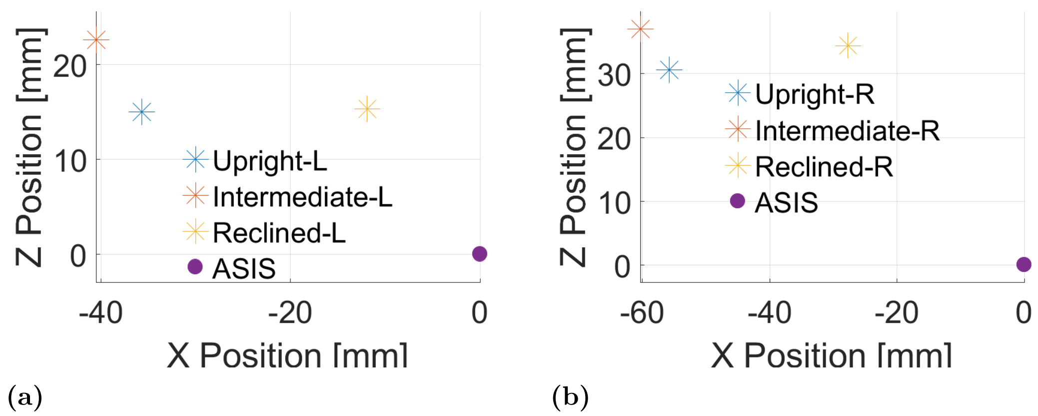

Figure 3.25: For THUMS50: Initial lap-belt position in relation to the ASIS blocks (a) Left (anchor side) and (b) right (buckle side)

3.1.14 Indicator 21 - Lever Arm

The lever arm on the left and right iliac wing is shown in Fig. 3.26, 3.27 and 3.28 for the span of the crash event for the HIII05, THOR50 and THUMS50 sitting in upright, intermediate reclined and reclined positions for the FFRB pulse. For HIII05 and THOR50, it can be seen in submarining cases that just after submarining time there is considerably amount of noise in the lever arm data with high fluctuations. This may be due to when the ASIS slips under the lap-belt, the force on the ASIS is reduced and thus the denominator in Equation 2.2 becomes small which in turn gives large values of the lever arm. It can also be seen for HIII05, THOR50 and THUMS50, that the lever arm has a negative value just before submarining, which indicates that the belt is located on the negative side of the Z-axis in the local coordinate system of the ASIS load cells as defined in Section 2.2. This is related to the sign of the Y-moment on the ASIS, which has a positive sign when the belt is located on the negative side of the Z-axis. It can also be seen for all occupant models, that in non-submarining cases of HIII05 and THOR50, the lever arm has significantly less noise. In THOR50 and THUMS50 initial drops in the lever arm can be seen at about 20-25 *ms* into the event, this is not part of submarining but may be due to the pre-tensioner firing.

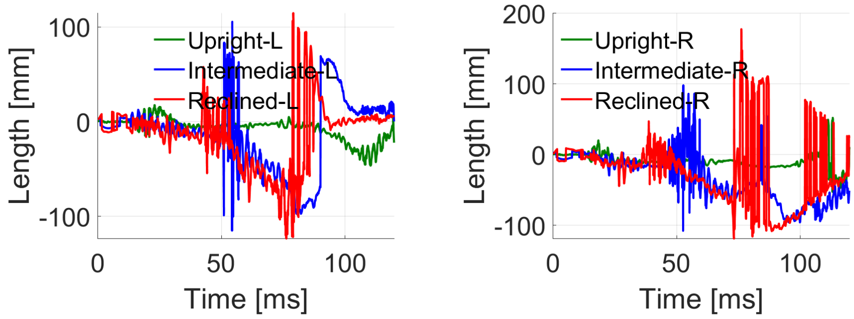

(a) **(b)**

Figure 3.26: HIII05: Iliac lever arm in the FFRB pulse. (a) Anchor side (b) Buckle side.

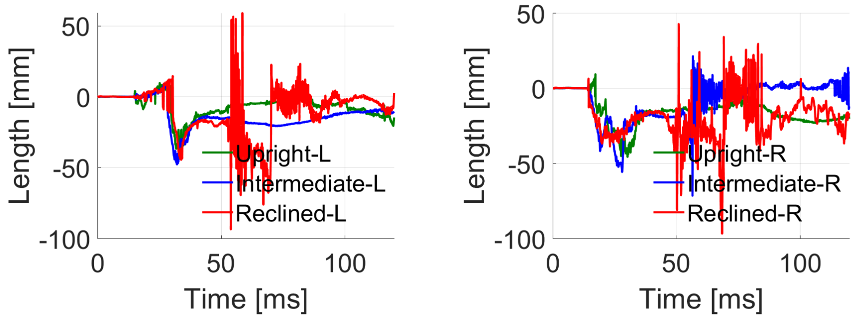

(a) **(b)**

Figure 3.27: THOR50: Iliac lever arm in the FFRB pulse. (a) Anchor side (b) Buckle side.

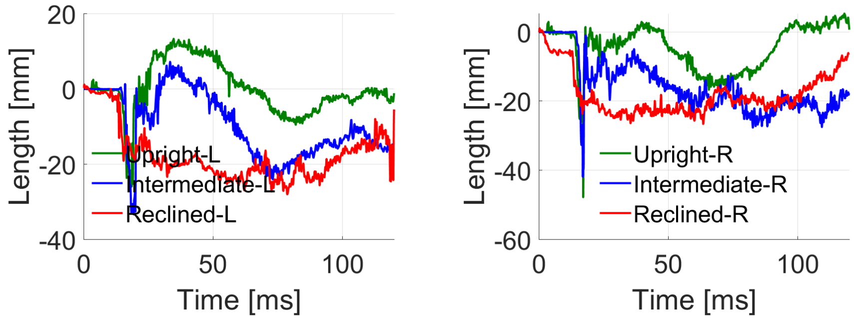

(a) **(b)**

Figure 3.28: THUMS50: Iliac lever arm in the FFRB pulse. (a) Anchor side (b) Buckle side.

3.2 FE Simulations: Oblique Left Pulse (Positive Yaw Rotation)

The second pulse used in this study is the oblique left pulse. The kinematics of this pulse makes the car occupant move towards the a-pillar in the car. The submarining and submarining time information as observed visually in simulation for HIII05, THOR50 and THUMS50 occupant models are tabulated in Table 3.3, corresponding to upright, intermediate reclined and reclined configurations of seat backrest. For the FFRB pulse all results are presented in the corresponding results section, while for this oblique left pulse, relative 2D angle between lap-belt and pelvis right, H-point trajectory, iliac/ASIS X forces, lumbar spine forces and moment, belt mid-point to spine X distance and ASIS/iliac (left/light) to belt X distance results are presented in the results section and remaining are omitted as they are not relevant due to angled movement of the occupant model.

Table 3.3: Oblique left pulse: submarining time information for HIII05, THOR50, THUMS50.

	Oblique left pulse (Positive Yaw)	
HIII05	Left Submarining	Right Submarining
Upright		
Intermediate		65 ms
Reclined		51 ms

THOR50	Left Submarining	Right Submarining
Upright		
Intermediate		72 ms
Reclined		52 ms

THUMS50	Left Submarining	Right Submarining
Upright		
Intermediate		68 ms
Reclined	75 ms	52 ms

Legend	
(green)	Non Submarining
(red)	Submarining

3.2.1 Indicator 3 - Relative Angle Between Lap-Belt and Pelvis (2D): Right

The change in relative 2D angle between lap-belt and pelvis, right side is shown in Fig. 3.29 for the span of the crash event for the HIII05, THOR50 and THUMS50 sitting in upright, intermediate reclined and reclined positions for the oblique left pulse . In HIII05 (Fig. 3.29 a), transients can be observed at the time when the two cases on right side are submarining. This gives information about the submarining time. The minimum angle trend as observed in the FFRB pulse is not as distinctive anymore as in Section 3.1.1. In THOR50 (Fig. 3.29 b), it can be seen that the initial angle decreases as the seat-backrest angle increases. The graphs do not give any nformation about the submarining time. In THUMS50 (Fig: 3.29 c), no trend is observed and the graph remains inconclusive.

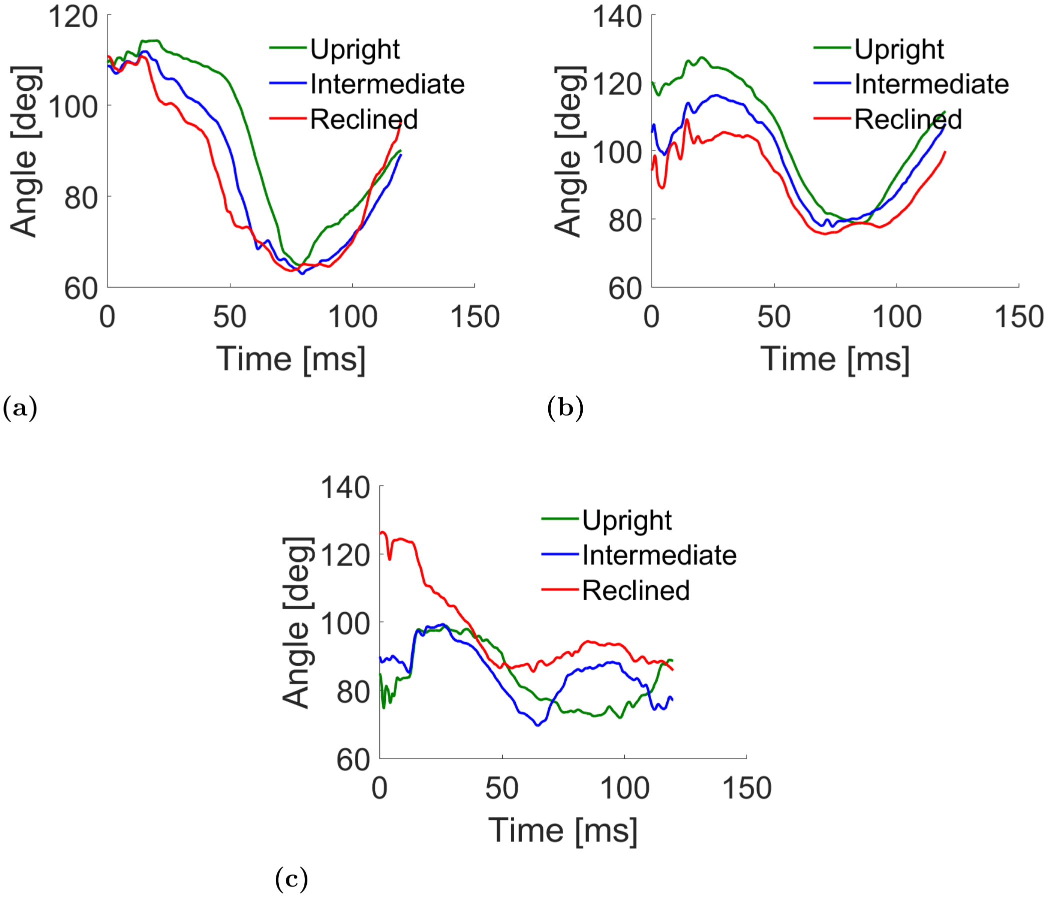

Figure 3.29: Relative 2D right angle between lap-belt and pelvis in the oblique left pulse . (a) HIII05, (b) THOR50, (c) THUMS50

3.2.2 Indicator 5 - H-Point XZ Trajectory

The H-point trajectory is shown in Fig. 3.30 for the span of the crash event for the HIII05, THOR50 and THUMS50 sitting in upright, intermediate reclined and reclined positions for the oblique left pulse . It can be seen from the the Figure 3.30 that all occupant models undergoing submarining have an exaggerated forward excursion (smaller X coordinate) and have a reduced vertical movement (larger Z coordinate). It can be seen in THUMS50 (Fig. 3.30 c), that the pelvis moves up in submarining cases and in HIII05 and THOR50 (Fig: 3.30 a, 3.30 b), the pelvis moves down in Z in all cases.

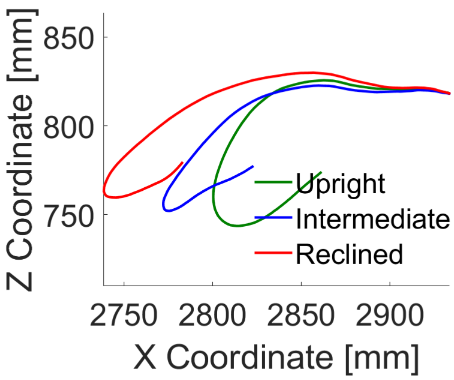

(a)

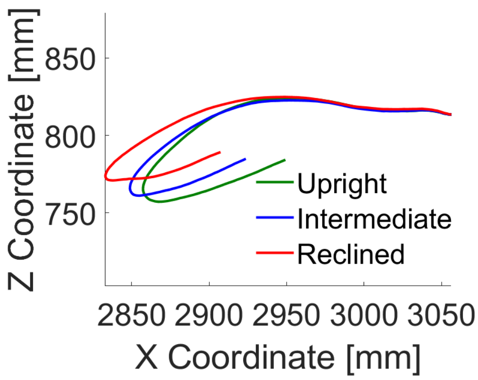

(b)

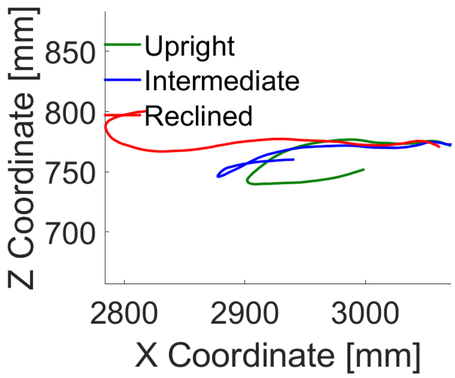

(c)

Figure 3.30: H-point XZ trajectory in the oblique left pulse . (a) HIII05, (b) THOR50, (c) THUMS50

3.2.3 Indicator 6 - Iliac/ASIS X Forces Left & Right

The iliac/ASIS X forces are shown in Fig. 3.31 for the span of the crash event for the HIII05, THOR50 and THUMS50 sitting in upright, intermediate reclined and reclined positions for the oblique left pulse . For all the occupant models it can be seen that, for the submarining cases, the force build-up and drops happens in a shorter time interval than non-submarining cases. This can give information about submarining and submarining time and may be considered as submarining flag. It can also seen for all occupant models that the left side forces are higher than the right side forces for the same seat-backrest angle, which may be related to the kinematics of the oblique left pulse, where the ATD moves towards the a-pillar which may cause a higher iliac/ASIS force on the left side when engaging with the lap-belt.

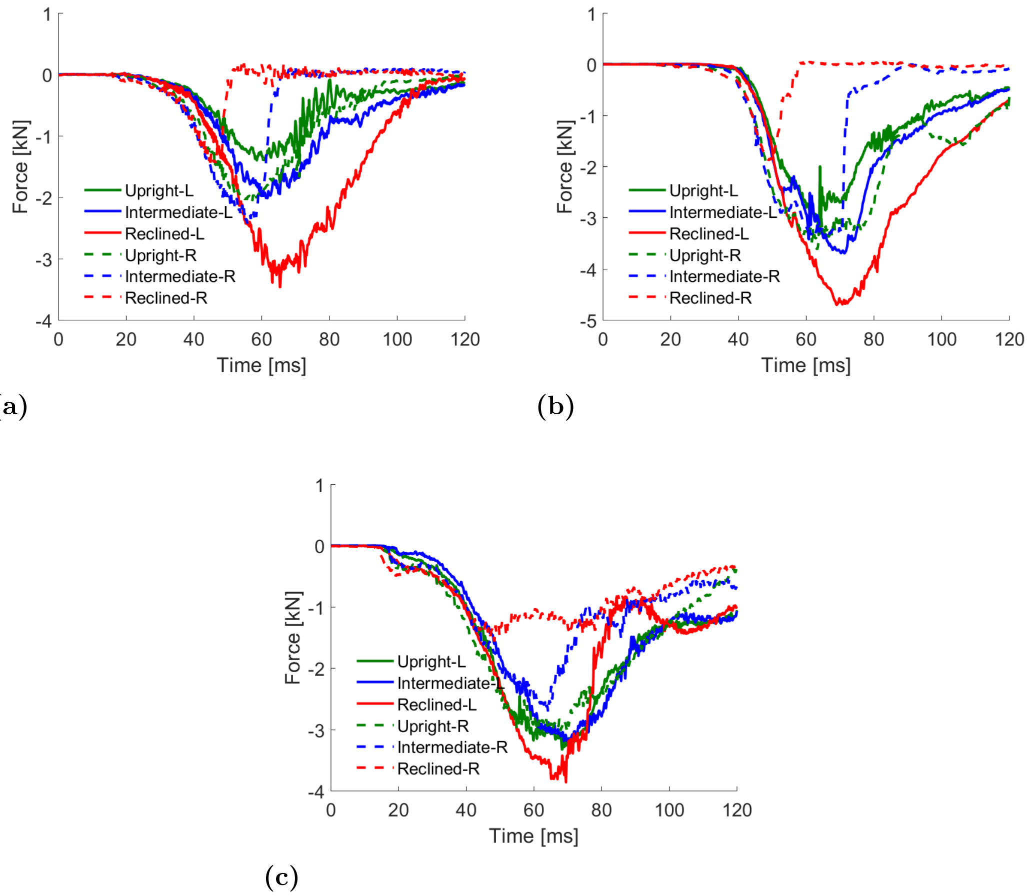

Figure 3.31: Iliac/ASIS X forces left & right in the oblique left pulse . (a) HIII05, (b) THOR50, (c) THUMS50

3.2.4 Indicator 9-10 - Lumbar Spine Forces & Moments

The lumbar spine forces and moments are shown in Fig. 3.32, 3.33 and 3.34 for the span of the crash event for the HIII05, THOR50 and THUMS50 sitting in upright, intermediate reclined and reclined positions for the oblique left pulse . For the lumbar spine forces measured in HIII05 (Fig: 3.32 a), it can be seen that the forces are higher for the submarining cases than for the non-submarining case. For the lumbar spine moments measured in HIII05 (Fig. 3.32 b), the same type of fluctuations as observed in the lumbar spine moments for the submarining cases in HIII05 in the FFRB pulse cannot be observed in the oblique left pulse . It can be seen for the lumbar spine forces measured in THOR50 (Fig. 3.33 a), that they do not provide any conclusive information about submarining occurrence and timing. The lumbar spine moments measured in THOR50 (Fig: 3.33 b) show that the moments are considerably higher in submarining cases than in non submarining cases. The higher moments for submarining cases observed in HIII05 and THOR50 may be a possible submarining flag. For THUMS50 (Fig: 3.34 b), both the lumbar spine forces and moments do not provide conclusive information about submarining.

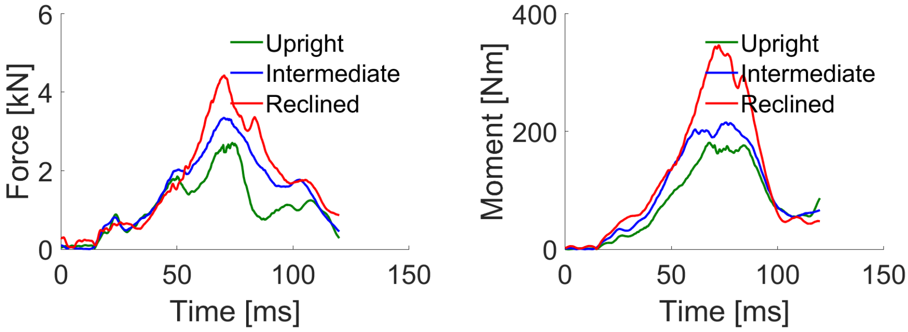

(a) **(b)**

Figure 3.32: For HIII05 in the oblique left pulse . (a) Lumbar spine forces and (b) Lumbar spine moments

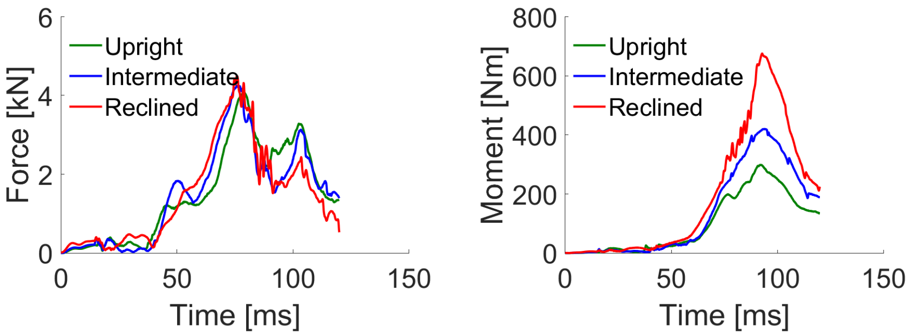

(a) **(b)**

Figure 3.33: For THOR50 in the oblique left pulse . (a) Lumbar spine forces and (b) Lumbar spine moments

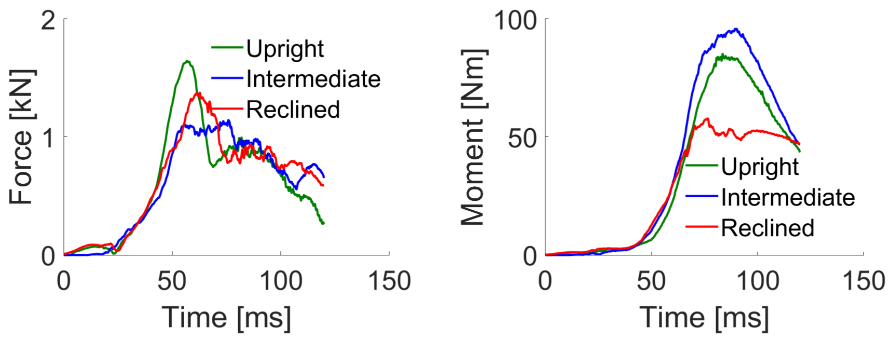

(a) **(b)**

Figure 3.34: For THUMS50 in the oblique left pulse . (a) Lumbar spine forces and (b) Lumbar spine moments

3.2.5 Indicator 12 - Belt Mid-Point to Spine X Distance

The belt mid-point to spine X distance is shown in Fig. 3.35 for the span of the crash event for the HIII05, THOR50 and THUMS50 sitting in upright, intermediate reclined and reclined positions for the oblique left pulse . For all occupant models (Fig: 3.35 a, 3.35 b & 3.35 c), the belt mid-point to spine X distance is smaller in the submarining cases than in the non submarining cases. This may be due to the belt intrusion into the abdomen in submarining cases. The smaller belt mid-point to spine X distance observed in submarining cases may be considered as a submarining flag. It can also be seen for the THOR50 ATD (Fig: 3.35 b), that there is a considerably lower minimum belt to spine X distance in the reclined position compared to in the intermediate reclined position. This may be due to the earlier submarining time for the THOR50 ATD in the reclined position, giving the belt more time to intrude further into the abdomen.

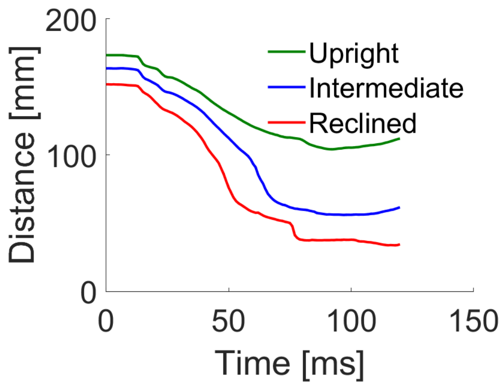

(a)

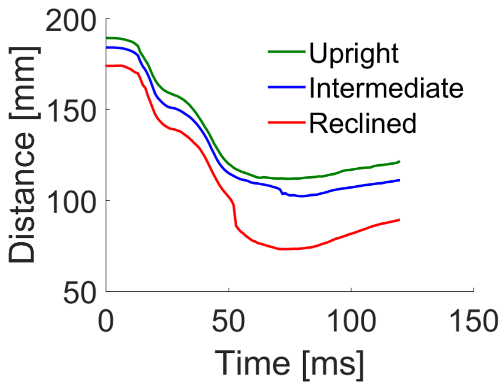

(b)

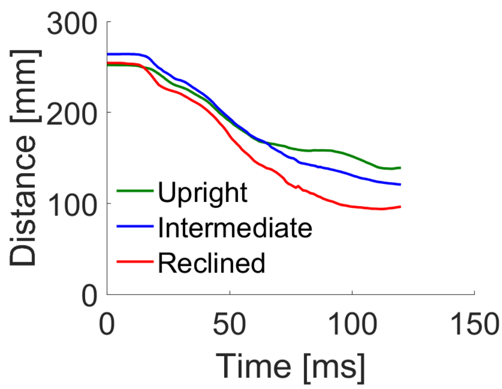

(c)

Figure 3.35: Belt mid to Spine X distance in the oblique left pulse . (a) HIII05, (b) THOR50, (c) THUMS50

3.2.6 Indicator 13-14 - ASIS/Iliac (Left/Right) to Belt X Distance

The ASIS/iliac (Left/Right) to belt X distance is shown in Fig. 3.36 for the span of the crash event for the HIII05, THOR50 and THUMS50 sitting in upright, intermediate reclined and reclined positions for the oblique left pulse. For all occupant models it is evident from the below figures that the when the graphs change sign, i.e. when the distance becomes negative, this coincides with the left and right sides submarining. When the distance goes from positive to negative represents that the ASIS/iliac has slid under the lap-belt . The graphs in which the distance has not become negative and is close to zero shows that the corresponding side has not submarined. The change of sign gives information about both of the occurrence and timing of submarining and may be considered as a submarining flag.

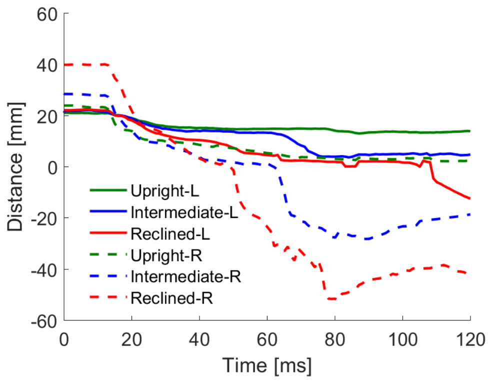

(a)

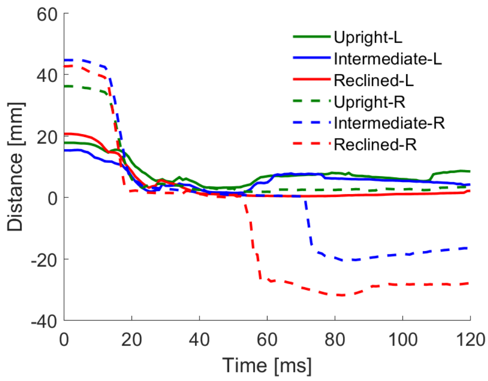

(b)

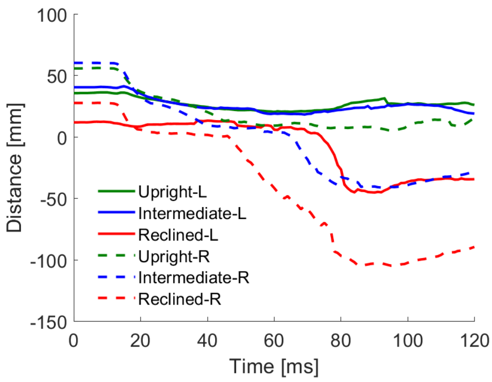

(c)

Figure 3.36: ASIS/Iliac (left/right) to belt X distance in the oblique left pulse . (a) HIII05, (b) THOR50, (c) THUMS50

3.2.7 Indicator 21 - Lever Arm

The lever arm on the left and right iliac wing is shown in Fig. 3.37, 3.38 and 3.39 for the span of the crash event for the HIII05, THOR50 and THUMS50 sitting in upright, intermediate reclined and reclined positions for the oblique left pulse. Similarly as described for the data for the FFRB pulse in Section 3.1, it can be seen in submarining cases for HIII05 and THOR50, that just after submarining time there is noise in the lever arm data with high fluctuations. This may be due to when the ASIS block slips under the lap-belt, the force reduces and thus the denominator in Equation 2.2 becomes small resulting in large values of the lever arm. In HIII05 and THOR50, the ASIS on anchor side did not submarine for any configuration of seatback angle, which can be seen from that the data in the corresponding graphs has less noise. It can also be seen for HIII05, THOR50 and THUMS50, that the lever arm has a negative value just before submarining, which indicates that the belt is located on the negative side of the Z-axis in the local coordinate system of the ASIS load cells as defined in Section 2.2. In THOR50 and THUMS50 initial drops in the lever arm can be seen at about 20-40 *ms* into the event, this may be due to pre-tensioner firing.

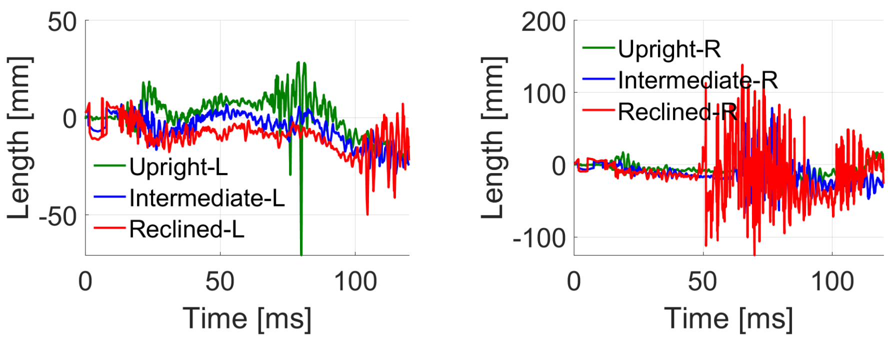

(a) **(b)**

Figure 3.37: HIII05: Iliac lever arm in the oblique left pulse. (a) Anchor side (b) Buckle side.

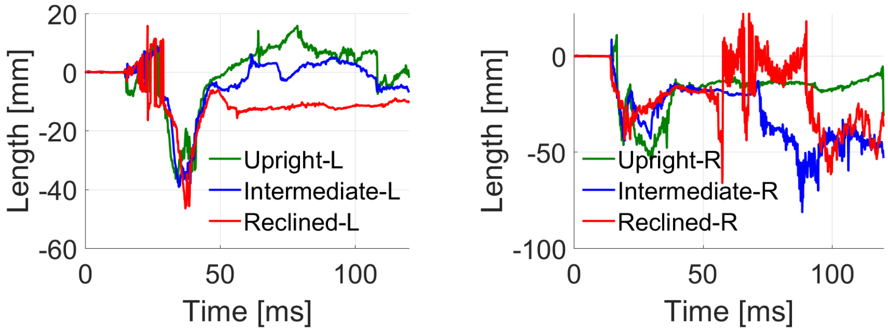

(a) **(b)**

Figure 3.38: THOR50: Iliac lever arm in the oblique left pulse. (a) Anchor side (b) Buckle side..

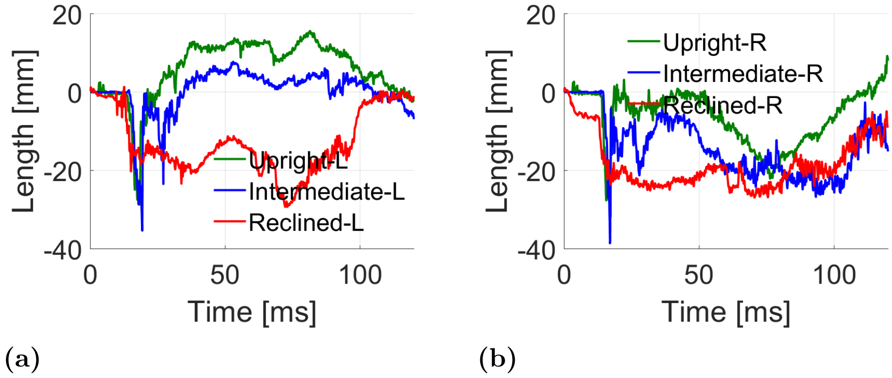

Figure 3.39: THUMS50: Iliac lever arm in the oblique left pulse. (a) Anchor side (b) Buckle side.

3.3 FE Simulations: Oblique Right Pulse (Negative Yaw Rotation)

The third pulse used in this study is oblique right pulse. The kinematics of this pulse makes the car occupant move towards the passenger/centre-console. The submarining and submarining time information as observed visually in simulation for HIII05, THOR50 and THUMS50 occupant models are tabulated in Table 3.4, corresponding to upright, intermediate reclined and reclined configurations of seat backrest. For the FFRB pulse all results are presented in the corresponding results section, while for this oblique right pulse, the H-point trajectory, cross-sectional forces of the lap-belt, lumbar spine forces and moment, belt mid-point to spine X distance and ASIS/Iliac (Left/Right) to Belt X distance results are presented in the corresponding results section and remaining are omitted as they are not relevant due to angled movement of the occupant model.

Table 3.4: Oblique right pulse: Submarining time information for HIII05, THOR50, THUMS50.

	oblique right pulse (Negative Yaw)	
HIII05	Left Submarining	Right Submarining
Upright		
Intermediate	76 ms	
Reclined	60 ms	58 ms

THOR50	Left Submarining	Right Submarining
Upright		
Intermediate		
Reclined		

Legend	
	Non Submarining
	Submarining

THUMS50	Left Submarining	Right Submarining
Upright		
Intermediate	74 ms	
Reclined	60 ms	60 ms

3.3.1 Indicator 5 - H-Point XZ Trajectory

The H-point trajectory is shown in Fig. 3.40 for the span of the crash event for the HIII05, THOR50 and THUMS50 sitting in upright, intermediate reclined and reclined positions for the oblique right pulse . It can be seen from the the figures that all occupant models undergoing submarining have an exaggerated forward excursion (smaller X coordinate) and have a reduced vertical movement (larger Z coordinate). It can also be seen, THOR50 (Fig.3.40 b) did not submarine for the oblique right pulse , so difference in H-point trajectory can not be seen in the graph and seems coinciding. It can be seen in THUMS50 (Fig. 3.40 c), that the pelvis moves up in submarining cases while in HIII05 and THOR50 (Fig. 3.40 a, 3.40 b), the pelvis moves down in Z in all cases.

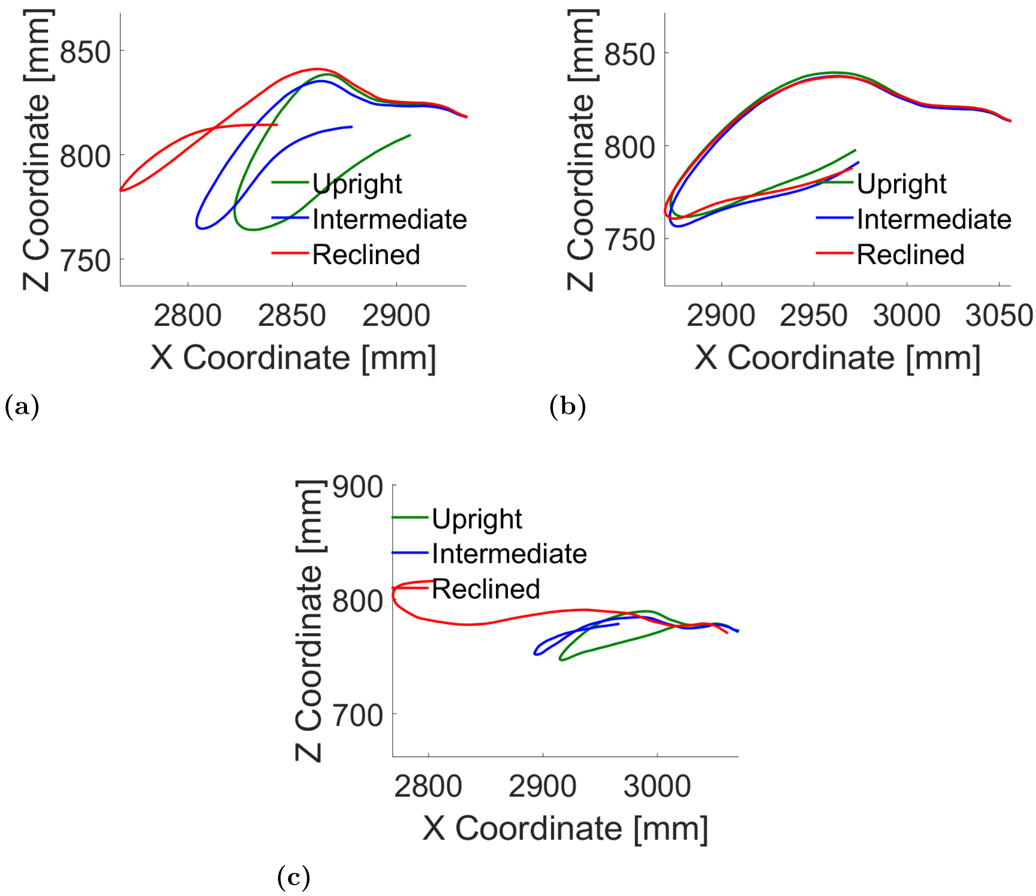

Figure 3.40: H-Point XZ trajectory in the oblique right pulse . (a) HIII05, (b) THOR50, (c) THUMS50

3.3.2 Indicator 8 - Lap-Belt Cross-Sectional Resultant Forces

The cross-sectional forces of the lap-belt are shown in Fig. 3.41 for the span of the crash event for the HIII05, THOR50 and THUMS50 sitting in upright, intermediate reclined and reclined positions for the oblique right pulse. For HIII05 (Fig. 3.41 a), it can be seen in the submarining cases, the force build up and drop happens in small time interval. It can also be seen that local minima/fluctuation in curve gives information about the submarining time. This can be a possible flag for submarining detection. THOR50 (Fig. 3.41 c) did not submarine for the oblique right pulse, so the lap-belt forces for all seating configurations are similar. For THUMS50 (Fig. 3.41 c), it can be seen that as seat back-rest angle increases, lap-belt forces decreases but there is not any information to identify submarining.

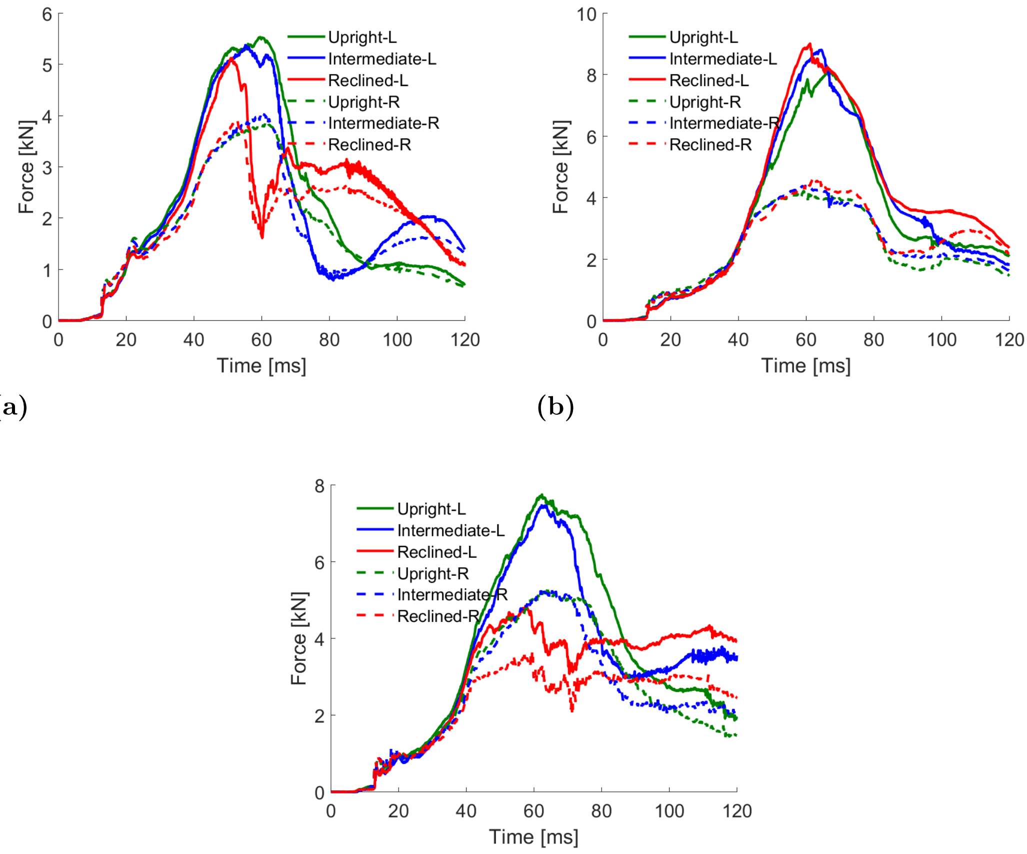

(a) (b) (c)

Figure 3.41: Lap-belt cross section resultant forces in the oblique right pulse . (a) HIII05, (b) THOR50, (c) THUMS50

3.3.3 Indicator 9-10 - Lumbar Spine Forces & Moments

The lumbar spine forces and moments are shown in Fig. 3.42, 3.43 and 3.44 for the span of the crash event for the HIII05, THOR50 and THUMS50 sitting in upright, intermediate reclined and reclined positions for the oblique right pulse . It can be seen for HIII05 (Fig. 3.42 a), cases undergoing submarining shows considerable higher lumbar spine forces. It can also be seen in Fig: 3.42 b, that the local minima/fluctuations in the curve shows occurrence of submarining and gives information about the submarining time. So, altogether it can be seen, for HIII05, high lumbar spine forces and minima/fluctuations in moment curve shows occurrence of submarining and which may be considered as a submarining flag. THOR50 (Fig. 3.43 a) did not submarine for the oblique right pulse and it can be seen that the peak forces increase as seat back-rest angle increases and moments remain inconclusive. For THUMS50 (Fig. 3.44), both forces and moments are inconclusive.

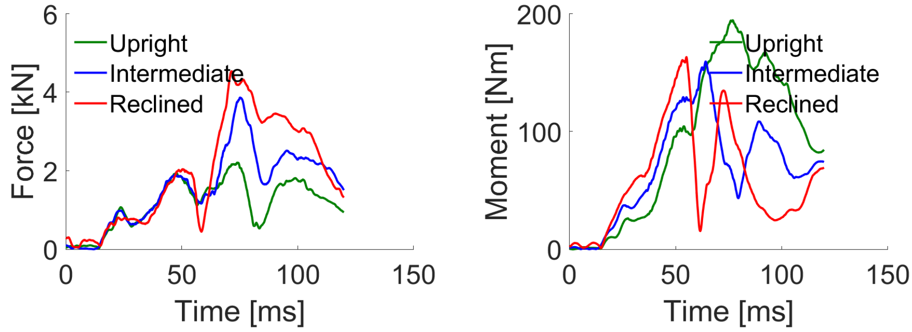

(a) **(b)**

Figure 3.42: For HIII05 in oblique right pulse . (a) Lumbar spine forces and (b) Lumbar spine moments

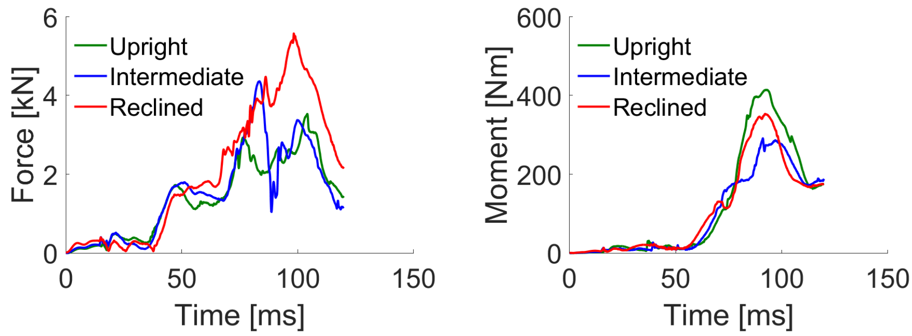

(a) **(b)**

Figure 3.43: For THOR50 in oblique right pulse . (a) Lumbar spine forces and (b) Lumbar spine moments

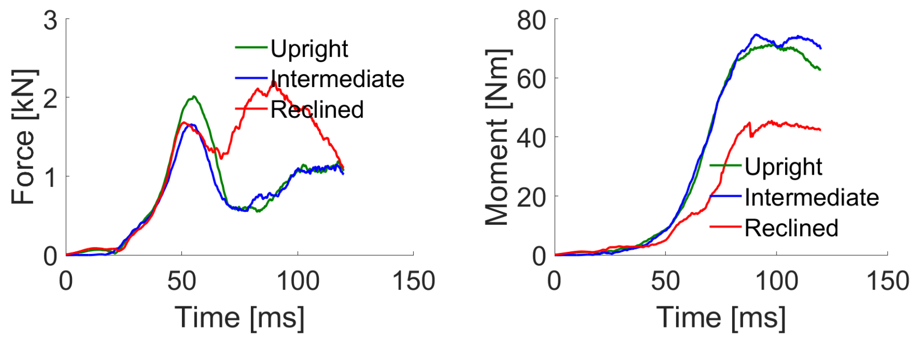

(a) **(b)**

Figure 3.44: For THUMS50 in oblique right pulse . (a) Lumbar spine forces and (b) Lumbar spine moments

3.3.4 Indicator 12 - Belt Mid-Point to Spine X Distance

The belt mid-point to spine X distance is shown in Fig. 3.45 for the span of the crash event for the HIII05, THOR50 and THUMS50 sitting in upright, intermediate reclined and reclined positions for the oblique right pulse . For HIII05 (Fig. 3.45 a), the distances are considerably smaller for the submarining cases. This can be because of the more belt-intrusion in abdomen in submarining cases. Smaller belt mid-point to spine X distance may be considered as a submarining flag for HIII05. THOR50 did not submarine for the oblique right pulse (Fig: 3.45 (a)), so the distances are similar and shows ASIS has not slid under the lap-belt. For THUMS50 (Fig: 3.45 c), the graph remains inconclusive.

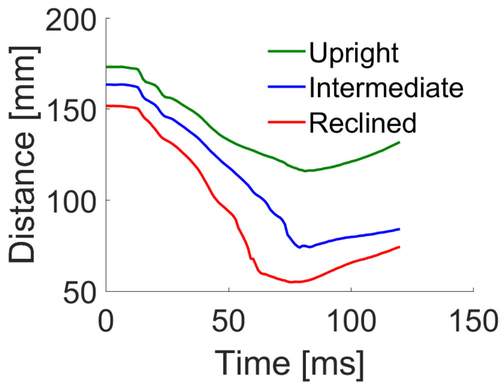

(a)

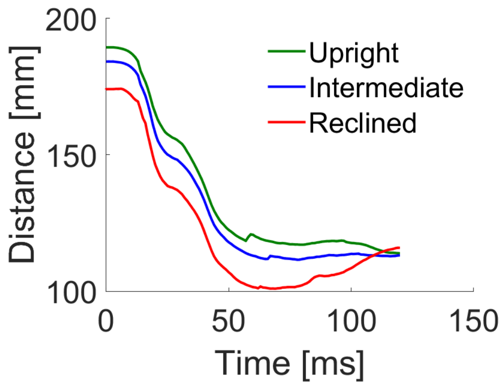

(b)

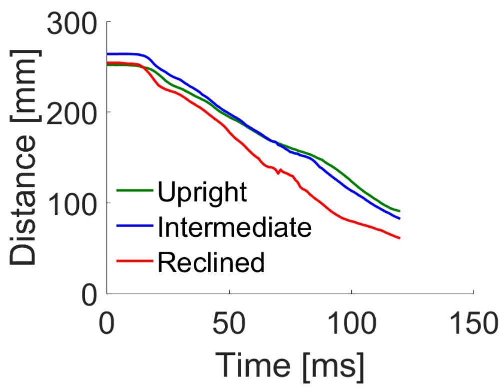

(c)

Figure 3.45: Belt mid to Spine X distance in the oblique right pulse . (a) HIII05, (b) THOR50, (c) THUMS50

3.3.5 Indicator 13-14 - ASIS/Iliac (Left/Right) to Belt X Distance

The ASIS/Iliac (Left/Right) to Belt X distance is shown in Fig. 3.46 for the span of the crash event for the HIII05, THOR50 and THUMS50 sitting in upright, intermediate reclined and reclined positions for the oblique right pulse. It can be seen, that the change in the sign of the distance shows submarining and submarining time for left and right submarining respectively. This represents that the ASIS/iliac has slid under the lap-belt at that particular instant of time. The cases where the distance does not become negative and is close to the zero line shows that the belt is still loading the ASIS/iliac block and ASIS/iliac has not slid under the lap-belt. The change in sign of distance may be considered as a submarining flag.

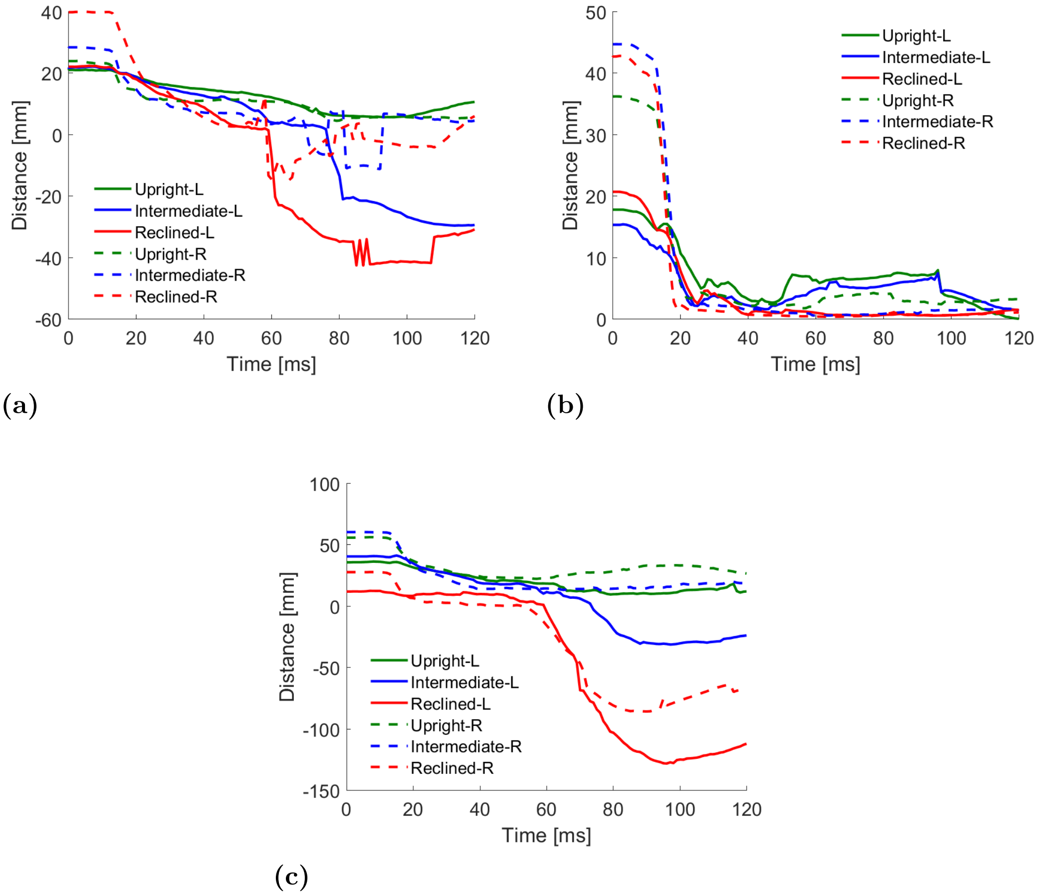

Figure 3.46: ASIS/Iliac (left/right) to belt X distance in the oblique right pulse . (a) HIII05, (b) THOR50, (c) THUMS50

3.3.6 Indicator 21 - Lever Arm

The lever arm on the left and right iliac wing is shown in Fig. 3.47, 3.48 and 3.49 for the span of the crash event for the HIII05, THOR50 and THUMS50 sitting in upright, intermediate reclined and reclined positions for the oblique right pulse. Similar noise in the lever arm for HIII05 and THOR50 as observed in the FFRB (3.1) and oblique left pulse (3.2) can be observed here in the data from oblique right pulse. It can also be seen for HIII05, THOR50 and THUMS50, that the lever arm has a negative value just before submarining, which indicates that the belt is located on the negative side of the Z-axis in the local coordinate system of the ASIS load cells as defined in Section 2.2. In the lever arm for THOR50 and THUMS50, initial drops can be seen at about 20-40 *ms* into the event, this may be due to the pre-tensioner firing.

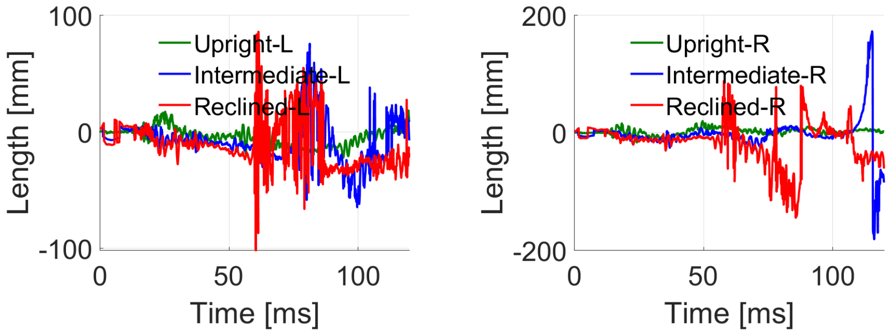

(a) **(b)**

Figure 3.47: HIII05: Iliac lever arm in the oblique right pulse. (a) Anchor side (b) Buckle side.

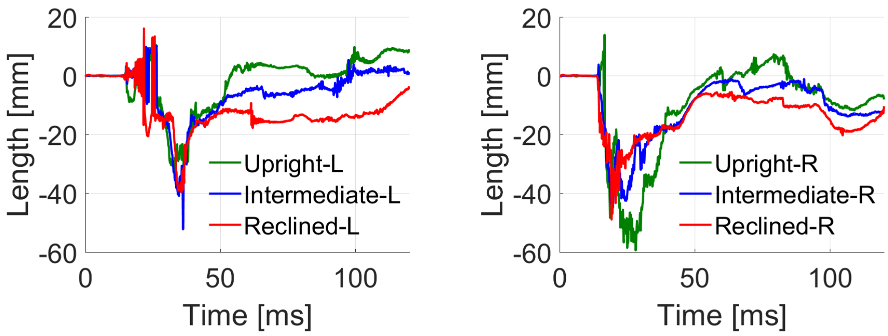

(a) **(b)**

Figure 3.48: THOR50: Iliac lever arm in the oblique right pulse. (a) Anchor side (b) Buckle side.

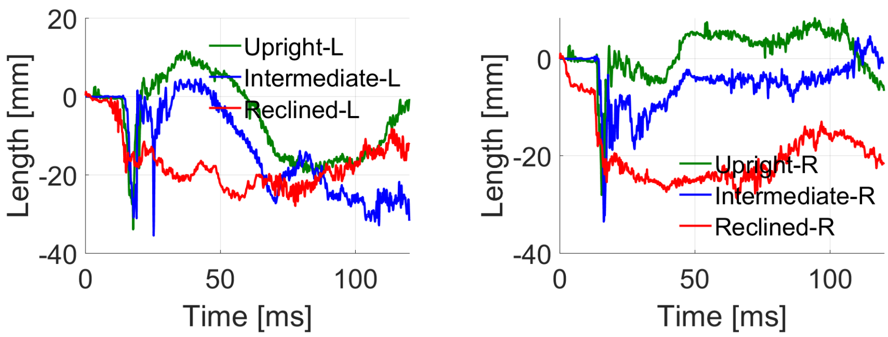

(a) **(b)**

Figure 3.49: THUMS50: Iliac lever arm in the oblique right pulse. (a) Anchor side (b) Buckle side.

3.4 Statistical Analysis

The statistical analysis' results have been divided according to side of submarining of the occupant model. The AIC value is shown in Table 3.5 for both anchor and buckle side respectively. It can be seen that the logistic regression models of individual predictors lever arm and minimum ASIS to belt X distance have least AIC values in both sides. It can also be seen, looking at the AU-ROC values in Table 3.6 that for models of individual predictors of both lever arm and minimum ASIS to belt X distance, the outcome is perfectly predicted i.e. 0s are predicted as 0s and 1s are predicted as 1s. The estimated model coefficients for anchor and buckle side can be found in the Appendix in Table A.5 and A.6.

Table 3.5: AIC values of logistic regression models of predictors and predictor combinations for buckle and anchor side data.

Logistic regression models of predictor and predictor combinations	AIC (anchor side)	AIC (buckle side)
1. Lever arm.	4.00	4.00
2. Minimum ASIS to belt X distance.	4.00	4.00
3. Maximum Force drop.	37.07	36.81
4. Minimum value of belt to pelvis relative angle.	37.10	28.68
5. Lever arm + Minimum ASIS to belt X distance.	6.00	6.00
6. Lever arm + Maximum Force drop.	6.00	6.00
7. Lever arm + Minimum value of belt to pelvis relative angle.	6.00	6.00
8. Minimum ASIS to belt X distance + Maximum Force drop.	6.00	6.00
9. Minimum ASIS to belt X distance + Minimum value of belt to pelvis relative angle.	6.00	6.00
10. Maximum Force drop + Minimum value of belt to pelvis relative angle.	35.51	27.51
11. Lever arm + Minimum ASIS to belt X distance + Maximum Force drop.	8.00	8.00
12. Lever arm + Minimum ASIS to belt X distance + Minimum value of belt to pelvis relative angle	8.00	8.00
13. Lever arm + Maximum Force drop + Minimum value of belt to pelvis relative angle.	8.00	8.00
14. Minimum ASIS to belt X distance + Maximum Force drop + Minimum value of belt to pelvis relative angle	8.00	8.00
15. Lever arm + Minimum ASIS to belt X distance + Maximum Force drop + Minimum value of beltto pelvis relative angle	10.00	10.00

Table 3.6: AU-ROC values of logistic regression models of predictors and predictor combinations.

Logistic regression models of predictor and predictor combination	AU-ROC (anchor side)	AU-ROC (buckle side)
1. Lever arm.	1.00	1.00
2. Minimum ASIS to belt X distance.	1.00	1.00
3. Maximum Force drop.	0.71	0.70
4. Minimum value of belt to pelvis relative angle.	0.64	0.86
5. Lever arm + Minimum ASIS to belt X distance.	1.00	1.00
6. Lever arm + Maximum Force drop.	1.00	1.00
7. Lever arm + Minimum value of belt to pelvis relative angle.	1.00	1.00
8. Minimum ASIS to belt X distance + Maximum Force drop.	1.00	1.00
9. Minimum ASIS to belt X distance + Minimum value of belt to pelvis relative angle.	1.00	1.00
10. Maximum Force drop + Minimum value of belt to pelvis relative angle.	0.74	0.91
11. Lever arm + Minimum ASIS to belt X distance + Maximum Force drop.	1.00	1.00
12. Lever arm + Minimum ASIS to belt X distance + Minimum value of belt to pelvis relative angle	1.00	1.00
13. Lever arm + Maximum Force drop + Minimum value of belt to pelvis relative angle.	1.00	1.00
14. Minimum ASIS to belt X distance + Maximum Force drop + Minimum value of belt to pelvis relative angle	1.00	1.00
15. Lever arm + Minimum ASIS to belt X distance + Maximum Force drop + Minimum value of beltto pelvis relative angle	1.00	1.00

3.4.1 Buckle Side (Right side)

Based on the steps described in the method Section 2.3, the logistic regression models of the lever arm and minimum ASIS to belt X distance are identified as the most optimal predictors, but for both predictors, Fig. 3.50 a and 3.51 a, the maximum likelihood of parameters does not exist due to the complete separation of data-points. The estimated coefficients perfectly separate failures from successes, which can also be seen in Fig. 3.50 c and 3.51 c, where AU-ROC is 1 and which indicates that both of the logistic regression models of individual predictors perfectly predicts the outcome.

Figure 3.50 a and b indicate that there is an increased probability of submarining the smaller the minimum belt to ASIS X distance becomes. It can also be seen in the same figure for HIII05, THOR50 and THUMS50 that these occupant models might submarine when the minimum ASIS to belt X distance becomes smaller than 2, 0 and 5 *mm* respectively for the three occupant models. This is indicated by the last data point at which that corresponding occupant model did not submarine. From a mechanical viewpoint, submarining is assessed as the event when the belt slips over the iliac wing. Thus, it is reasonable that the threshold of minimum ASIS to belt X distance at which submarining might occur is close to 0 *mm*.

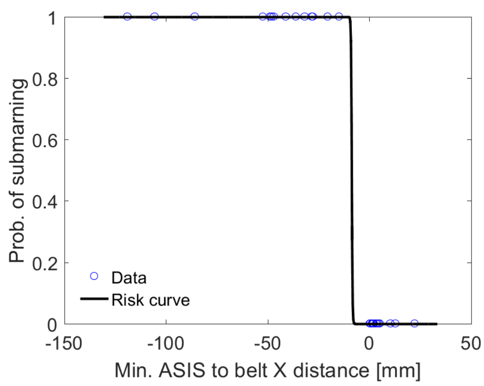

(a)

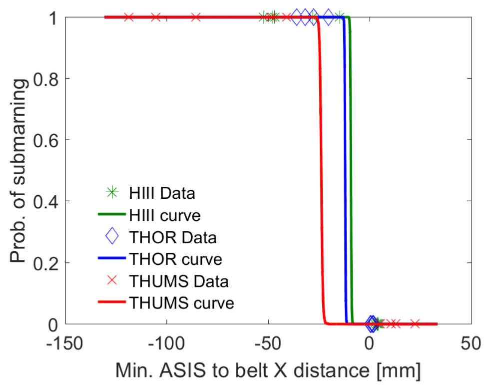

(b)

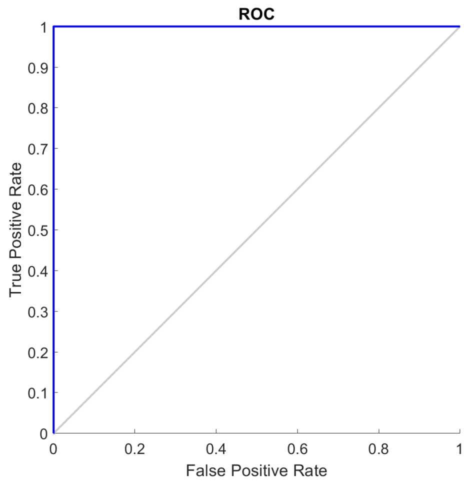

(c)

Figure 3.50: Buckle side optimal predictor: Minimum ASIS to belt X distance. (a) probability curve for submarining, (b) probability curve for submarining - occupant model (c) ROC graph

For the lever arm, Figure 3.51 indicates that, the smaller the lever arm becomes, the probability of submarining increases . HIII05, THOR50 and THUMS50 might submarine when the lever arm becomes smaller than approximately -10, -14 and -10 *mm* respectively. This is indicated by the last data point at which that corresponding occupant model did not submarine. It has to be noted that the possible threshold values mentioned for the models using either the individual predictor minimum ASIS to belt X distance or the lever arm are based on very few data-points, because of this the possible threshold values might change if more data would be present.

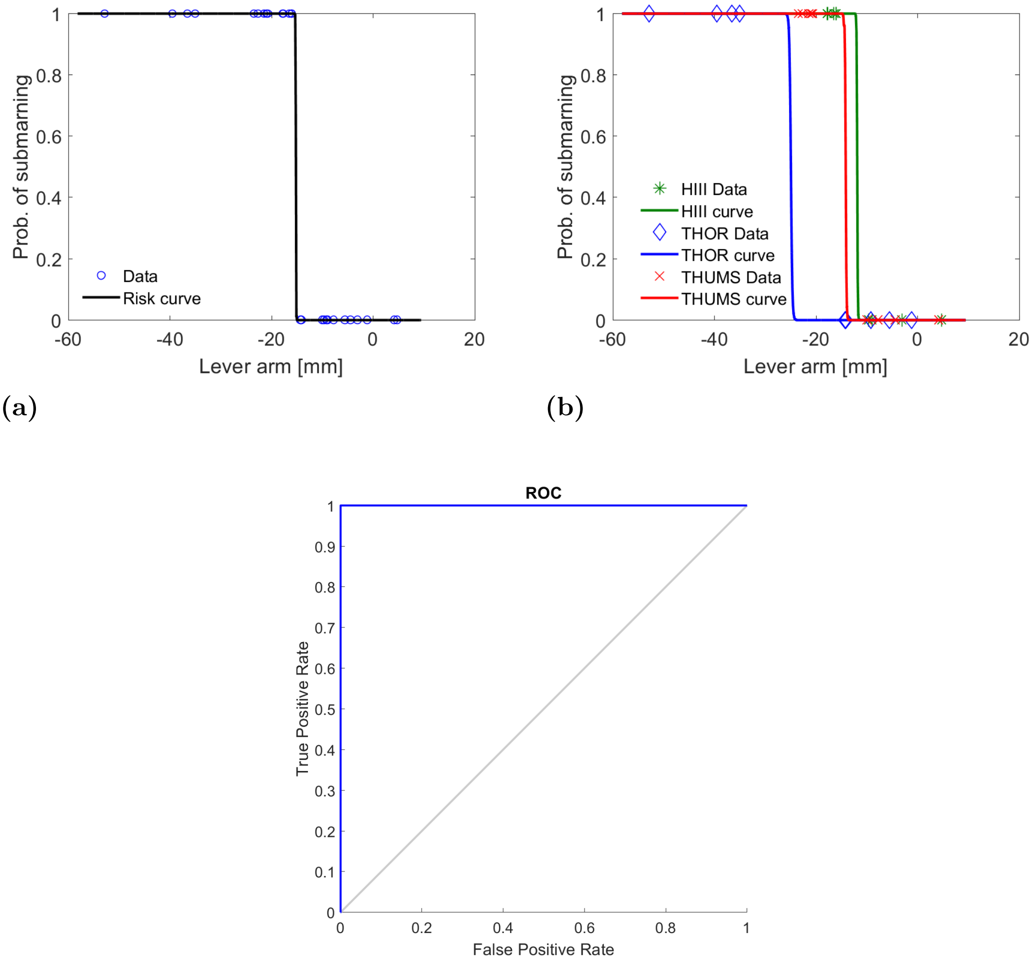

(a) **(b)** **(c)**

Figure 3.51: Buckle side optimal predictor: Lever arm. (a) probability curve for submarining, (b) probability curve for submarining - occupant model (c) ROC graph

The models of combinations of predictors where the minimum ASIS to belt X distance and lever arm are included are not considered for the next best predictor since they on their own already perfectly separate failures from successes. So next best model of individual predictor (Fig. 3.52), minimum relative angle between lap-belt and pelvis is selected according to the method mentioned in Section 2.3. It can be seen in Fig. 3.52 b, that all occupant models show different probability curve for submarining and which are not overlapping, which indicates that the predictor is occupant model specific. It can also be seen in Fig. 3.52 b, that for HIII05 there is a complete separation of data-points. This may be because of fewer data-points as each curve in Fig. 3.52 b is drawn based on one third of the number of data-points (9 data-points) compared to Fig. 3.52 a (27 data-points). The AU-ROC for the model including the single predictor minimum relative angle between lap-belt and pelvis is 0.86, which can be considered good as mentioned in Section 2.3.
Figure 3.52 a and b indicate that the probability of submaring occurrence increases with decreased minimum relative angle between lap-belt and pelvis. In the same

figure it can be seen that there is a 50% probability of submarining at a minimum relative angle between lap-belt and pelvis of approximately 75 and 72 ° for THOR50 and THUMS50 respectively. In the same figure, a step curve can be seen for HIII05 with approximately 65 ° threshold value. The perfect separation may be because of very few data-points and with more number of data-points, a sigmoid curve may be obtained.

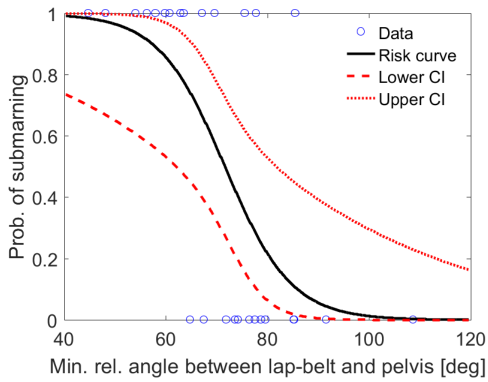

(a)

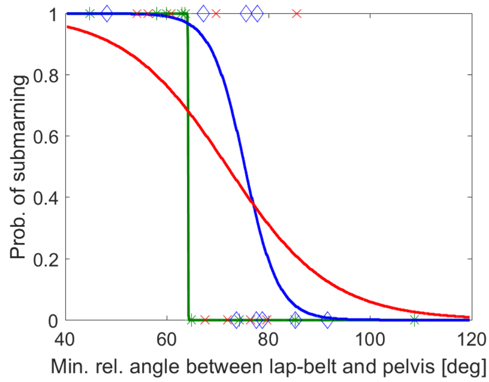

(b)

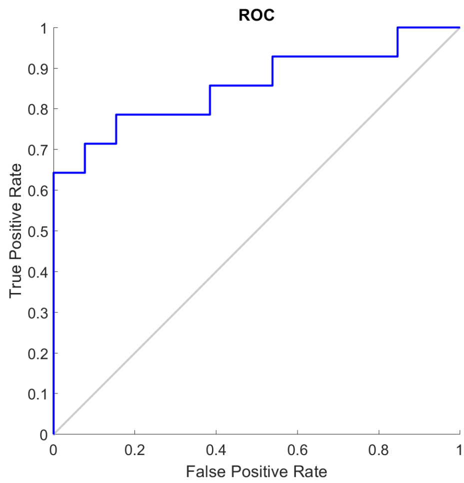

(c)

Figure 3.52: Buckle side optimal predictor: Minimum relative angle between lap-belt and pelvis. (a) probability curve for submarining showing 95% confidence intervals, (b) probability curve for submarining - occupant model, HIII05: ______, THOR50: ______, THUMS50: ______ (c) ROC graph

3.4.2 Anchor Side (Left side)

Based on the steps in the method Section 2.3, the logistic regression models of the lever arm and minimum ASIS to belt X distance are identified as the most optimal predictors, but for both predictors (Fig. 3.53 a and 3.54 a), the maximum likelihood of parameters does not exist due to complete separation of data-points (Fig. 3.53 a). The estimated coefficients perfectly separate failures from successes. It can also be seen for the lever arm, that there is just one data-point for which THOR50 submarines, so the graph is according to the best theoretical estimate in that case.

Figure 3.53 a and b indicate that, the smaller the minimum ASIS to belt X distance becomes, there is an increased probability of submarining. It can also be seen in the same figure for HIII05, THOR50 and THUMS50 that these occupant models might submarine when the minimum ASIS to belt X distance becomes smaller than 0, 0 and 10 mm respectively for the three occupant models. This is indicated by the last data point at which that corresponding occupant model did not submarine. In a similar manner, for the lever arm, Figure 3.54 indicates that the probability of submarining increases, the smaller the lever arm becomes. HIII05, THOR50 and THUMS50 might submarine when the lever arm becomes smaller than approximately -9, -17 and -8 mm respectively. This is indicated by the last data point at which that corresponding occupant model did not submarine. It has to be noted that the possible threshold values mentioned for the models using either the individual predictor minimum ASIS to belt X distance or the lever arm are based on very few data-points, because of this the possible threshold values might change if more data would be present.

Similar to the buckle side, the next best logistic regression model of an individual predictor for anchor side (Fig. 3.55) is chosen, which is the maximum force drop. It can be seen in Fig. 3.55 b that all occupant models show different probability curve for submarining and which are not overlapping, which indicates that the maximum force drop predictor is occupant model specific. It can also be seen in Fig. 3.55 b, that for THUMS50, there is a complete separation of data-points. This may be because of very less data-points for THUMS50. The AU-ROC for the maximum force drop is 0.71 which can be considered good as mentioned in Section 2.3.

As shown in Figure 3.55 a and b, the probability of submarining occurrence increases with increased maximum force drop. In the same figure it can be seen that there is a 50% probability of submarining at a maximum force drop of approximately 0.8 and 1 kN for HIII05 and THOR50 respectively. In the same figure it can also be seen for THUMS50, that this occupant model might submarine when the maximum force drop becomes larger than 0.4 kN. It has to be noted that the possible threshold values mentioned above are based on very few data-points, because of this the possible threshold values might change if more data would be present.

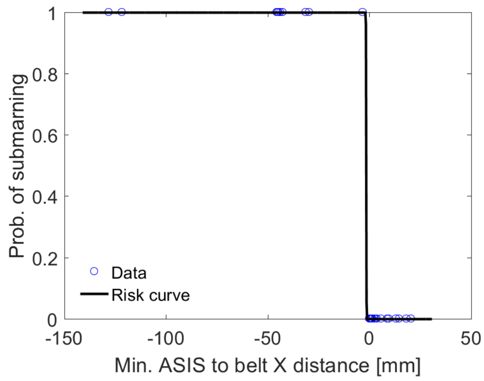

(a)

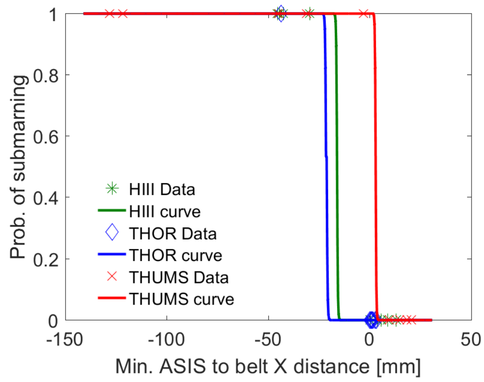

(b)

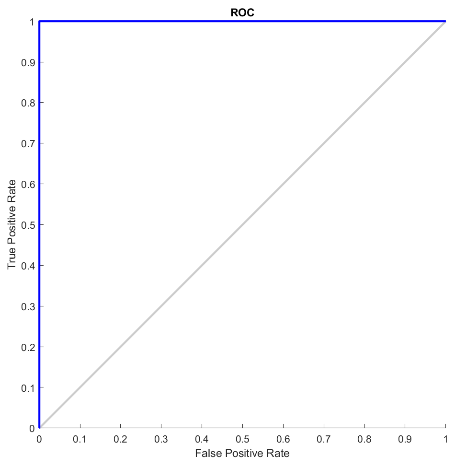

(c)

Figure 3.53: Anchor side optimal predictor: Minimum ASIS to belt X distance. (a) probability curve for submarining, (b) probability curve for submarining - occupant model (c) ROC graph

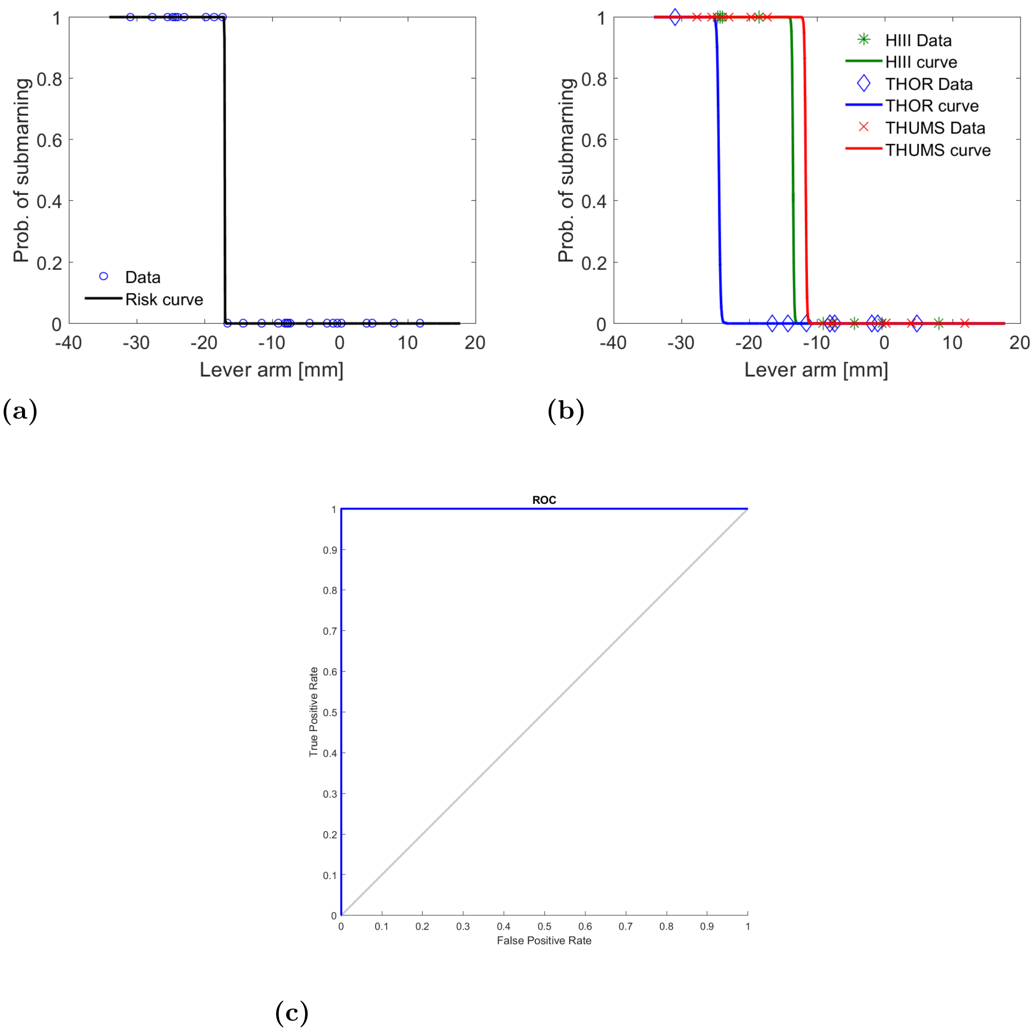

Figure 3.54: Anchor side optimal predictor: Lever arm. (a) probability curve for submarining, (b) probability curve for submarining - occupant model (c) ROC graph

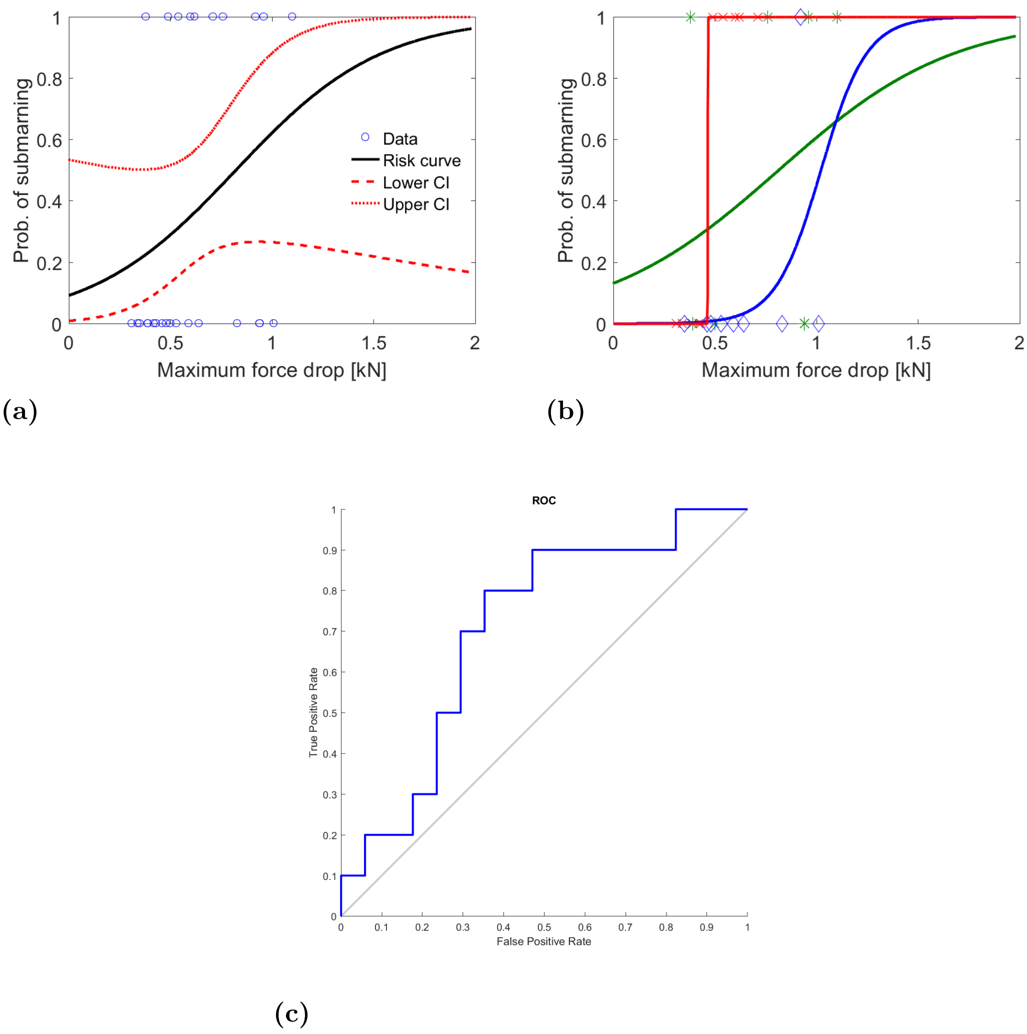

Figure 3.55: Anchor side optimal predictor: Maximum force drop. (a) probability curve for submarining showing 95% confidence intervals, (b) probability curve for submarining - occupant model, HIII05: ———, THOR50: ———, THUMS50: ——— (c) ROC graph

4
Discussion

Several submarining indicators (Table 2.1) were investigated for the occupant models (HIII05, THOR50 and THUMS50) and it was found that the ASIS lever arm, ASIS to belt X distance, ASIS X force and relative angle between lap-belt and pelvis showed trends with submarining occurrence. Optimal predictors in relation to submarining were determined from the logistic regression analysis and the logistic regression models using the individual predictors ASIS lever arm and minimum ASIS to belt X distance were found to be optimal predictors. Probability curve for submarining were drawn according to the methodology mentioned in Section 2.3.

4.1 FE Simulations

The identified submarining indicators were analysed for all three pulses, three seating configurations and three occupant models used in this study and those which showed the most interesting trends in relation to submarining occurance for both the ATDs and the HBM were shortlisted and tabulated in Table 4.1. It was also seen that some indicators show a trend for submarining but they do not tell on which side the occupant model is going to submarine, these are tabulated in Table 4.2. It was observed that one occupant model did not show submarining for one pulse irrespective of the posture used in the study (THOR50 for oblique right pulse). It was also seen that some indicators (lumbar spine forces and moments) showed some trend in relation to submarining, but these were not investigated in further detail due to their location far away from the region of interest in which submarining occurs (pelvis region). The submarining indicators which showed good trend (Table 4.1) were used as an input in the statistical analysis.

Table 4.1: Submarining indicators for occupant models for all pulses.

	Candidate
1.	Lever arm
2.	Belt to ASIS X distance
3.	ASIS/Iliac forces
4.	Relative angle between lap-belt and pelvis

Table 4.2: Submarining indicators for occupant models (not side specific).

	Candidate
1.	H-Point XZ Trajectory
2.	Belt mid to spine X distance

The first submarining indicator chosen to be used in the statistical analysis was the ASIS lever arm. This indicator consistently showed a trend in relation to submarining for all the used occupant models, pulses and seating positions. In Section 3, a consistent trend of the lever arm value close to or at submarining time was observed for all occupant models. Considerable amount of noise was also observed for two of the occupant models (HIII05 and THOR50) when submarining occurred. These two trends were identified as a motivation for the indicator to be used in the later statistical analysis.

The second submarining indicator chosen for further statistical analysis was the ASIS to belt X distance. In the results Chapter 3, it was presented that at submarining time in submarining cases, the ASIS to belt X distance changed sign and became negative, while for most non-submarining cases the distance did not become negative and is close to the zero line. The minimum distance was therefore identified as an appropriate measure to quantify if the ASIS has slid under the lap-belt in any occupant model, since a minimum distance of around zero may indicate that ASIS has not slid under the lap-belt and a minimum distance that is negative may indicate that the ASIS block has slid under the lap-belt.

The third submarining indicator chosen for the further statistical analysis was the ASIS X forces. This indicator showed for most simulations that there was a force build-up and drop on the ASIS force gauges within a shorter time interval than for non-submarining cases (see Section 3). This indicates that when submarining occurs, i.e. the pelvis (ASIS/iliac wings) slides under the lap-belt, the force exerted by the lap-belt on the pelvis is reduced suddenly and therefore, measuring a force drop over a short period of time was considered to be an appropriate measure.

The fourth submarining indicator chosen for the statistical analysis was the relative angle between lap-belt and pelvis in 2D. For this indicator transients in curve were observed in some simulations which showed information about submarining occurrence and timing (see Section 3). Another trend observed was that when the backrest was further reclined the minimum relative angle between lap-belt and pelvis became smaller for numerous simulations. The first trend mentioned is difficult to quantify for further analysis in logistic regression, since for non-submarining cases there is no suitable value comparable to the local minima in submarining cases. The second trend, minimum relative angle between lap-belt and pelvis, is therefore easy to quantify and was therefore used for statistical analysis.

The H-point XZ trajectory and belt mid to spine X distance were observed to show trend in relation to submarining occurrence. The H-point trajectory consistently showed that the displacement in X was larger for submarining cases than for non-submarining cases. The H-point trajectory may work for comparative studies of the same setup, but may not work for analysing novel environments as the expected x-displacement of the occupant H-point might be unknown. The belt mid to spine X distance showed for many simulations that the distance became smaller for submarining cases compared to non-submarining cases (see Section 3). However, both of these submarining indicators cannot give information about the submarining timing and side (anchor or buckle) of submarining, which is of interest, therefore these indicators were not used for further statistical analysis.

The lever arm consist of the ASIS X forces and Y moments which both can be measured in testing and FE simulations. The minimum ASIS to belt X distance is difficult to measure in testing, since markers on the belt might become obstructed from the camera view when the ATD torso bends in front. Data corresponding to extrapolation of obstructed marker positions in films may not be accurate. Although, in FE simulations, this indicator is easy to measure. The force drop on ASIS blocks is already used in Euro NCAP (2017) testing protocol as a standard submarining identification in combination with video analysis. The maximum force drop can also be measured in FE simulation post-processing. The minimum relative angle between lap-belt and pelvis in 2D can be measured in sled-testing using markers and sensors in the ATDs, however in full vehicle testing, it seems hard to measure as the films of marker movements are hard to record due to interior obstruction. The minimum relative angle between lap-belt and pelvis in 2D can be measured in FE simulation post-processing.

The difference in results and kinematics within occupant models can be because of difference in anthropometry and relative position of ASIS to lap-belt. The HIII05 ATD was positioned forward in X compared to THOR50 and THUMS50.

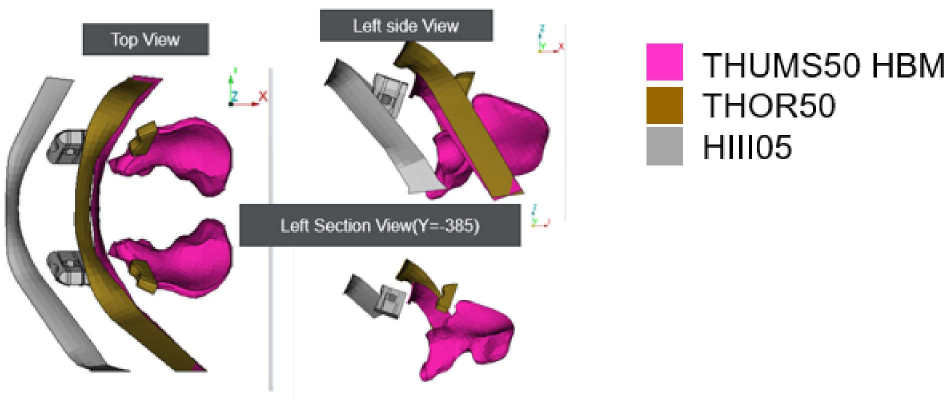

Figure 4.1: Lap-belt to pelvis block relative position for upright seating configuration

4.2 Statistical Analysis

The objective of this part of the study was to find an optimal predictor in relation to submarining and to develop a methodology to derive probability curve for submarining that shows a way forward that a probabilistic prediction of submarining is feasible using the probability curve for submarining. Simulations were done to obtain the data-set for probability curve for submarining and demonstrate its feasibility. Here only simulation data were used and was one of the major limitation for the derived probability curve for submarining. The first step was therefore to choose the most appropriate logistic regression model of predictor or predictor combinations that predicts submarining outcome.

The first step of statistical analysis was to choose the most appropriate logistic regression model of predictor or predictor combinations that predicts submarining outcome. The relevant extracted data corresponding to the indicators identified from Section 4.1 and Table 4.1 were used as an input for the statistical analysis. It was seen that there was perfect separation for the data-points for logistic regression models of lever arm and minimum ASIS to belt X distance predictors in the probability curve for submarining. Since there were just twenty-seven data-points used for the logistic regression analysis, it may be possible with more number of data-points, the probability of obtaining more values for the response may become higher and thus might eliminate the data separation. The same observations were seen in the probability curve for submarining for the occupant models. The threshold value based on the few data-points can not be precisely determined. The 95% confidence interval cannot be drawn for a perfect separation. It was also seen that the probability curve for submarining drawn are occupant model specific and one common curve for all occupant models cannot be drawn. Since there were very few data-points, the sample could not be separated in test and training data for AU-ROC and the AU-ROC values can be slightly higher because of in-sample testing and over-fit. Assessing out-of-sample prediction accuracy of a model with more number of data-points can be used to further reduce over-fitting.

The lever arm and ASIS to belt minimum X distance showed the least AIC value (AIC value=4) for both anchor and buckle sides of submarining and perfectly predicted the outcomes as explained in Section 3.4. With more number of data points for lever arm, a more precise threshold can be found but the curve might still remain steep.

The pivot around which iliac wing is rotating is assumed to be located in centre of the load cell and the local coordinate system is shown in Fig. 4.2. The distance from pivot to upper end of the iliac wing (local -Z direction) may be similar to threshold lever arm value. Therefore, it can be said that once the ASIS block has sled under the lap-belt, the lever arm value may have passed the threshold value. So, it seems like the threshold value depends on the geometry of the pelvis of the occupant model. With more number of data-points for lever arm, a more precise threshold than the threshold obtained in results section can be found but the curve might become sigmoid but still remain steep because of mechanical explanation of lever arm as explained above.

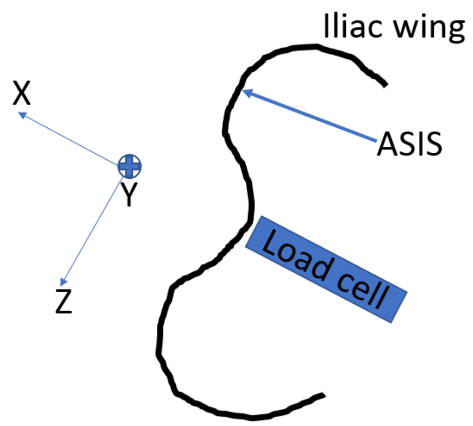

Figure 4.2: Schematic description of the left iliac wing with the ASIS load cell location and local coordinate directions.

The step curve was obtained for minimum ASIS to belt X distance with a narrow threshold range and no confidence interval. It was seen for the investigated data-set that the overall probability to submarine for the both anchor and buckle side is one for negative distances. With more data-points, the threshold can be precisely determined and expected to be close to zero. As explained in results Section 3, and according to the submarining mechanical definition i.e. once the ASIS block slides under the lap-belt, the minimum ASIS to belt X distance becomes negative. So, even with more number of data-points, it does not seem likely to obtain a sigmoid curve for minimum ASIS to belt X distance predictor.

For the buckle side the minimum relative angle between lap-belt and pelvis was identified as the next optimal individual predictor. The minimum value in submarining cases is less in numerous cases than in the non-submarining cases. So, it seems that the less the minimum relative angle between lap-belt and pelvis is, the occupant model is more likely to submarine.

For the anchor side, the third best individual predictor was found to be force drop. It was seen that the belt did not build up much force with the ASIS block for the submarining cases in reclined seat position, which resulted in similar force drop values as in non-submarining cases in upright position (Section 3). This might be because of poor lap-belt engagement with the ASIS block in submarining cases in reclined seat position. So there might be a possible influence of seat backrest angle on the performance of the maximum force drop predictor.

5
Conclusion

The most promising submarining indicators which were identified from the FE simulations were: ASIS Lever arm, ASIS to belt X distance, ASIS/Iliac X forces, and relative angle between lap-belt and pelvis. The minimum ASIS to belt X distance separated the submarining and non submarining in most cases and can be a good measure to identify submarining in simulations, however in testing environment this indicator may be hard to measure. The lever arm indicator is a derived measure from ASIS X forces and ASIS Y moments from post-processing and it is possible to measure this indicator in testing. The indicators involving acceleration measurement (T1, T4, T12 and pelvis resultant accelerations) were inconclusive in the study, since they did not show any trends in relation to submarining occurrence.

The logistic regression analysis was performed to obtain probability curve for submarining. The logistic regression models for both individual ASIS lever arm and minimum ASIS to belt X distance predictors were identified as the optimal logistic regression models by having the least AIC and the highest AU-ROC value for both buckle and anchor side. For both optimal individual predictors, a step probabilistic injury risk curve for submarining occurrence was obtained without confidence interval instead of a sigmoid curve with confidence intervals, which suggests threshold values for submarining for these indicators. The threshold values for optimal predictors were determined with few data-points in this study and the precise threshold values may be determined with more data points.

5.1 Limitations

- There are a number of limitations associated with the FE simulation part of this thesis. For instance, the study was performed without a frontal airbag, knee airbag, centre console, steering wheel and instrument panel in the model. So the occupant model did not have any interactions with the aforementioned parts. Additionally, the position of buckle, anchor, cushion angle and D-ring were kept fixed.
- There are few limitations in the statistical analysis study i.e. all the derived probability curves for submarining are based on the few data-points (27 data-points).
- The probability curves for submarining are derived using only simulation data. Scaling of data for different age groups was not done in the study.

6
Future Work

The present work is subjected to limitations mentioned in the Section 5.1. Following points can be explored and investigated in future.

1. The statistical analysis study is performed with few data-points, it would be desirable to obtain more data-points for the generation of probability curves for submarining.
   - With more number of data-points, the predictor models can be divided in the training and test data and therefore, the out of sample prediction accuracy testing can be done for the model performance evaluation.
   - The threshold values mentioned can be refined with the help of more data-points.
   - The obtained probability curves for submarining can be drawn with a better maximum likelihood fit with more number of data-points. Additionally, narrow confidence intervals can be obtained.
   - The derived probability curves for submarining are based on simulation data, the performance and validity of curves can be assessed on the testing data and real life data.
2. It would be desirable to have the data-sets when all interiors are modelled in the experimental setup. In future, more data-points can be collected after performing simulations with frontal airbag, knee airbag, centre-console, instrument panel and steering wheel modelled in the experimental set-up. It would also be desirable to generate data-points with changed buckle, D-ring and anchor positions, and with different seat-cushion angles.
3. The probability curves for submarining were only assessed for the occupant model dependency, they can also be assessed for seat backrest angle and pulse dependency in the future.
4. The logistic regression model using the combination of maximum force drop and minimum relative angle between lap-belt and pelvis can be explored in the future with both predictors modelled on individual axes and the probabilistic outcome on a separate axis to obtain a 3D probability curve for submarining.

Bibliography

Bohlin, N. (1977). “Fifteen Years with the Three-Point Safety Belt. (English)”. In: Sixth International Conference of the International Association for Accident and Traffic Medicine - Melbourne (Australia), pp. 142–159.

Norin, H., G. Carlsson, and J. Korner (1984). “Seat Belt Usage in Sweden and Its Injury Reducing Effect. (English)”. In: *SAE Technical Papers*, pp. 10–28.

Håland, Y. and G. Nilsson (1991). “Seat belt pretensioners to avoid the risk of submarining – a study of lapbelt slippage factors. (English)”. In: Proceedings of the $13^t h$ International Technical Conference on the Enhanced Safety of Vehicles (ESV) - Paris (France).

Lizee, E. et al. (1998). “Development of a 3D Finite Element Model of the Human Body. (English)”. In: 42nd Stapp Car Crash Conference Proceedings, pp. 1–23.

Håland, Y. (2006). “THE EVOLUTION OF THE THREE POINT SEAT BELT FROM YESTERDAY TO TOMORROW. (English)”. In: IRCOBI Conference - Madrid (Spain), pp. 3–15.

Uriot, J., P. Baudrit, et al. (2006). “Investigations on the Belt-to-Pelvis Interaction in Case of Submarining. (English)”. In: *Stapp Car Crash Journal* 50, pp. 53–73.

Swedish Transport Administration (Trafikverket) (2011). *Analysis of Road Safety Trends 2010: Management by Objectives for Road Safety Work, Towards the 2020 Interim targets. (English)*. 2011:118. Borlänge, Sweden. URL: https://www.unece.org/fileadmin/DAM/trans/doc/2011/wp1/Informal_Document_No.5_Sweden.pdf.

Girard, B. and S. Cirovic (2012). “DEVELOPMENT OF KINEMATIC CRITERIA FOR DETECTION OF SUBMARINING. (English)”. In: vol. 45, Supplement 1:S84. ESB2012 - 18th Congress of the European Society of Biomechanics, s84–s84.

Luet, C., X. Trosseille, P. Drazétic, et al. (2012). “Kinematics and Dynamics of the Pelvis in the Process of Submarining using PMHS Sled Tests. (English)”. In: *Stapp Car Crash Journal* 56, pp. 411–442.

Luet, C., X. Trosseille, P. Potier, et al. (2012). “Investigation on the interindividual differences influence on submarining in frontal crash. (English)”. In: *COMPUTER METHODS IN BIOMECHANICS AND BIOMEDICAL ENGINEERING* 15:sup1, pp. 306–308.

Petitjean, A. et al. (2012). “Injury Risk Curves for the WorldSID 50^{th} Male Dummy. (English)”. In: *Stapp Car Crash Journal* 56, pp. 323–347.

Reed, M. P., S. M. Ebert, and J. J. Hallman (2013). “Effects of Driver Characteristics on Seat Belt Fit. (English)”. In: *Stapp Car Crash Journal* 57, pp. 43–57.

Saunders, J. and D. Parent (2013). "Repeatability of a Small Overlap and an Oblique Moving Deformable Barrier Test Procedure. (English)". In: *SAE Int. J. Trans. Safety* 1(2), pp. 309–327.

Beck, B., J. Brown, and L. E. Bilston (2014). "Assessment of Vehicle and Restraint Design Changes for Mitigating Rear Seat Occupant Injuries. (English)". In: *Traffic Injury Prevention* 15.7, pp. 711–719.

Nakane, K. et al. (2015). "Analysis of Abdominal Injuries Caused by the Submarining Phenomenon in the Rear Seat Occupants. (English)". In: 24th International Technical Conference on the Enhanced Safety of Vehicles (ESV) - Gothenburg (Sweden), pp. 15–23.

Poplin, G. S. et al. (2015). "Nature and etiology of hollow-organ abdominal injuries in frontal crashes. (English)". In: *Accident Analysis and Prevention* 78, pp. 51–57.

Richard, O. et al. (2015). "Occupant restraint optimisation in frontal crash to mitigate the risk of submarining in out-of-position situation. (English)". In: IRCOBI Conference - Lyon (France), pp. 84–100.

Uriot, J., P. Potier, P. Baudrit, X. Trosseille, P. Petit, et al. (2015). "Reference PMHS Sled Tests to Assess Submarining. (English)". In: *Stapp Car Crash Journal* 59, pp. 203–223.

Uriot, J., P. Potier, P. Baudrit, X. Trosseille, O. Richard, et al. (2015). "Comparison of HII, HIII and THOR dummy responses with respect to PMHS sled tests. (English)". In: IRCOBI Conference - Lyon (France), pp. 435–451.

Yoganandan, N. et al. (2016). "Deriving injury risk curves using survival analysis from biomechanical experiments. (English)". In: *Journal of Biomechanics* 49.14, pp. 3260–3267.

Euro NCAP (2017). *EUROPEAN NEW CAR ASSESSMENT PROGRAMME (Euro NCAP). ASSESSMENT PROTOCOL - ADULT OCCUPANT PROTECTION. (English).* Version 8.0.2. Leuven, Belgium.

Dozza, M. (2018). *Active Safety Course: Introduction to Automated Driving. (English). Lecture in TME192 Active Safety at Chalmers University of Technology.*

Shaw, G. et al. (2018). "Pelvic Restraint Cushion Sled Test Evaluation of Pelvic Forward Motion. (English)". In: *Traffic Injury Prevention* 19.3, pp. 250–255.

Trosseille, X. et al. (2018). "Reference PMHS Sled Tests to Assess Submarining of the Small Female. (English)". In: *Stapp Car Crash Journal* 62, pp. 93–118.

UN - United Nations (2018). *17 Goals to Transform Our World. (English).* URL: `https://www.un.org/sustainabledevelopment/`.

WHO - World Health Organization (2018a). *GLOBAL STATUS REPORT ON ROAD SAFETY 2018. (English).* ISBN 978-92-4-156568-4. Geneva, Switzerland. Licence: CC BY-NC-SA 3.0 IGO.

– (2018b). *SUMMARY GLOBAL STATUS REPORT ON ROAD SAFETY 2018. (English).* WHO/NMH/NVI/18.20. Geneva, Switzerland. Licence: CC BY-NC-SA 3.0 IGO. URL: `https://apps.who.int/iris/bitstream/handle/10665/277370/WHO-NMH-NVI-18.20-eng.pdf?ua=1`.

A

Appendix 1

A.1 HIII05 Instrumentation

The following measurement capabilities (Table A.1) of HIII05 dummy can be used in testing to measure the submarining indicators.

Table A.1

Location	Description	Channels
Thorax:	3 Accelerometers in a triaxial array Five-Axis Thoracic Spine Load Cell	Ax,Ay,Az Fx,Fy,Fz,Mx,My
Lumbar Spine:	Five-Axis Lumbar Spine Load Cell	Fx,Fy,Fz,Mx,My
Pelvis:	3 Accels or 1 Triax pack A.S.I.S. Load Cell (Iliac Wings)	Ax, Ay, Az Fx,My (per side)

A.2 THOR50 Instrumentation

The following measurement capabilities (Table A.2) of THOR dummy can be used in testing to measure the submarining indicators.

Table A.2

Location	Description
Spine and Thorax:	T1 Accelerometer (Tri-pack) Thorax Accelerometer (Tri-pack) T12 Accelerometer (Tri-pack) T12 Load Cell
Pelvis:	Acetabulum Load Cell (Left) Acetabulum Load Cell (Right) A.S.I.S Load Cell (Left) A.S.I.S Load Cell (Right)

A.3 Data Aggregation for Statistical Analysis

The following two tables contain the data aggregated for the statistical analysis for anchor side (Table A.3) and buckle side (Table A.4). In the test nr. column for both tables, number 1-3, 10-12 and 19-21 refer to simulations with the FFRB pulse, number 4-6, 13-15 and 22-24 refer to simulations with the oblique left pulse and number 7-9, 16-18 and 25-27 refer to simulations with the oblique right pulse.

Table A.3: Biomechanical matrix - Indicator data for anchor side.

Anchor side						
Occupant model	**Test nr.**	**Outcome (0/1)**	**Submarining indicator**			
			Lever arm	**Minimum ASIS to belt X distance**	**Maximum force drop**	**Rel. angle betw. lap-belt and pelvis (2D)**
HIII05	1	0	-4.47	8.69	0.39	85.56
	2	1	-23.99	-45.59	1.1	78.32
	3	1	-18.58	-44.7	0.38	65.55
	4	0	7.97	13.02	0.94	96.58
	5	0	-0.41	3.66	0.39	72.62
	6	0	-7.65	0.17	0.5	51.86
	7	0	-9.12	5.66	0.94	83.09
	8	1	-24.3	-29.59	0.96	83.69
	9	1	-24.68	-42.54	0.76	79.11
THOR50	10	0	-8.07	2.48	0.59	84.26
	11	0	-16.6	0.98	0.35	63.46
	12	1	-30.94	-43.8	0.92	53.87
	13	0	4.76	3.11	1.01	87.19
	14	0	-1.92	1.47	0.83	76.20
	15	0	-11.58	0.42	0.53	58.98
	16	0	-1.04	0.05	0.46	85.37
	17	0	-7.36	1.37	0.48	80.32
	18	0	-14.27	0.58	0.64	70.53
THUMS50	19	0	0.21	14.67	0.42	76.1
	20	1	-17.35	-3.24	0.62	63.74
	21	1	-25.47	-121.6	0.6	45.89
	22	0	11.79	20.42	0.31	81.54
	23	0	3.92	18.27	0.43	61.21
	24	1	-27.69	-45.16	0.71	35.21
	25	0	-7.82	9.54	0.34	84.78
	26	1	-19.77	-31.24	0.49	80.61
	27	1	-23	-128.1	0.54	88.12

Table A.4: Biomechanical matrix - Indicator data for buckle side.

Buckle side						
Occupant model	**Test nr.**	**Outcome (0/1)**	**Submarining indicator**			
			Lever arm	**Minimum ASIS to belt X distance**	**Maximum force drop**	**Rel. angle betw. lap-belt and pelvis (2D)**
HIII05	1	0	-9.69	3.38	0.53	85.19
	2	1	-16.49	-46.9	0.74	57.99
	3	1	-16.06	-48.01	0.33	44.79
	4	0	-9.02	2.16	0.7	64.82
	5	1	-17.83	-28.21	0.83	62.9
	6	1	-17.74	-52.32	0.78	63.56
	7	0	4.71	4.49	0.39	108.7
	8	0	-3.12	3.89	0.83	74.22
	9	1	-16.07	-14.89	1.23	59.9
THOR50	10	0	-14.14	1.32	0.49	77.59
	11	1	-35.06	-27.72	0.91	67.14
	12	1	-39.53	-36.1	0.5	48.14
	13	0	-14.33	1.82	0.6	78.76
	14	1	-36.58	-20.41	2.11	77.79
	15	1	-52.87	-31.8	0.62	75.57
	16	0	-1.22	1.77	0.39	91.57
	17	0	-5.62	0.58	0.26	85.28
	18	0	-9.22	0.36	0.27	73.62
THUMS50	19	0	-7.8	10.38	0.3	67.52
	20	1	-21.47	-48.8	0.49	56.3
	21	1	-22.72	-118.85	0.29	54.08
	22	0	-10.01	5.21	0.3	71.91
	23	1	-20.73	-41.03	0.45	69.66
	24	1	-21	-105.5	0.25	85.49
	25	0	4.11	22.25	0.39	76.46
	26	0	-4.45	12.73	0.42	79.62
	27	1	-23.49	-85.72	0.55	60.77

A.4 Model Estimates

Table A.5: Model estimates for anchor side.

	Predictor combination	Model coefficient				
		β_0	β_1	β_2	β_3	β_4
Anchor side	1. Lever arm.	-1423.13	-83.84			
	2. Min. ASIS to belt X distance.	-31.45	-19.6			
	3. Max. force drop.	-2.29	2.79			
	4. Min. rel. angle betw. lap-belt and pelvis.	2.72	-0.04			
	5. Lever arm + min. ASIS to belt X distance.	-144.47	-7.55	-14.39		
	6. Lever arm + max. force drop.	-664.03	-32.47	255.35		
	7. Lever arm + min. rel. angle betw. lap-belt and pelvis	-2868.45	-77	24.55		
	8. Min. ASIS to belt X distance + max. force drop.	-68.31	-17.47	71.13		
	9. Min. ASIS to belt X distance + min. rel. angle betw. lap-belt and pelvis.	-23.91	-19.36	-0.11		
	10. Max force drop + min. rel. angle betw. lap-belt and pelvis	1.39	3.65	-0.06		
	11. Lever arm + min. ASIS to belt X distance + max force drop.	-516.89	-24.55	-0.91	198.68	
	12. Lever arm + min. ASIS to belt X distance + min. rel. angle betw. lap-belt and pelvis.	-194.67	-7.96	-14.32	0.68	
	13. Lever arm + max. force drop + min. rel. angle betw. lap-belt and pelvis.	-799.1	-31.67	185.21	2.72	
	14. Min. ASIS to belt X distance + max. force drop + min. rel. angle betw. lap-belt and pelvis.	-53.72	-17.33	114.19	-0.64	
	15. Lever arm + min. ASIS to belt X distance + max. force drop + min. rel. angle betw. lap-belt and pelvis.	-83.02	-13.72	-2.8	207.22	-4.04

Table A.6: Model estimates for buckle side.

	Predictor combination	Model coefficient				
		β_0	β_1	β_2	β_3	β_4
Buckle side	1. Lever arm.	-605.92	-39.88			
	2. Min. ASIS to belt X distance.	-48.46	-5.57			
	3. Max. force drop.	-1.76	3.37			
	4. Min. rel. angle betw. lap-belt and pelvis.	11.03	-0.15			
	5. Lever arm + min. ASIS to belt X distance.	-90.4	-3.34	-4.8		
	6. Lever arm + max. force drop.	-606	-39.87	0.58		
	7. Lever arm + min. rel. angle betw. lap-belt and pelvis	16.09	-15.49	-3.58		
	8. Min. ASIS to belt X distance + max. force drop.	-147.36	-3.7	128.69		
	9. Min. ASIS to belt X distance + min. rel. angle betw. lap-belt and pelvis.	99.76	-4.73	-2.08		
	10. Max force drop + min. rel. angle betw. lap-belt and pelvis	9.5	2.49	-0.15		
	11. Lever arm + min. ASIS to belt X distance + max force drop.	-159.01	-2.55	-2.85	106.31	
	12. Lever arm + min. ASIS to belt X distance + min. rel. angle betw. lap-belt and pelvis.	117.38	-8.06	-1.4	-3.8	
	13. Lever arm + max. force drop + min. rel. angle betw. lap-belt and pelvis.	-20.59	-15.52	13.02	-3.2	
	14. Min. ASIS to belt X distance + max. force drop + min. rel. angle betw. lap-belt and pelvis.	-49.7	-3.48	122.32	-1.24	
	15. Lever arm + min. ASIS to belt X distance + max. force drop + min. rel. angle betw. lap-belt and pelvis.	-77.94	-2.3	-2.72	105.3	-1.04